

**EFFECT OF MICRON ARCHITECTURAL
MODIFICATIONS ON THE FRACTURE OF
IMPLANT-CEMENT INTERFACES**

By

YANLING LI

Master of Science in Mechanical Engineering

University of Central Oklahoma

Edmond, Oklahoma,

2015

MASTERS THESIS

Submitted to the Faculty of the
Graduate College of the
University of Central Oklahoma
in partial fulfillment of
the requirements for the Degree of
MASTER OF SCIENCE

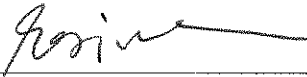
May, 2015

**EFFECT OF MICRON ARCHITECTURAL
MODIFICATIONS ON THE FRACTURE OF
IMPLANT-CEMENT INTERFACES**

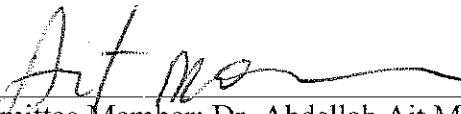
Thesis Approved:



Committee Chair: Dr. Morshed Khandaker



Committee Member: Dr. Mohammad Hossan



Committee Member: Dr. Abdellah Ait Moussa

ACKNOWLEDGMENTS

I am grateful to thank my graduate adviser, Dr. Morshed Khandaker for his excellent care and guidance throughout my graduate studies and in the preparation of my master's thesis. I would also like to express my sincere gratitude to Dr. Mohammad Hossan and Dr. Abdellah Ait Moussa for their valuable suggestions in developing my research work. The support of this research was National Institute of General Medical Sciences of the National Institutes of Health under award number 8P20GM103447. I would like to thank for the support from my student research supports.

I would like to specially thank my research mates Shahram Riahinezhad, Charles Collins, Ryan Jordan, Kooroush Azartash-Namin for their friendship, cooperation and guidance. I am also grateful to the Department of Physics & Engineering at University of Central Oklahoma, which presented me with this wonderful opportunity to pursue graduate studies.

Finally I would like to express my boundless gratitude to my parents, my husband Mujie Ji, my best friend Stefano Tarantini and all the other friends who have always inspired me and helped me in building my academic career.

Effect of Micron Architectural Modifications on the Fracture of Implant/Cement Interfaces

Yanling Li

May, 2015

Abstract

The majority of cemented hip replacements fail due to implant loosening. One design feature that may affect loosening rates is the fracture performance of implant-cement interface. The goal of the study is to develop an effective solution for cemented fixation. It is hypothesis that adding the micron or nano-size bioactive particles or monomer into the cement mantle or coating the micron fibers onto the implant surface can increase the mechanical interlock of the implant-cement interface and eventually solve the implant loosening problem.

For cement mantle, bioactive particles (MgO, hydroxyapatite (HAp), chitin (CT), chitosan (CS), Barium sulfate (BaSO_4) and Silica (SiO_2)) were mixed with polymethylmethacrylate (PMMA) beads and Glycidyl methacrylate (GMA) was added into MMA monomer to prepare various bone cement specimens for improving the conventional PMMA cement mechanical thermal and biological properties. This study found that with GMA, PMMA bone cement without any particle additives has the greatest flexural strength and fracture toughness. Without GMA, SiO_2 can significantly increase the fracture toughness and flexural strength of PMMA bone cement. This study has also found that the fracture toughness of bone-PMMA with micro MgO particles and nano MgO particles interfaces were significantly higher comparing to the result of the bone-PMMA interface. For Titanium (Ti) implant, in vitro static test has been performed on implant-cement interface with fiber coated to evaluate the effect of fiber architecture on the fracture strength of Ti-cement interfaces. It has been manifested that either heating up Titanium before coating PCL-acetone fiber or directly coating PCL-PMMA-acetone fiber on the Titanium surface can greatly gain larger fracture strength than cement-Ti without fiber. Additionally, static/fatigue test gripper for the fracture test of implant-cement interface have been designed and analyzed by experiment and ANSYS. It has been manifested that due to the elastic property of the plastic, plastic cement holder can only be used for static test not for fatigue test. Multiple fatigue test gripper have been designed and tried in experiment, which can be used for future fatigue experiments of any bi-material samples.

TABLE OF CONTENTS

ACKNOWLEDGMENTS	ii
LIST OF TABLES	ix
LIST OF SYMBOLS	xiii
LIST OF ABBREVIATION	xiv
1 INTRODUCTION	1
1.1 Summary.....	1
1.2 Titanium implant	1
1.3 Bone cement	2
1.4 Implant fixation technique.....	3
1.5 Implant fixation problem	3
1.6 Surface modification of implant-cement interface	4
1.7 Measurement approaches for evaluation fixation quality.....	5
1.8 Hypothesis	6
1.9 Research questions.....	6
1.10 Motivation and goals	7
1.11 Objectives	7
1.12 Organization of the thesis	8
1.13 Figures	9
2 BIOACTIVE ADDITIVES AND FUNCTIONAL MONOMERS EFFECT ON PMMA BONE CEMENT: MECHANICAL PROPERTIES[26]	11
2.1 Summary.....	11
2.2 Background and specification.....	12
2.2.1 Introduction	12
2.2.2 Research questions	14
2.2.3 Scope of work.....	14
2.3 Material and method	15
2.3.1 Sample Preparation.....	15
2.3.2 Experiments and analysis	16
2.3.3 Data analysis.....	16
2.3.4 Statistical Analysis	17
2.4 Results and Discussion	17
2.5 Conclusion	19
2.6 Figures	20
2.7 Tables.....	25
3 MICRO AND NANO MGO PARTICLES FOR THE IMPROVEMENT OF FRACTURE TOUGHNESS OF BONE-CEMENT INTERFACES[40]	27
3.1 Summary.....	27
3.2 Background and specification.....	27
3.2.1 Introduction	27
3.2.2 Research questions	28

3.2.3 Scope of work.....	28
3.3 Material and method.....	29
3.3.1 Sample Preparation.....	29
3.3.2 Experiments and analysis.....	30
3.4 Results and Discussion.....	33
3.5 Conclusion.....	34
3.6 Figures.....	35
3.7 Tables.....	39
4 EFFECT OF SPECIMEN HOLDER ON STATIC AND FATIGUE TESTS ON TITANIUM/CEMENT INTERFACES.....	40
4.1 Summary.....	40
4.2 Introduction.....	40
4.2.1 Static and fatigue tests specimen holder.....	40
4.2.2 Factors that affect Ti-cement interface.....	41
4.2.3 Motivation and Objectives.....	41
4.2.4 Scope of work.....	42
4.3 Material and Method.....	42
4.3.1 Static Test Experiment.....	42
4.3.2 Finite Element Analysis.....	43
4.4 Results and discussion.....	45
4.4.1 Control Experiment.....	45
4.4.2 Finite Element Analysis.....	46
4.4.2.1 Mesh sensitivity analysis.....	46
4.4.2.2 Frictional coefficient for stem-cement and holder-cement interfaces.....	47
4.4.2.3 FEA static and fatigue results for cement with different thickness	47
4.4.2.4 FEA static and fatigue results for plastic and aluminum holders .	48
4.5 Conclusions.....	49
4.6 Figures.....	51
4.7 Tables.....	60
5 EFFECT OF FIBER ARCHITECTURE ON THE FRACTURE STENGTH OF IMPLANT/CEMENT INTERFACES.....	62
5.1 Summary.....	62
5.2 Background and Specification.....	63
5.2.1 Joint replacement implant.....	63
5.2.2 Electrospinning.....	64
5.2.3 Factors that affects the quality of fiber coatings on implant.....	64
5.2.4 Motivation and Objectives.....	65
5.2.5 Scope of Work.....	65
5.3 Material and Method.....	66
5.3.1 Material.....	66

5.3.2 Fiber Deposition	67
5.3.3 Static Test	68
5.4 Results	69
5.4.1 Relation between fiber topography and interface fracture strength	69
5.4.2 Relation between fiber thickness and interface fracture strength.....	69
5.4.3 Relation between fiber stiffness and interface fracture strength	70
5.5 Conclusions	71
5.6 Figures	72
5.7 Tables.....	80
6 DESIGN OF GRIPPERS FOR FATIGUE TESTS ON BI-MATERIAL INTERFACES	
.....	82
6.1 Summary.....	82
6.2 Specification and Background.....	82
6.2.1 Introduction	82
6.2.2 Problems of conventional gripper	83
6.2.3 Motivation and Objectives	83
6.3 Material and Method.....	84
6.3.1 Material	84
6.3.2 Fatigue Test	84
6.3.3 Setup Design Concept Evaluation	85
6.3.3.1 Concept I.....	85
6.3.3.2 Concept II.....	85
6.3.3.3 Concept III	86
6.3.3.4 Concept IV	86
6.4 Results	87
6.4.1 Surface Roughness for different polishing technique	87
6.4.2 Control Experiment	87
6.4.2.1 Concept I.....	87
6.4.2.2 Concept II.....	88
6.4.2.3 Concept III	88
6.4.2.4 Concept IV	88
6.5 Conclusions	89
6.6 Figures	90
6.7 Tables.....	95
7 CONCLUSION AND FUTURE WORKS	96
7.1 Conclusions	96
7.2 Future works	97
8 REFERENCES	99

LIST OF TABLES

Table 2.1 Particulate size of PMMA additives	25
Table 2.2 Variation of flexural strength of bone cements due to the variation of additives and alternative monomer.....	25
Table 2.3 Variation of work of fracture of different kinds of CBC and composite cement specimens	26
Table 3.1 Some particle-size parameters and specific surface	39
Table 3.2 Experimental parameters determined for the tensile test on the flat dumbbell-shaped cement CBC (n=3), mCBC (n=3) and nCBC (n=3) specimen	39
Table 3.3 Descriptive statistics of the experimental single edge sandwiched bone-cement specimen data.....	39
Table 4.1 Material Properties used for the fatigue test of bi-material samples	60
Table 4.2 Static result of plastic and aluminum fatigue holders.....	60
Table 4.3 Relations between implant-cement contact frictional coefficient and displacement	60
Table 4.4 Relationship between cement-aluminum holder frictional coefficient and displacement	61
Table 4.5 Mesh sensitive of FEA model at the Ti-cement union	61
Table 4.6 Mesh sensitive of FEA model at Ti-cement-holder union.....	61
Table 5.1 SEM image of produced PCL-acetone 1 round fiber distribution	80
Table 5.2 Static results of Ti-cement union with and without PCL-acetone fiber (n=3) .	80
Table 5.3 Static results of Ti-cement union with and without heating up Ti before PCL-acetone fiber (n=3).....	80
Table 5.4 SEM image of produced PCL-PMMA-acetone fiber distribution.....	81
Table 5.5 Static results of Ti-cement union with PCL or PCL-PMMA fiber and without fiber	81
Table 5.6 Static results of Ti-cement union with and without heating up Ti rod before PCL-PMMA fiber	81
Table 6.1 Surface roughness for different polishing technique	95
Table 6.2 Control experiment result of fatigue test_3 step polishing using concept IV...	95
Table 6.3 Control experiment result of fatigue test for Ti_2 step polishing using concept IV	95

LIST OF FIGURES

Figure 1.1 Ti-6Al-4V material specification	9
Figure 1.2 Cobalt bone cement	9
Figure 1.3 Schematic of cemented hip replacement	10
Figure 1.4 Flowchart of the study outline	10
Figure 2.1 (a) 3D solid model and (b) fabricated mold using 3D printer used for the preparation of bone cement specimens	20
Figure 2.2 Experimental setup used for bone-cement interface study	20
Figure 2.3 Alignment of SENB specimen on Evex tensile test stage	21
Figure 2.4 Stress-strain plot of composite bone cement made with hydroxyapatite and glycidyl methacrylate	21
Figure 2.5 Line diagram of the variation of flexural strength of various bone cement samples due to the variation of additives and GMA	22
Figure 2.6 Variation of bending modulus of various bone cement samples due to the variation of additives and GMA	22
Figure 2.7 Load-displacement plot of composite bone cement made with hydroxyapatite and glycidyl methacrylate	23
Figure 2.8 Variation of fracture toughness of various bone cement samples due to the variation of additives and GMA. Each additive incorporated CBC samples was grouped in two categories: samples without GMA and samples with GMA	23
Figure 2.9 Line diagram of the variation of WOF of various bone cement samples due to the variation of additives and GMA	24
Figure 3.1 Fabricated mold used for the preparation of cement and bone-cement specimens	35
Figure 3.2 (a) Tension test on a flat dumbbell-shaped cement specimen to measure the Young's modulus and Poisson's ratio of the cement specimen, (b) schematic diagram and dimension of the flat dumbbell-shape specimen, (c) schematic diagram and dimension of the single edge sandwiched bone-cement specimen, and (d) tension test setup for the measurement of the interface fracture toughness of bone-cement specimen	35
Figure 3.3 Particle-size distribution of the MgO powders: (a) micro size and (b) nano size	36
Figure 3.4 (a) Longitudinal stress vs. longitudinal strain plots of a CBC, mCBC and nCBC specimen (b) transverse strain vs. longitudinal strain plots of a CBC, mCBC and nCBC specimen calculated at 30 sec and 60 sec test time (c) dot plots of the Poisson's ratios of three CBC, mCBC and nCBC samples	37
Figure 3.5 Load versus displacement graphs of (a) bone-CBC, (b) bone-mCBC and (c) bone-nCBC specimens	38
Figure 4.1 Fabricated aluminum and plastic cement holder using CNC machining and 3D printer	51
Figure 4.2 (a) Static tests setup in UTM before curing; (b) during curing	51

Figure 4.3 (a) Meshed model of Ti-cement samples with element size of 0.8mm; (b) meshed model of Ti-cement-holder samples with element size of 3mm.....	52
Figure 4.4 Load vs displacement plot before static test to determine preload caused by curing (a) with plastic holder; (b) with aluminum holder.....	52
Figure 4.5 Load vs displacement plot for plastic and aluminum cement holder	53
Figure 4.6 (a) Boundary conditions of the Ti-0.11 inch cement model; (b) boundary conditions of the Ti-cement-holder model.....	54
Figure 4.7(a) Frictional coefficient of Ti-cement interface (b) frictional coefficient of cement-aluminum interface	54
Figure 4.8 Ti-cement union fatigue life variations with different meshing element sizes	54
Figure 4.9 (a) Displacement contour plot in Z direction of Ti-0.22 inch cement interface;	55
Figure 4.10(a) Von-Mises stress contour plot of 0.22 inch cement; (b) Von-Mises stress contour plot of 0.11 inch cement	55
Figure 4.11 (a) Fatigue life contour plot of 0.22 inch cement; (b) fatigue life contour plot of 0.11 inch cement.....	56
Figure 4.12 Ti-cement-holder union fatigue life variations with different meshing element sizes.....	56
Figure 4.13(a) Displacement contour plot in Z direction of the Ti-cement-plastic holder union; (b) displacement contour plot in Z direction of the Ti-cement-plastic holder union	57
Figure 4.14(a) Displacement at Z axis contour plot of cement in plastic holder; (b) displacement at Z axis contour plot of cement in aluminum holder.....	57
Figure 4.15 Von-Mises stress contour plot of cement in plastic holder; (b) Von-Mises stress contour plot of cement in aluminum holder.....	58
Figure 4.16(a) Fatigue life contour plot of the Ti-cement-plastic holder union; (b) fatigue life contour plot of the Ti-cement-aluminum holder union	58
Figure 4.17 (a) Fatigue life contour plot of the cement in plastic holder; (b) fatigue life contour plot of the cement in aluminum holder.....	59
Figure 5.1 (a) Customized made dis used for polishing round sample using Buehler isomet low speed cutter; (b) Buehler isomet low speed cutter; (c) polishing setup...	72
Figure 5.2 (a) Sonic vitro & sonication device used for sonication; (b) Corning heating & magnetic stirring cell.....	72
Figure 5.3 (a) Schematic representation of the electrospinning process; (b) electrospinning unit; (c) infusion pump; (d) power supplies	73
Figure 5.4 Flowchart showing the steps of determining the topography, stiffness and thickness effect on the fracture of Ti-cement interface.....	74
Figure 5.5 Universal Test Resources (UTM).....	75
Figure 5.6 Static test setup in UTM (a) before curing; (b) during curing.....	75
Figure 5.7 (a) Scanning electron microscope images (SEM) of with 1 rounds of PCL-acetone fiber sample (sample #1); (b) SEM of 2 rounds of PCL-acetone fiber sample; (c) SEM of 3 rounds of PCL-acetone fiber sample.....	76

Figure 5.8 Typical load-displacement plot of Ti-cement interface without fibers	77
Figure 5.9 Comparison of fracture load of Ti-cement interface with different round of fiber	77
Figure 5.10 Scanning electron microscope images of PCL-PMMA-acetone fiber samples	78
Figure 5.11 Typical load-displacement plot of Ti-cement union with and without fiber under static test	78
Figure 5.12 Comparison of fracture load of Ti-cement union with different fiber and with or without heating	79
Figure 6.1(a) Geared Head Milling & Drilling Machine; (b) polishing setup.....	90
Figure 6.2 (a) Top side of the cement holder of concept I; (b) bottom side of the cement holder of concept I; (c) fatigue test setup before cemented; (d) setup during curing the cement	91
Figure 6.3 (a) Bottom side of the cement holder of concept II; (b) fatigue test setup before cemented; (c) setup during curing the cement	92
Figure 6.4 (a) Top side of the aluminum cement holder of concept III; (b) bottom side of the cement holder of concept III; (c) corner support for the cement holder; (d) fatigue test setup before cemented; (f) setup during curing the cement	92
Figure 6.5 (a) Titanium rod sample with a drill hole; (b) fabricated top specimen holder for fatigue test; (c) fatigue test setup of Concept IV	93
Figure 6.6 Surface roughness respond to Ti with 2-step polished using Geared Head Milling & Drilling machine generated by Leica.....	93
Figure 6.7 Surface roughness respond of Ti with 3-step polished using Geared Head Milling & Drilling machine generated by Leica.....	94

LIST OF SYMBOLS

B	Thickness of the 3PB specimen
d	Deflection of the 3PB specimen
E	Young's modulus
K_{IC}	Fracture toughness
N	Number of fatigue cycles
P	Load
S	Span of the 3PB specimen
σ_f	Flexural strength or Fracture Strength
ν	Poisson's ratio
W	Width of the 3PB specimen
WOF	Work of fracture

LIST OF ABBREVIATION

PMMA	Polymethylmethacrylate
GMA	Glycidyl methacrylate
HAp	Hydroxyapatite
CT	Chitin
CS	Chitosan
BaSO ₄	Barium sulfate
CBC	Cobalt™ HV bone cement
mCBC	PMMA with micro MgO particles
nCBC	PMMA with nano MgO particles
PCL	Polycaprolactone

CHAPTER 1

INTRODUCTION

1.1 Summary

The cemented hip prosthesis is one of the most frequent operations in the orthopedic fields. Titanium (Ti) implant is the most widely used material for hip replacement. Poly methyl methacrylate (PMMA) bone cements are widely used to fix artificial joints for filling the free space between bone and prostheses. The big challenges of orthopedic research are the implant loosening or the breakage at the implantation sites and improve the bonding between the interface materials [1]. The mechanical failure of the stem-cement interfaces has been proposed as one of the most possible causes leading to the eventual clinical loosening of cemented hip replacement. The goal is to develop an optimal implant-cement interface by surface modification on Ti implant surface and cement mantle surface. The tensile tests on bioactive particles and alternative monomer added cement were conducted to see whether the particles or the monomer would improve the mechanical properties of cement mantle. The static as well as fatigue tests for implant-cement interfaces have been conducted to see whether the micron fibers would improve the bonding strength of implant and cement interface.

1.2 Titanium implant

Metal alloys exhibit attractive properties such as biocompatibility, mechanical strength, corrosion resistance, safety and ductility. Titanium (Ti) is used as a dental metal for excellent biocompatibility [2]. The dissolution of Ti into body is very trivial because Ti metal surface can spontaneously form a stable and inert layer of titanium dioxide (Ti_2O), which will prevent Ti metal from reacting with body fluid [3]. Ti has its excellent biocompatibility (high corrosion resistance, low ion-formation tendency, low level of electronic conductivity, etc.) mostly owing to this oxide layer. Comparing to commercial

pure Ti, Ti alloys such as Ti-6Al-4V exhibit solid solution hardening and have lower fusion temperatures and better ductility [4]. Among the various Ti alloys, Ti-6Al-4V, which was used in this study, is the most widely used as implant because of its better physical and mechanical properties in comparison to pure Ti. Figure 1.1 shows the material specification of Ti-6Al-4V used in this study.

1.3 Bone cement

Bone cement is used in various orthopedic surgeries. Among the many potential bone cement materials, polymethylmethacrylate (PMMA) bone cement has been successfully used in orthopedic surgeries mostly because of its strong mechanical bonding with implant. PMMA bone cements are provided as two-component materials, a powder (PMMA beads) and a liquid (MMA monomer). These two components are mixed at 2:1 ratio and polymerization occurs. The current most commercially available PMMA bone cements are Cobalt (Biomet, Inc.), Simplex (Stryker, Inc.), and Palacos (Heraeus Company). However, several drawbacks associated with PMMA bone cement limit its efficacy. For example, PMMA cement adheres inadequately to the bone surfaces (no bioactivity) [5], has a high exothermic reaction temperature [6] and exhibits monomer toxicity [7]. Particularly, enough bonding strength of cement with the implant and bone is required for the design of optimal bone cement. Whereas, increasing the bonding strength of implant-cement interfaces is imperative. It may be accomplished by increasing the surface interlock of implant-cement or bone-cement interfaces through enlarging the surface roughness of the cement mantle or the implant surface. The typical bone cement used in this study was Cobalt HV PMMA bone cement (Figure 1.2). One of the objectives of this study is to improve the mechanical biological and thermal properties of Cobalt HV PMMA bone cement.

1.4 Implant fixation technique

The hip is an important multifunctional joint in the human musculoskeletal system. Since the hip is subject to position change, bending, and extreme force, much wear is imposed on the joint. For these reasons, along with age, health, and weight, a hip replacement is sometimes required through a total hip replacement (THR) surgery. The most common practice in THR is the use of titanium implants secured in the patients' femur using cement to press between femoral stem and bone for providing the stability to the implant, which is called cemented fixation (Figure 1.3). Cemented fixation is more common for osteoporotic bone, where the bone cement is used to hold the implant in place [8]. For healthy bone, bone can grow into the surface of the implant by osseointegration. Cementless fixation is more expensive and has less long-term stability when compared to cemented fixation. Furthermore, bone cuts require a perfect match with the component for cementless fixation [9]. The purpose of the thesis is to improve the union of both implant-cement and bone-cement interface for cemented implant.

1.5 Implant fixation problem

Although cemented fixation provides more long-term stability, the clinical loosening of cemented replacement has been reported. In USA, there are approximately 600,000 cases of poor union and 100,000 cases of nonunion of implant with surrounding tissue each year [10]. Many manufacturers have recalled their hip implants (including Johnson & Johnson, DePuy, and Zimmer Durom) [11]. A patient's age, sex, weight, diagnosis, activity level, surgery condition and implant choice influence the longevity of the device. The primary cause of failure of cemented joint replacements is aseptic loosening of the components, which may arise from mechanical failure of the cement mantle surrounding the implant [12]. It has been pointed out that the debonding of stem-cement interface enables gapping and sliding between the stem and cement [13, 14]. Revision surgeries are required for implant failures that are costly and painful.

1.6 Surface modification of implant-cement interface

A wide variety of surface modifications techniques have been developed with the aim to solve implant fixation problem. The current main surface modification techniques are mostly relative to increasing surface roughness or surface energy. The augmentation of the surface roughness or surface energy allows for developing mechanical interlock of implant and bone cement interface, which can improve the bonding characteristics of implant-cement interface [15]. Hosein *et.al* [16] pointed out that circumferential-grooved stems offered improved stability under compression relative to the smooth stems. It has been revealed that porous coating of femoral stems dramatically improved push-out strengths and fatigue properties of the stem-cement interface through increasing surface roughness [17]. Additionally, various implant coatings, including titanium-dioxide with integrated copper ions (TiO_2Cu), plasma polymerized allylamine (PPAAm), calcium phosphate (CaP) and titanium nitride (TiN) have been investigated regarding the adhesion strength and wear resistance [18]. Apart from the implant surface modification, elastic modulus as well as the mechanical properties of the cement mantle could play an important role in the bonding of implant-cement interface. Several research groups found improvement of PMMA bone cements surface roughness properties by incorporating different kinds of nanoparticle additives to PMMA cement [19-23]. Gabureck *et al.* [24] proposed the modified PMMA cement by adding 5-20% 3-methacryloxypropyl-trimethoxysilane to PMMA monomer as a coupling agent to achieve more hydrolysis resistant covalent bonding of implant-cement interface.

There are two approaches of surface modification of implant-cement interface in this study. One approach is surface modification by adding micron/nano particles or monomer into the cement for the purpose of the increment of surface roughness or the elastic property of bone cement. The other approach is surface modification of implant by coating fibers on Ti implant in order to increase the surface roughness of Ti implant

surface, which may increase the mechanical interlock and ensure long lasting bond between implant and cement interface [25].

1.7 Measurement approaches for evaluation fixation quality

To evaluate the impact of the surface modification on cement mantle using bioactive particles and an alternative monomer, the mechanical performance (flexural strength and fracture toughness) of modified cement were measured. In this study, the flexural strength and fracture toughness of various composite bone cements were compared. Three Point Bending (3PB) tests using Evex Tensile stage were performed at room temperature on bone specimen and Single Edge Notch Tensile (SENB) specimen to test the flexural stress-strain properties of the composite bone cements with various particles or monomer. The main reason of using 3PB test is the ease of specimen preparation and testing. The flexural strength and fracture toughness of the cement mantle were calculated based on the test result so as to determine the suitable additives for optimal fracture performance of the bone cement.

Subsequently the fracture toughness of bone-cement interface, bone-micron additive-cement interface and bone-nanosize additive-cement interface were compared to determine whether the micron or nanosize additive has any effect on the bonding strength of the bone-cement union. Fracture toughness is a quantitative way of expressing a material's resistance to fracture, which is related to the material elastic (Young's modulus, Poisson ratio) and the maximum load taking the material to break. Tension tests were conducted on the flat dumbbell-shaped at room temperature using Evex Tensile stage to find the Young's modulus, Poisson's ratio of bone cement with and without micron or nanosize additive. Tension test were conducted on wet biomaterial samples of bone-cement interface, bone-micron additive-cement interface and bone-nanosize additive-cement interface to find out the critical load that breaks the interface. Such study would show the effect of additive particle size on the fracture toughness.

Besides, micron fibers were coated on the implant surface by electrospinning for the purpose of increasing the fracture strength and fatigue life of Ti-implant interface. Fracture strength is the stress when a specimen failed. Fatigue life defines the number of stress cycles of a specified character that a specimen sustains before failure of a specified nature occurs. Test Resources 800LE4 universal testing machine (UTM) was used to conduct the static and fatigue compressing/pulling test. Firstly, multiple static and fatigue test gripper of implant-cement interface were analyzed through finite element analysis (FEA) in ANSYS to explore a suitable test gripper. The suitable test gripper was used to conduct the experimental static test to determine the fracture strength of implant-cement interface with or without fibers. The effect of fiber architecture on the fracture performance of implant-cement interface under static loads was evaluated to develop a suitable implant surface texture. Furthermore, a couple of experimental cyclical test gripper were designed and tested to develop an effective fatigue test fixture for future interface fracture test.

1.8 Hypothesis

The hypothesis of the study is that either adding the micron bioactive particles or monomer into the cement mantle or coating the micron fibers onto the implant surface can increase the mechanical interlock of the implant-cement interface. The independent or combined treatment of the above technique can enhance the bonding strength of implant-cement interfaces and eventually solve the implant loosening problem.

1.9 Research questions

This thesis addressed the following questions: (1) is there any significant difference in the mechanical performances between a PMMA and an additive incorporated PMMA cement that contains GMA as alternative monomer? (2) Is there any significant difference in the mechanical performances between a PMMA and additive

incorporated PMMA cement that do not contain GMA as alternative monomer? (3) Do MgO particles have any influence on the bonding strength between bone and cement? (4) Is there any difference in the mechanical performances of Ti-cement union between 0.22 inch thick cement and 0.11 inch thick cement? (5) Is there any difference in the mechanical performances of Ti-cement union between using plastic cement holder and using aluminum cement holder? (6) Is there any significant differences in the fracture strength of Ti-cement with one round, two rounds and five rounds of PCL fiber under static load; (7) Is there any significant differences in the fracture strength of Ti-cement with PCL fiber and PCL-PMMA fiber under static load; (8) Is there any significant differences in the fracture strength of Ti-fiber-cement with and without heating up Ti before fiber under static load; (9) Is there any suitable fatigue test fixture which can conduct the fatigue test on Ti -cement union?

1.10 Motivation and goals

The motivation of this thesis is to explore a sufficient solution for the mechanical failure of the cemented joint. The goal of this study is to determine the most suitable additives and alternative monomer that can enhance the mechanical performances of PMMA bone cement and to develop fiber coating technique that can enhance the mechanical performance of Ti-cement interface.

1.11 Objectives

This thesis has five objectives: (1) to evaluate whether the micron particles such as MgO, hydroxyapatite (HAp), chitin (CT), chitosan (CS), Barium sulfate (BaSO_4) and Silica (SiO_2) or alternative monomer such as glycidyl methacrylate (GMA) enhance the mechanical performance of PMMA bone cement; (2) to evaluate whether the micron and nanosize MgO enhance the bonding strength between PMMA bone cement and bone; (3) to develop and validate the static/fatigue experimental cement holder by finite element analysis; (4) to evaluate whether the fiber architecture (topography, stiffness and

thickness) improve the in vitro fracture strength of conventional Ti implant; (5) to develop and validate the fatigue test gripper by fatigue experiments.

1.12 Organization of the thesis

The outline of this thesis is simplified in Figure 1.4. There were six chapters. Chapter 1 is the introduction. Chapters 2 to 6 are corresponding to objective 1 to 5, respectively. In Chapter 2, a comparative study of PMMA bone cement with various bio-particles such as MgO, hydroxyapatite (HAp), chitin (CT), chitosan (CS), Barium sulfate (BaSO_4) and Silica (SiO_2) and alternative functional monomers such as glycidyl methacrylate (GMA) on the mechanical properties was conducted. In chapter 3, MgO was used to quantify the elastic properties of PMMA, PMMA with micro MgO particles and PMMA with nano MgO particles cements. In chapter 4, experimental static test of Ti-cement interface was conducted and finite element analysis was performed based on the experiment test result to evaluate the effect of the cement holder on the static/fatigue test of Ti-cement interface. In chapter 5, the fracture toughness of bone-PMMA, bone-PMMA with micro MgO particles and bone-PMMA with nano MgO particles interfaces was determined. In chapter 6, multiple fatigue test grippers have been designed and validated to explore a suitable gripper for fatigue test of Ti-cement interface.

1.13 Figures

IN REGARD TO YOUR

Purchase Order No.: 16922-P
 Sales Order No.: 142727
 Item No.: 1
 Description: Ti 6Al-4V ELI
 Condition: Mill Finish, Annealed @ 1100-1450 Deg F +/-25 Deg F for 30 Min to 1 Hour
 Diameter: 0.164" (+/-0.002")
 Length: 144" (+6"-0")
 Specifications: ASTM F136-08, AMS 4930F, ASTM B348-08a GR 23, ISO 5832 PT 3 1996, M000105 Rev J, ASME SB348-04, ASTM F136-02a and Purchase Order
 Date: June 26, 2009
 Weight: 270 lbs.
 Heat / Lot No. : H82W
 Batch No.: TIW-205062

INGOT CHEMISTRY: (in Wt. %)

Element	Alpha Spec.	Spec. Min.	Spec. Max.	Top	Bottom
Al		5.50	6.50	5.95	5.99
C		0	0.08	0.007	0.007
Fe		0	0.25	0.19	0.17
H		0	0.012	0.0005	<0.0003
N		0	0.03	0.003	0.004
O		0	0.130	0.101	0.109
V		3.50	4.50	3.97	3.95
Y		0	0.005	<0.0005	<0.0005
Others each		0	0.10	<0.05	<0.05
Others total		0	0.40	<0.20	<0.20
Ti	BALANCE				
Beta transus				1763	1761

MECHANICAL TEST RESULTS:

	Ultimate Tensile Strength	Yield Strength	Elongation (4D)	Elongation (5D)	Reduction In Area
Specification:	125 ksi (min)	115 ksi (min)	10% (min)	10% (min)	25% (min)
Test Result 1:	159.5	142.8	23.2	20.4	47

Figure 1.1 Ti-6Al-4V material specification



Figure 1.2 Cobalt bone cement

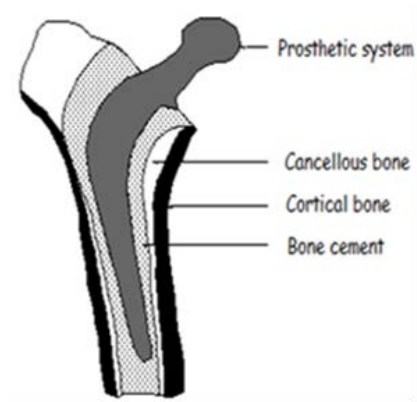


Figure 1.3 Schematic of cemented hip replacement

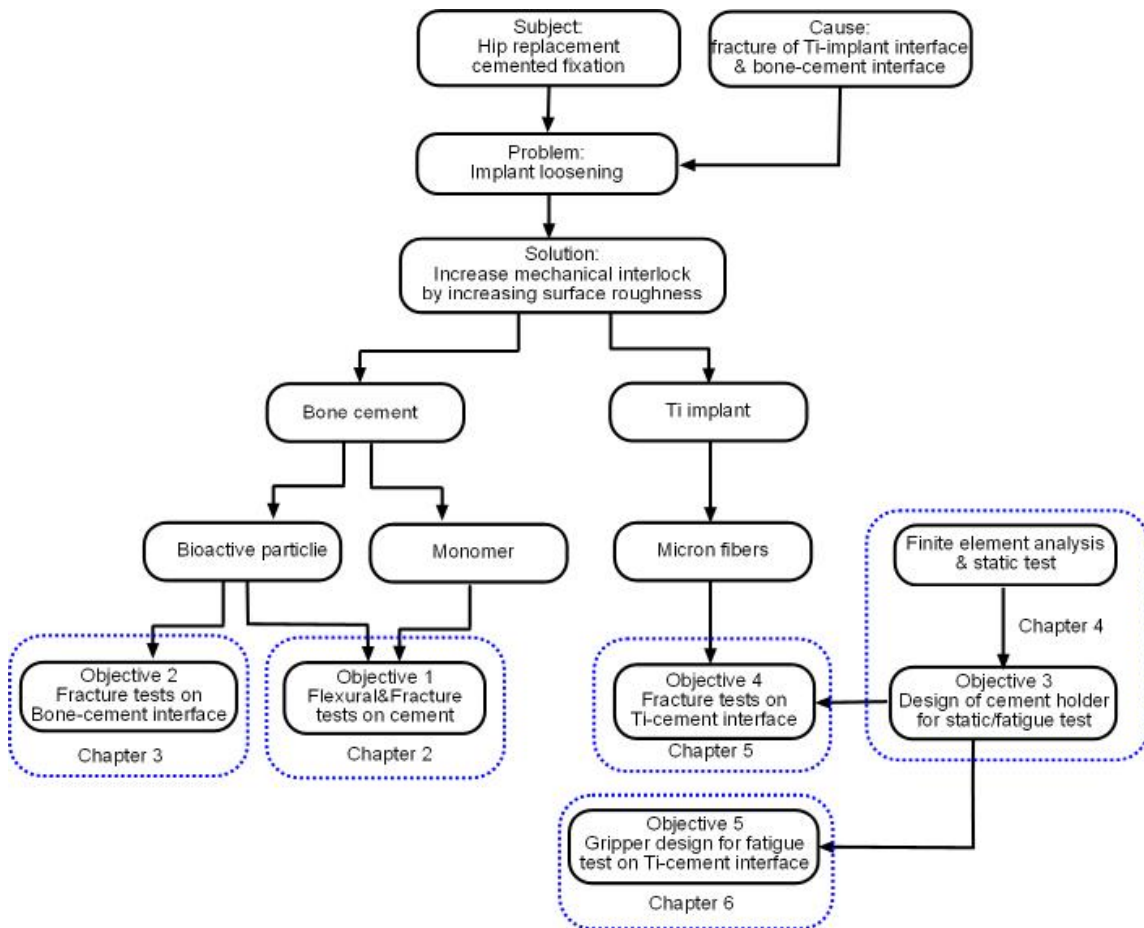


Figure 1.4 Flowchart of the study outline

CHAPTER 2

BIOACTIVE ADDITIVES AND FUNCTIONAL MONOMERS EFFECT ON PMMA BONE CEMENT: MECHANICAL PROPERTIES[26]

2.1 Summary

The most common bone cement material used clinically today for orthopedic surgeries is poly methyl methacrylate (PMMA). In general, poly Methyl MethAcrylate (PMMA) beads are added to MMA monomer with bead and monomer ratio of 2:1 to prepare the PMMA bone cement. Conventional PMMA bone cement has several mechanical and biological disadvantages. To overcome these disadvantages, researchers investigated several bioactive additives to PMMA bone cement, such as MgO, Hydroxyapatite (HAp), Chitosan (CS). Additionally, functional monomer, such as glycidyl methacrylate (GMA) was used in addition or substitution to MMA to enhance the properties of PMMA bone cement. A comparative study is required to evaluate the effect that different bio-additives and monomers have on the mechanical and biological performances of PMMA bone cement. The goal of this study is to determine the most suitable additives and alternative monomer for PMMA bone cement that can enhance the mechanical and biological performances of PMMA bone cement. Cobalt™ HV bone cement (referred as CBC), a commercial orthopedic bone cement, was used in this study as PMMA bone cement. MgO, hydroxyapatite (HAp), chitin (CT), chitosan (CS), Barium sulfate (BaSO₄) and Silica (SiO₂) were mixed with PMMA beads to prepare CBC-MgO, CBC-HAp, CBC-CT, CBC-CS, CBC-BaSO₄ and CBC-SiO₂ specimens. Additives included CBC were referred as composite specimen. CBC and composite specimens were further grouped according to the application of GMA as replacement of MMA monomer. Two groups of CBC and composite specimen were prepared. In the first group, CBC and composite specimens were prepared using MMA monomer only, referred as without GMA specimen. In the second group, CBC and composite specimens were prepared using GMA and MMA monomers, referred as with GMA specimen. There are three general research questions: (1) is there a significant difference in the mechanical

performances between CBC (control) and different composite specimens that contain GMA? (2) Is there a significant difference in the in the mechanical performances between CBC (control) and different composite specimens that do not contain GMA? And (3) is there a significant difference in the mechanical performances between specimens mixed with and without GMA? Elastic and fracture properties of different CBC and composite cements were calculated from three point bend experiments. This study found that flexural strength and fracture toughness of the CBC specimens that contain GMA is significantly greater than the flexural strengths of all other specimens that contain GMA. In contrast, flexural strength and fracture toughness of the CBC-SiO₂ specimens that do not contain GMA is significantly greater than the flexural strengths of all other specimens that contain GMA.

2.2 Background and specification

2.2.1 Introduction

Bone cement is used in various orthopedic surgeries. For example, during total hip replacement surgery bone cement is pressed between femoral stem and bone for providing the stability to the implant. The most common bone cement material used clinically today is poly(methyl methacrylate), or PMMA. PMMA cement is associated with several drawbacks that limit its efficacy (such as strong exothermic reactions, weak radiopacity and poor mechanical strength compare to host bone). The most challenging issue associated with commercially available PMMA bone cements such as Cobalt (Biomet, Inc.), Simplex (Stryker, Inc.), Palacos (Heraeus company) for the application of total joint replacement is their poor osseointegration (incorporation of the cement with surrounding bone tissues) [27]. Problems about infection and loosening of the bone cements at the bone-cement interface have been reported in literature [19]. One way to reduce loosening would be to increase mechanical interlock between bone and cement [15, 28]. This can be done by enhancing the surface roughness of the PMMA cement.

Several research groups found improvement of PMMA bone cements surface roughness properties by incorporating different kinds of nanoparticle additives to PMMA cement [19-23]. Ricker *et al.* [23] researched on the influence of nano MgO and BaSO₄ particle size additives on thermal, surface and cytocompatibility properties of PMMA cement. Authors reported that compared to PMMA with micro MgO and BaSO₄, PMMA with nano MgO and BaSO₄ reduced harmful exothermic reactions of PMMA during solidifications and increased radiopacity as well as increased osteoblast cell functions. Serbetci *et al.* [29] study found that addition of HA into low viscosity cement compositions caused an increase in compressive strength and compressive elastic modulus (addition of 7.7% (w/w) and 14.3% (w/w) HA); but caused a decrease in tensile strength. Tunney *et al.* [30] research found that incorporating chitosan into gentamicin-loaded Palacos® R bone cement for use in revision surgery has no clinical antimicrobial benefit and the detrimental effect on mechanical properties could adversely affect the longevity of the prosthetic joint. Hong *et al.* [31] study found improved glass transition temperature, surface hardness, flexural strength as well as impact strength of the silica-nanoparticle reinforced PMMA compared to PMMA alone. According to author's knowledge, there is no study conducted on evaluating the mechanical and biological functions of PMMA bone cement impregnated with chitin.

In general, PMMA beads were added to MMA monomer in a solid: liquid ratio of 2: 1 to prepare PMMA bone cement. Functional monomer in addition or substitution to MMA is required for the appropriate preparation of additive incorporated PMMA bone cement. Glycidyl methacrylate (GMA) has been investigated as a monomer for wide variety of additives incorporated bone cements [32-35] .

A comparative study is required to determine the effect that different bio-additives and functional monomers on the mechanical and biological properties of PMMA bone cement. The suitability of inclusion of the bioactive additives and functional monomers to overcome problems of conventional PMMA bone cement for the orthopedic applications requires complete understanding of the influence of the additives and monomers on the mechanical and biological properties compared to conventional PMMA

cements. Also such studies are required for the design of novel PMMA based composite bone cement.

ASTM 399 standard three point bend (3PB) flexural and fracture tests were conducted on each specimen. Flexural strength and bending modulus of each specimen will be calculated from 3PB flexural test. Fracture toughness and work of fracture of each specimen will be calculated from 3PB notched specimen.

2.2.2 Research questions

This study was conducted based on three research questions: (1) Is there a significant difference in the mechanical performances between CBC (control) and different composite specimens that contain GMA? (2) Is there a significant difference in the mechanical performances between CBC (control) and different composite specimens that do not contain GMA? And (3) is there a significant difference in the mechanical performances between specimens mixed with and without GMA?

2.2.3 Scope of work

The scope of work for this study was: (1) to determine the Flexural strength, σ_f , of CBC-MgO, CBC-HAp, CBC-CT, CBC-CS, CBC-BaSO₄ and CBC-SiO₂, (2) to determine the fracture toughness, K_{IC} , of CBC-MgO, CBC-HAp, CBC-CT, CBC-CS, CBC-BaSO₄ and CBC-SiO₂, (3) to determine the Flexural strength, σ_f , of CBC-GMA-MgO, CBC-GMA-HAp, CBC-GMA-CT, CBC-GMA-CS, CBC-GMA-BaSO₄ and CBC-GMA-SiO₂, (4) to determine the fracture toughness, K_{IC} , of CBC-GMA-MgO, CBC-GMA-HAp, CBC-GMA-CT, CBC-GMA-CS, CBC-GMA-BaSO₄ and CBC-GMA-SiO₂.

2.3 Material and method

2.3.1 Sample Preparation

Cobalt™ HV bone cement (CBC), a commercial orthopedic bone cement, was used in this research as PMMA bone cement. MgO, hydroxyapatite (HAp), chitin (CT), chitosan (CS), and Barium sulfate (BaSO₄) additives were used as the additives for the PMMA bone cements. Particulate size of additives used in this research is shown in Table 2.1.

Two groups of composite bone cements were prepared to find the effects of additives and GMA monomers on the mechanical and cytocompatibility properties of CBC. In the first group of composite cements, composite bone cements were prepared using MMA only i.e. without GMA. In the second group of composite bone cements were prepared with 90% MMA and 10% GMA. Group 1 specimen referred as CBC-MgO, CBC-HAp, CBC-CT, CBC-CS, CBC-BaSO₄ and CBC-SiO₂ specimens. Group 2 includes CBC-GMA-MgO, CBC-GMA-HAp, CBC-GMA-CT, CBC-GMA-CS, CBC-GMA-BaSO₄ and CBC- GMA-SiO₂ specimens.

According the Biomet, Inc. recommendation, 10 grams of poly Methyl MethAcrylate (PMMA) beads was as added to 5 ml of MMA monomer to prepare the CBC specimen. Selected 10 % (w/w) of the nanoparticulate additives were mixed with PMMA beads and then the mixer was added into the MMA and MMA-GMA monomers maintaining the same solid:liquid ratio of 2:1 for the preparation of group 1 and 2 samples, respectively. A mold was designed (using ProE solid modeling software, Figure 2.1(a)) and fabricated (using dimension elite 3D printer, Figure 2.1(b)) to cure the bone cement block of dimension 20×8×10 mm. The mold was made of tough ABS plastic. Glass slides were glued at the interior boundaries of the mold to avoid contact of PMMA with ABS plastic during curing. Sets of weights were placed at the top of the mold to provide total 60 kPa pressure (clinically achievable range[36]) to the bone cements samples during the curing process. The pressure was initiated at exactly three minutes

after the onset of mixing and was sustained throughout the curing period[37]. To prepare samples for flexural and fracture tests, (20×4×2) mm blocks were cut from a (20×8×10) mm block using Buehler isomet low speed cutter. To prepare the SENB test samples, a center notch was cut at the middle of the (20×4×2) mm cement samples using the Buehler isomet low speed cutter. A (4×.012×1/2) in. wafer blade was used for cutting the samples.

2.3.2 Experiments and analysis

Three-point bend (3PB) tests were conducted on bend and SENB specimens at room temperature using Evex SEM tensile tester (300 N load cell) as shown in Figure 2.2. The specimens were mounted on the 3PB holder in the test stage. All specimens were loaded with a loading rate equal to 3μm/s. The load and displacement were continuously recorded until the failure of the specimens using Evex nano-analysis software.

During the SENB test, an optimal microscope (Nikon SMZ 1000 stereomicroscope with DS-Fi-1 camera and U2 controller) was used to align the notch center of the specimen and the center of indenter round edge. Figure 2.3 shows alignment of the SENB specimen notch center with the center of the 3PB indenter on the Evex test stage. Nikon NIS BR visualization software was used for the alignment.

2.3.3 Data analysis

Several mechanical performance parameters were derived from the 3PB flexural and fracture tests on various bone cement bend specimens. From 3PB flexural test load and displacement data, stress and strain was calculated using $\sigma=3PS/2BW^2$ and $6dW/S^2$ equations, respectively, where P is the incremental load, d is the incremental deflection, S is the standard loading span for the 3PB specimen, B is the thickness, and W is the width of the specimen. Flexural strength, σ_f , was calculated using [38]: $\sigma_f=3P_{max}S/2BW^2$, where P_{max} is the ultimate load (force at failure). The value of bending modulus, E for a three-

point bend specimen was measured from the slope of the stress-strain curve at the elastic region. From SENB test, the maximum load, P_{max} , at the onset of crack extension from the notch tip was recorded from load-displacement data. P_{max} was used to calculate the mode I fracture toughness, K_{IC} using relationship [39] : $K_{IC}=P_{max}Sf(\alpha)/BW^{3/2}$, where α is the normalized initial crack length ($\alpha=a/W$) and $f(\alpha)$ is a dimensionless geometric function. The following equation can be used to calculate $f(\alpha)$ [39]:

$$f(a) = \frac{3(a)^{1/2}[1.99 - (a)(1-a) \times (2.15 - 3.93a + 2.7(a)^2)]}{2(1+2(a))(1-a)^{3/2}} \quad (2.1)$$

2.3.4 Statistical Analysis

A two-factor (additive and GMA) analysis of variance (ANOVA) with subsampling was performed in SAS version 9.1. No of cells on the substrate of interest were also analyzed statistically using ANOVA techniques. For all statistical analysis, statistical significance was considered as $P < 0.5$.

2.4 Results and Discussion

Figure 2.4 shows the typical stress-strain plot of bone cement samples found from the bend experiment. The stress-strain characteristics of all bone cement specimens exhibited a long elastic and inelastic region before catastrophic failure.

Table 2.2 shows the mean flexural strengths of various composite cements (MgO, hydroxyapatite, chitin, chitosan, BaSO₄ and SiO₂ incorporated CBC samples) with respect to the mean flexural strength of CBC. Figure 2.5 shows the line diagram of the effect of inclusion of GMA with MgO, hydroxyapatite, chitin, chitosan, BaSO₄ and SiO₂ incorporated CBC samples on flexural strength of those samples. In case of specimens with GMA, results show that (1) the mean flexural strength of the CBC specimens is significantly greater than the mean flexural strengths of all other specimens, (2) the mean

flexural strength of the SiO₂ specimens is significantly greater than the mean flexural strengths of the chitin and HA specimens, and (3) The mean flexural strengths of the chitosan and MgO specimens are significantly greater than the mean flexural strength of the chitin specimens. Rest of sample does not have significant differences. In case of specimens without GMA, results show that (1) the mean flexural strength of the SiO₂ specimens is significantly greater than the mean flexural strengths of all other specimens, (2) the mean flexural strength of the BaSO₄ specimens is significantly greater than the mean flexural strengths of the chitin and MgO specimens and (3) the mean flexural strength of the chitin specimens is significantly greater than the mean flexural strength of the MgO specimens. Rest of sample does not have significant differences.

Figure 2.6 compares the bending modulus of various composite cements (MgO, hydroxyapatite, chitin, chitosan, BaSO₄ and SiO₂ incorporated CBC samples) with respect to the bending modulus of CBC. Statistical analysis found that the influence of additive and GMA on the bending modulus of different samples is not significant (p=0.1108).

Figure 2.7 shows the typical load-displacement plot of a bone cement sample found from a SENB experiment. The load-displacement response of all specimens is characterized as initially elastic response, followed by a short inelastic region and then stable descending response.

Figure 2.8 compares the fracture toughness of various composite cements with respect to the fracture toughness of CBC. Also Figure 2.9 shows the effect of inclusion of GMA with MgO, hydroxyapatite, chitin, chitosan, BaSO₄ and SiO₂ incorporated CBC samples on fracture toughness of those samples. Results show that incorporation of additives with CBC influences the fracture toughness of the CBC. Furthermore, result shows that fracture toughness of GMA incorporated CBC samples were higher than the fracture toughness of CBC samples without GMA.

Table 2.3 shows the variation of the WOF of various composite cements with respect to the WOF of CBC for specimens with and without GMA. Figure 2.9 shows the line diagram of the effect of inclusion of GMA with different additives incorporated CBC samples on the WOF of those samples. In case of specimens with GMA, results show that the mean WOF of the CBC specimens is significantly greater than the mean flexural strengths of all other specimens. In case of specimens without GMA, results show that the mean WOF of the chitosan impregnated CBC specimens is significantly greater than the mean WOF of all other specimens.

2.5 Conclusion

This study found that flexural strength and fracture toughness of the CBC specimens that contain GMA is significantly greater than the flexural strengths of all other specimens that contain GMA. In contrast, flexural strength and fracture toughness of the CBC-SiO₂ specimens that do not contain GMA is significantly greater than the flexural strengths of all other specimens that do not contain GMA. Results also show that the influence of additive and GMA on the bending modulus of different samples is not significant ($p=0.1108$). The mean work of fracture of the chitosan impregnated CBC specimens is significantly greater than the mean WOF of all other specimens.

2.6 Figures

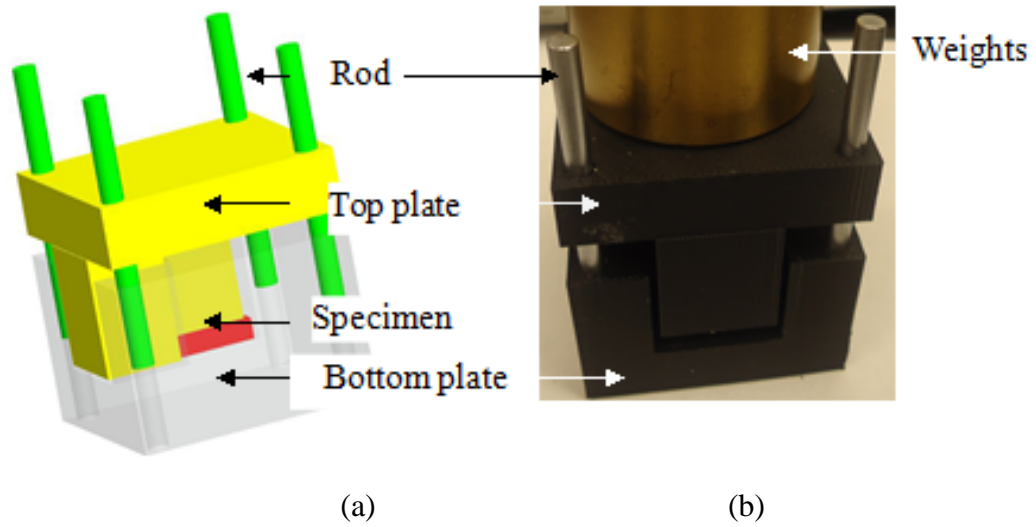


Figure 2.1 (a) 3D solid model and (b) fabricated mold using 3D printer used for the preparation of bone cement specimens

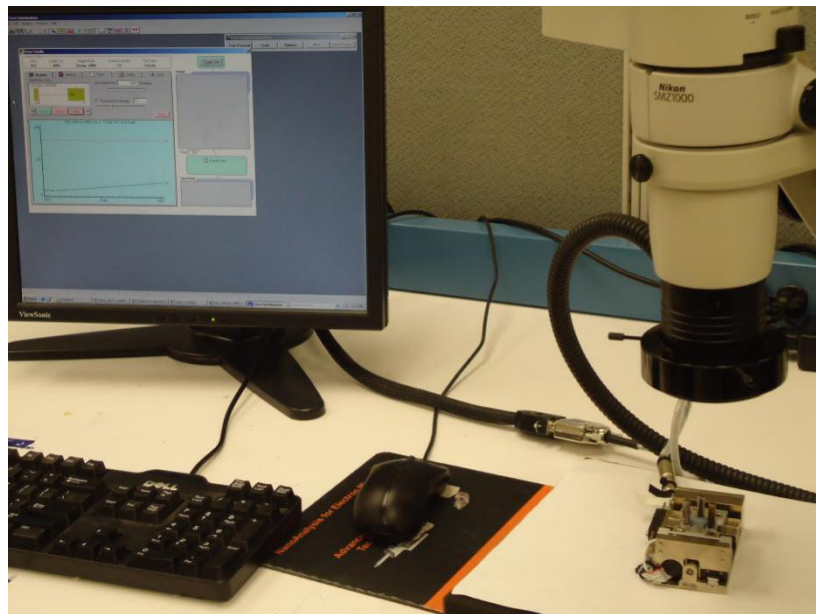


Figure 2.2 Experimental setup used for bone-cement interface study

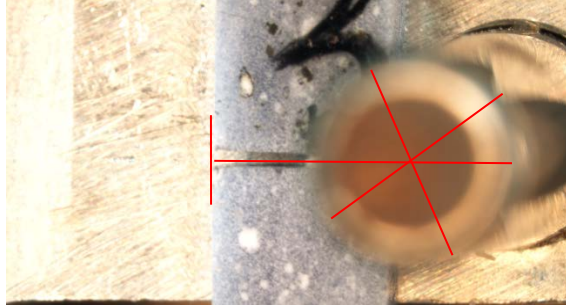


Figure 2.3 Alignment of SENB specimen on Evex tensile test stage

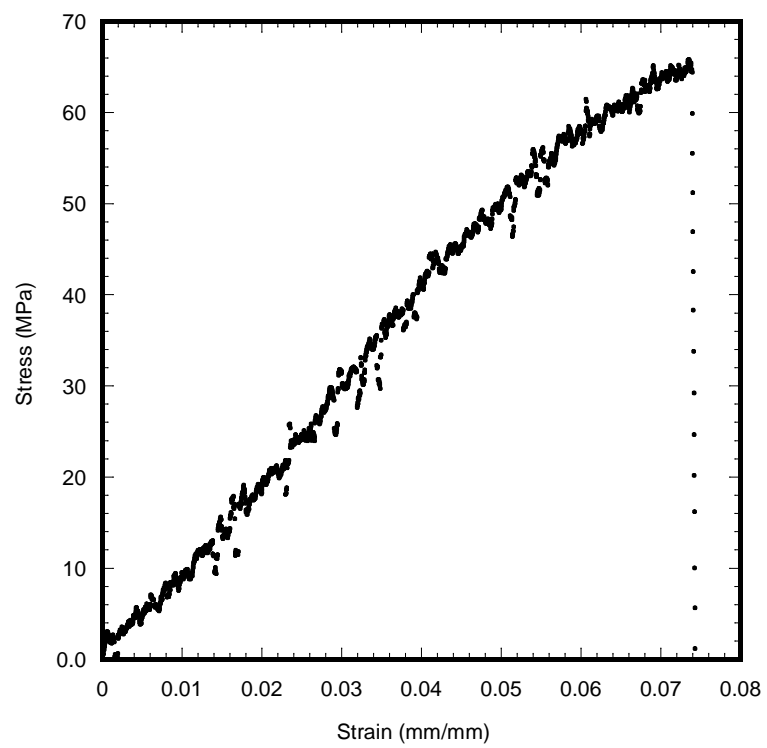


Figure 2.4 Stress-strain plot of composite bone cement made with hydroxyapatite and glycidyl methacrylate

With GMA:	Chitin	HA	BaSO ₄	Chitosan	MgO	SiO ₂	CBC
	51.89	55.09	58.73	61.62	64.63	66.69	86.7
	a	ab	abc	bc	bc	c	d
Without GMA:	Chitin	MgO	Chitosan	CBC	HA	BaSO ₄	SiO ₂
	47.27	60.52	63.06	63.74	65.93	69.6	82.56
	a	b	bc	bc	bc	c	d

Figure 2.5 Line diagram of the variation of flexural strength of various bone cement samples due to the variation of additives and GMA

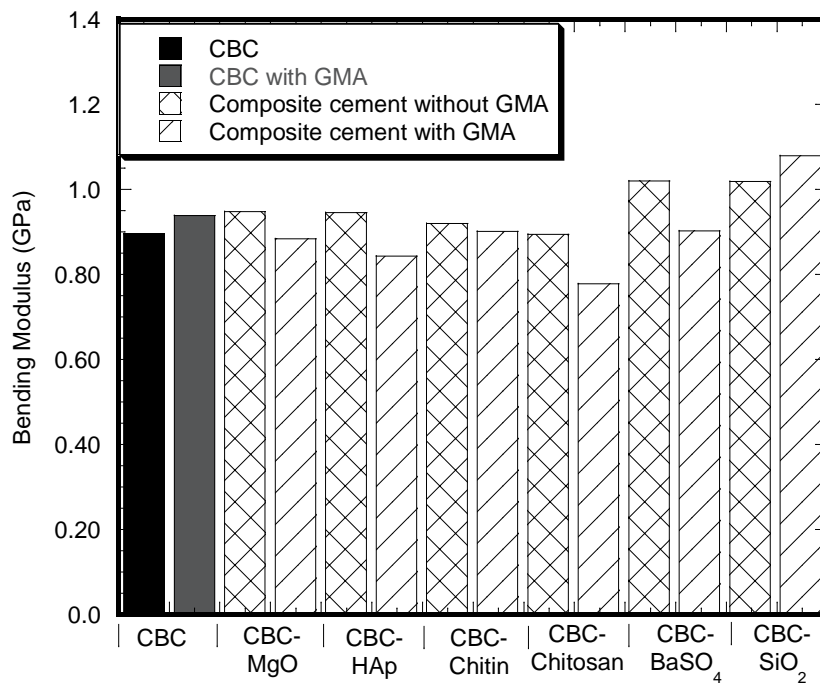


Figure 2.6 Variation of bending modulus of various bone cement samples due to the variation of additives and GMA

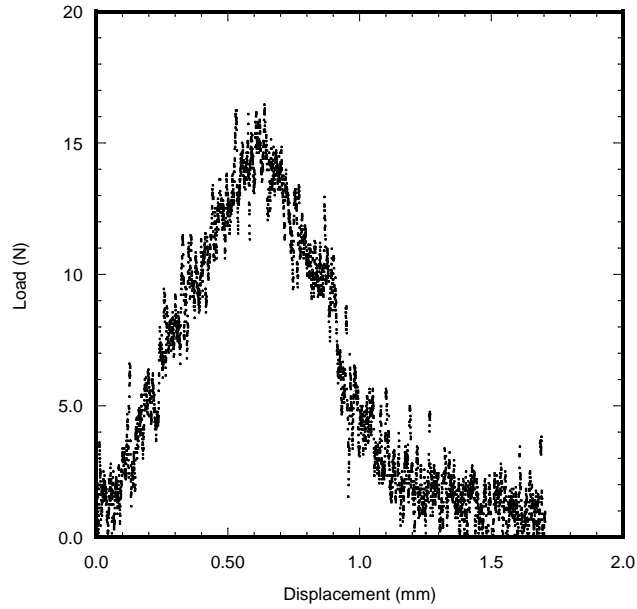


Figure 2.7 Load-displacement plot of composite bone cement made with hydroxyapatite and glycidyl methacrylate

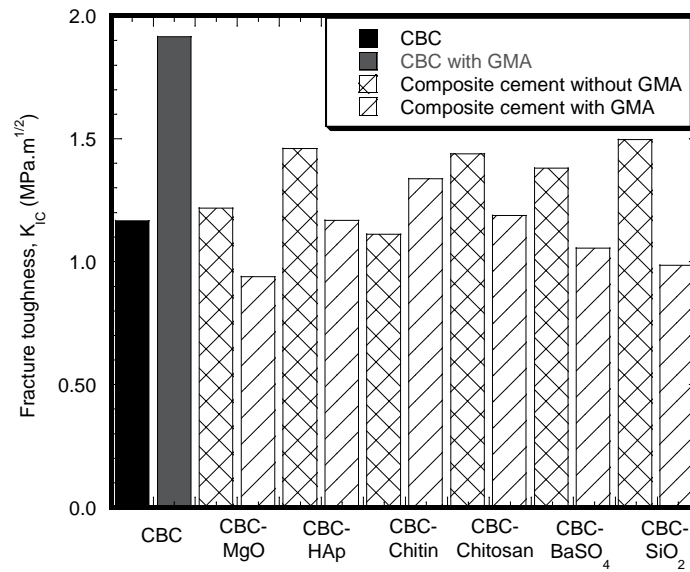


Figure 2.8 Variation of fracture toughness of various bone cement samples due to the variation of additives and GMA. Each additive incorporated CBC samples was grouped in two categories: samples without GMA and samples with GMA

With GMA:	SiO ₂	MgO	BaSO ₄	HA	Chitosan	Chitin	CBC
	138.71	186.79	238.62	262.32	279.85	454.78	687.18
	a	ab	b	b	b	c	d
Without GMA:	BaSO ₄	MgO	Chitin	SiO ₂	CBC	HA	Chitosan
	177.87	260.80	273.71	356.86	373.76	420.62	463.03
	a	ab	abc	bcd	cde	de	e

Figure 2.9 Line diagram of the variation of WOF of various bone cement samples due to the variation of additives and GMA

2.7 Tables

Table 2.1 Particulate size of PMMA additives

Bone cement additives	Average particulate size
MgO	36 μm
Hydroxyapatite	less than 200 nm
Chitin	N/A (fibrous)
Chitosan	less than 50 μm
BaSO ₄	0.85 μm ~1.05 μm
SiO ₂	less than 12 nm

Table 2.2 Variation of flexural strength of bone cements due to the variation of additives and alternative monomer

Additives	With GMA	Without GMA	p-value
CBC	86.70	63.74	<0.0001
CBC-MgO	64.63	60.52	0.3824
CBC-HA	55.09	65.93	0.0255
CBC-Chitin	51.89	47.27	0.2889
CBC-Chitosan	61.62	63.06	0.7726
CBC-BaSO ₄	58.73	69.60	0.0251
CBC-SiO ₂	66.69	82.56	0.0030
p-value	<0.0001	<0.0001	

Table 2.3 Variation of work of fracture of different kinds of CBC and composite cement specimens

Additive	With GMA	Without GMA	p-value
CBC	687.18 d	373.76 cde	<0.0001
CBC-MgO	186.79 ab	260.80 ab	0.1416
CBC-HA	262.32 b	420.62 de	0.0031
CBC-Chitin	454.78 c	273.71 abc	0.0009
CBC-Chitosan	279.85 b	463.03 e	0.0008
CBC-BaSO ₄	238.62 b	177.87 a	0.2247
CBC-SiO ₂	138.71 a	356.86 bcd	<0.0001
p-value	<0.0001	<0.0001	

CHAPTER 3

MICRO AND NANO MGO PARTICLES FOR THE IMPROVEMENT OF FRACTURE TOUGHNESS OF BONE-CEMENT INTERFACES[40]

3.1 Summary

The objective of this study was to determine whether inclusion of magnesium oxide (MgO) in micro and nanoparticulate forms in poly Methyl MethAcrylate (PMMA) cement has any influence on the fracture toughness of bone-cement interfaces. An interfacial fracture mechanics technique was used to compare the values of fracture toughness (K_{IC}) among bone-PMMA, bone-PMMA with micro MgO particles and bone-PMMA with nano MgO particles interfaces. This study found that the values of K_{IC} of bone-PMMA with micro MgO particles and bone-PMMA with nano MgO particles interfaces were significantly higher when compared to the values of K_{IC} of the bone-PMMA interface ($p < 0.0001$). The results indicated that the addition of the micro and nano MgO particles to PMMA improves the quality of bone-cement union.

3.2 Background and specification

3.2.1 Introduction

The fracture mechanics at the bone-cement interface is a critical issue for the cemented implant fixation. Several research groups reported improvement of PMMA cement strength, osteoblast cell growth, and surface roughness properties by incorporating additives such as MgO, hydroxyapatite, chitosan to PMMA[19, 20, 22]. The effects of these additives to PMMA on the mechanical strength of bone-PMMA interfaces are unknown. Our study found that MgO is one of the most suitable additives to PMMA, since osteoblast cell adhesion to the MgO included PMMA specimens is significantly higher than the cell adhesion to PMMA cement only specimens ($P < 0.001$) and no significant change of mechanical strength was observed due to the addition of

MgO to PMMA [26]. Ricker *et al.* [23] demonstrated that compared to micro particles, PMMA with nanoparticles of MgO reduced harmful exothermic reactions of PMMA during solidification and increased radiopacity. The suitability of incorporating micro and nanoparticles of MgO additives to PMMA for orthopedic applications necessitates estimating the K_{IC} of the respective bone-cement interfaces.

3.2.2 Research questions

This study was conducted based on two research questions: (1) Do micron MgO particles have any influence on the bonding strength between bone and cement? (2) Do nano size MgO particles have any influence on the bonding strength between bone and cement?

3.2.3 Scope of work

The scope of work for this study was: (1) to quantify elastic properties (Young's modulus and Poisson's ratio) of PMMA, PMMA with micro MgO particles and PMMA with nano MgO particles cements, (2) to determine the fracture toughness, K_{IC} , of bone-PMMA, bone-PMMA with micro MgO particles and bone-PMMA with nano MgO particles interfaces. Several researchers investigated the nominal strength of bone-PMMA interfaces where no defects were introduced in the test specimen [41, 42]. This study used a fracture mechanics technique developed by Wang and Agrawal [43], since it is more fundamental and meaningful estimation of interface fracture toughness of bone-cement than nominal strength measurement technique used by the previous authors. Cortical bone was used in place of trabecular bone [37] in the test specimen to reduce variability of test results due to bone porosity.

3.3 Material and method

3.3.1 Sample Preparation

Cobalt™ HV bone cement (CBC) (Biomet Inc., Warsaw, IN) was used as the PMMA cement. Micron MgO (Sial) and nanometer MgO (Aldrich) particles were purchased from Sigma-Aldrich. Their size distributions were characterized by Microtrac Inc. (Montgomeryville, PA) Nanotrac S3500 and Ultra instruments, respectively. According to manufacturer recommendations, CBC specimens were prepared by hand mixing 2.2 grams of PMMA powder with 1.1 ml of methyl methacrylate (MMA) monomer using powder: monomer ratio of 2:1. Ten wt% (0.22 gram) of micro and nano MgO particles were mixed with 1.98 grams of PMMA beads to prepare PMMA with micro MgO particles (mCBC) and PMMA with nano MgO particles (nCBC) cements, respectively. The mixers were added with 1.1 ml of MMA monomers maintaining the same powder: monomer ratio of 2:1 for the preparation of mCBC and nCBC samples. All samples were cured in a custom made mold (Figure 3.1) under 60 KPa pressure (clinically applied pressure during orthopedic surgeries [36]) to a block of size (22×12×4) mm. Each block was milled to a flat dumbbell-shaped specimen (Figure 3.2(a)) according to ASTM E855-90 standards [44]. This standard is suitable for the tensile test of a small size biological sample [45]. Specially, the length to width ratio at the gage section of the specimen is suitable for the tensile stage (accommodate maximum 24 mm long sample) and the microscope used in this study.

To prepare the bimaterial specimen (Figure 3.2(b)), a fresh bovine femur of unknown age and post mortem period was used. Cortical bone coupon was extracted from the mid-diaphysis of the femur. The coupon was milled to bars of size (22×12×2) mm using a constant cutting speed (1000 rev/min) and feed rate (50 mm/min) to ensure consistent bone surface roughness. The longitudinal axis of the bars was parallel to the longitudinal axis of the bone. The cement was packed and pressurized (60 KPa) on the one bar in the mold (Figure 3.1), which was a fabricated mold used for the preparation of cement and bone-cement specimens. The base plate contains (22×12×25) mm curing

chamber, which has front, back and top openings. Two ABS plastic blocks were used to cover the front and back sides of the chamber. A custom made clamp was used to restrict the side blocks movement. The top plate can slide freely to the curing chambers using 4 round rods. The top plate has (22×12×23) mm extruded block at the center that can close the top side of the curing chamber and apply pressure during curing. A set of weights were placed at the top plate to provide 60 KPa pressure[36]. Variable thickness of cement blocks (22×12×2~10 mm) were successfully cured using the mold. The mold was covered (12×6) mm at one of the side edges by a thin plastic sheet. The plastic sheet was accessed through the side blocks in the mold. The plastic sheet was pulled manually after curing. Bone-cement samples were carefully glued with two ABS plastic holders (made using Dimension 3D printer) by cyanoacrylate adhesive. The bone bars were maintained wet in saline during sample preparation.

3.3.2 Experiments and analysis

Tension tests were conducted on the flat dumbbell-shaped and wet bimaterial samples at room temperature and loading rate 0.01 mm/sec using Evex tensile stage (Evex Analytical Instruments Inc. , Princeton, NJ) as shown in Figure 3.2(a). Tension test on a flat dumbbell-shaped cement specimen was to measure the Young's modulus and Poisson's ratio of the cement specimen. Evex tensile stage, displacement variable reluctant transducer, and Nikon stereo microscope was used to record load, longitudinal displacement and transverse displacement during the experiment. Figure 3.2(b) is the schematic diagram and dimension of the flat dumbbell-shape specimen. The depth of the specimen is 4 mm. Figure 3.2(c) is the schematic diagram and dimension of the single edge sandwiched bone-cement specimen. The depth of the holder and specimen is 12 mm. Figure 3.2 (d) shows tension test setup for the measurement of the interface fracture toughness of bone-cement specimen. Young's modulus and Poisson's ratios, were calculated from three flat dumbbell-shaped CBC, mCBC, and nCBC samples in this study. Load was applied to the cement specimen below elastic limit to measure E and ν

values of cements. A displacement variable reluctant transducer (DVRT) (MicroStrain, Inc, Williston, VT) was secured along the gauge length (8~10 mm) to measure longitudinal displacement. A Nikon SMZ stereomicroscope (10X magnification) was used to sequentially capture images at 10 sec intervals to measure transverse displacement at the center of the gauge section. The load from Evex tensile stage, longitudinal displacement from DVRT and transverse displacement were continuously recorded using Evex nanoanalysis, National Instrument LabView 10.0 and Nikon NIS BR softwares, respectively. The slopes of longitudinal stress-longitudinal strain curves were used to calculate E . The transverse strain was calculated directly by dividing the transverse displacement by the initial width of the specimen. The transverse strains were calculated at 30 and 60 sec test times. Two values of ν were calculated from the ratio of the transverse strains and longitudinal strains for the corresponding test times.

The load and displacement were continuously recorded until the failure of the bi-material specimens. The K_{IC} values of bone-cement samples were calculated according to Wang and Agrawal [43] for a 0° loading angle. In short, K_{IC} of bone-cement interface were calculated using [43]:

$$K_{IC} = \frac{P_c \lambda^\nu Y \sqrt{\pi a}}{BW} \quad (3.1)$$

where K_{IC} is the mode I fracture toughness, P_c is the critical load that breaks the interface, and λ is a scale factor determined using:

$$\lambda = \sqrt{\frac{1-\alpha}{1-\beta}} \quad (3.2)$$

where α and β are Dundurs parameters, which estimate the elastic mismatch across the bi-materials interface [46], given by

$$\alpha = \frac{E_1(1-\nu_2^2) - E_2(1-\nu_1^2)}{E_1(1-\nu_2^2) + E_2(1-\nu_1^2)} \quad (3.3)$$

$$\beta = \frac{E_1(1-\nu_2 - 2\nu_2^2) - E_2(1-\nu_1 - \nu_1^2)}{2E_1(1-\nu_2^2) + 2E_2(1-\nu_1^2)}$$

where E_1 , E_2 , and ν_1 , ν_2 are elastic moduli and Poisson's ratios of the cement and bone, respectively. In Eq. (3.1), ψ is a correction factor determined using[43]:

$$\psi = e^{5.506(h/W)^{0.777}} \quad (3.4)$$

and Y is a shape function determined using [43]:

$$Y = \frac{1}{1-\rho} \sqrt{\frac{0.26 + 2.65 \frac{\rho}{1-\rho}}{1 + 0.55 \frac{\rho}{1-\rho} - 0.08 \left(\frac{\rho}{1-\rho}\right)^2}} \quad (3.5)$$

where $\rho = a/W$. Initial crack length, thickness and width of the specimen are given by a , B , and W , respectively.

The data were analyzed using SAS version 9.1 (SAS Institute, Inc., Cary, NC). The statistical analyses (1-way ANOVA) were performed on the means of the 3 groups for the p-values calculations of experimental parameters (E , ν , and K_{IC}). The groups were CBC, mCBC, and nCBC for E and ν , whereas the groups were bone-CBC, bone-mCBC, and bone-nCBC for K_{IC} . The average values of E and ν of cements, dimensions and fracture forces of bone-cement specimen were used for the calculation of K_{IC} . The values of E and ν for longitudinal bovine cortical bone were considered to be 20.4GPa [47] and 0.33 [48], respectively. For all statistical analysis, $p < 0.05$ was considered statistical significant.

3.4 Results and Discussion

Figure 3.3 and Table 3.1 show the particle size distributions and parameters of the micro and nano MgO particles, respectively. It is clear that the sizes of MgO particles are in the ranges of micron and nanometers, respectively. Figure 3.4(a) and (b) shows the linearity of longitudinal stress-longitudinal strain and transverse strain-longitudinal strain curves of CBC, mCBC and nCBC specimens, respectively. Figure 3.4(c) shows the variation of ν values of all tested cement samples. Plots show the two Poisson's ratio measurements for each sample at 30 sec and 60 sec test times. Table 3.2 reports the E and ν of cement samples. Results of the 1-way ANOVA indicate a significant difference for the experimental parameters (E and ν). It also shows that the variation of E is opposite to the variation of ν due to the incorporation of MgO particles to CBC. Decrease of E values and increase of ν was observed due to the addition of MgO particles to CBC. Figure 3.5 compares the load-displacement curves of various bone-cement specimens. The load-displacement response of bone-CBC specimens is characterized as elastic response and then sudden failure of the specimen without noticeable inelastic region. The maximum loads for the fracture of the bone-cement specimen were recorded for the calculation of the fracture toughness of bone-cement specimen. Table 3.3 presents statistics for K_{IC} of bone-cement specimens. Results show the K_{IC} (KPa.m^{1/2}) of bone-mCBC (25.05±5.00) and bone-nCBC (27.24±5.25) interfaces are significantly higher ($p < 0.0001$) when compared to the K_{IC} of the bone-CBC (9.71±2.23) interface.

This observed result is due to the differences in surface roughness, modulus, and residual stress at the interfaces of bone-cement with MgO in cement compared to that without MgO. Our separate study found that PMMA that contained micro or nano MgO particles possessed greater interface surface roughness as compared to those without MgO [49]. Increase of surface roughness led to a decrease of micro movement of cracks at the interface of bone-cement, and increased the load and elongation at the fracture (Figure 3.5). This behavior is consistent with published research [50-52], where it was found that increased surface roughness helped strengthen the interfacial mechanical

properties of bone-cement or implant-cement joints. Cements with micro or nano MgO particles exhibited lower elastic modulus (Table 3.2) and higher exothermic temperatures while curing [23] compared to those without MgO. The lower modulus cement can diminish local contact stresses at the bone-cement interface [53]. The residual stresses, which are caused by the exothermic temperature difference, can influence the fracture energies at the bone-cement interface [54]. The accumulation of stresses due to modulus and temperature differences at the interface of bone-cement with MgO can be lower than without MgO, resulted in higher K_{IC} for bone-cement with MgO than without MgO.

There is no publication on E and ν of CBC or K_{IC} of bone-CBC interface to compare our results. However, the value of E of CBC (740.41 ± 16.41 MPa) in this study is in close agreement with E of PMMA (674 MPa) found by Gillani *et al.* [55]. The value of K_{IC} of bone - CBC interface in this study was lower than that of Wang and Agrawal [43] (about $0.4 \text{ MPa}\cdot\text{m}^{1/2}$) between bovine cortical bone and Great Lakes Orthodontic's Splint dental cement ($E=2.5\text{GPa}$, $\nu=0.25$). This difference was reasonable since the cement used in this study is different from the test specimen used by Wang and Agrawal.

3.5 Conclusion

This study has demonstrated that the incorporation of micro and nanoparticles of MgO to PMMA enhanced the fracture toughness of bone-PMMA interfaces. This finding suggests that adding MgO particles to PMMA should be further investigated with respect to applications in total joint arthroplasty (TJA). The results of the mechanical properties (E , ν , K_{IC}) obtained from this study can be used in the finite element modeling of TJA. The optimal concentration of MgO particles to PMMA to enhance mechanical and biological performances is currently under investigation.

3.6 Figures

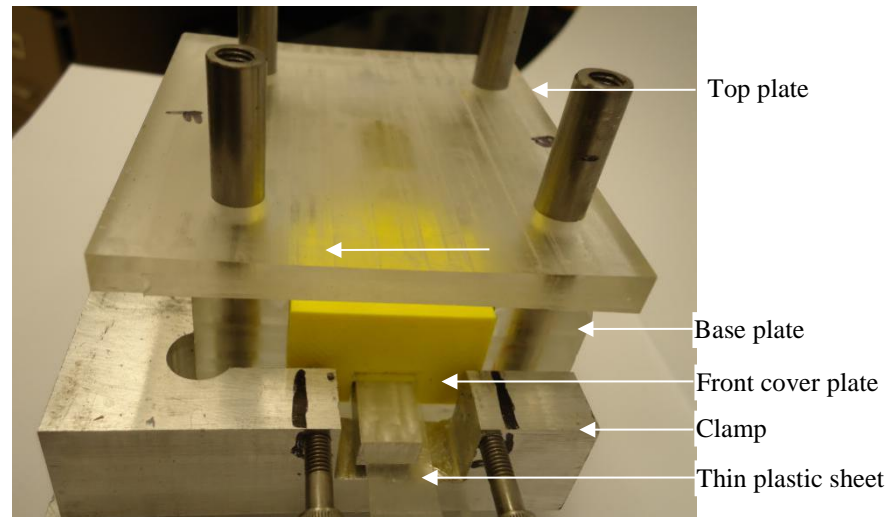


Figure 3.1 Fabricated mold used for the preparation of cement and bone-cement specimens

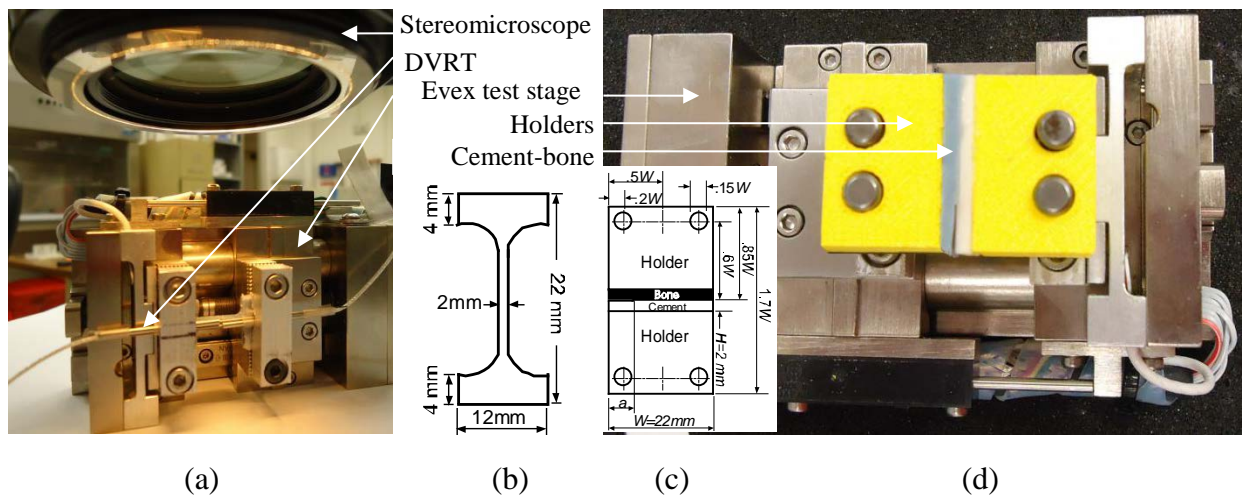
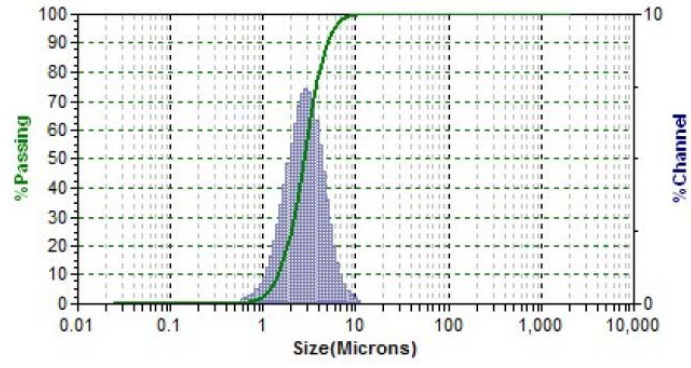
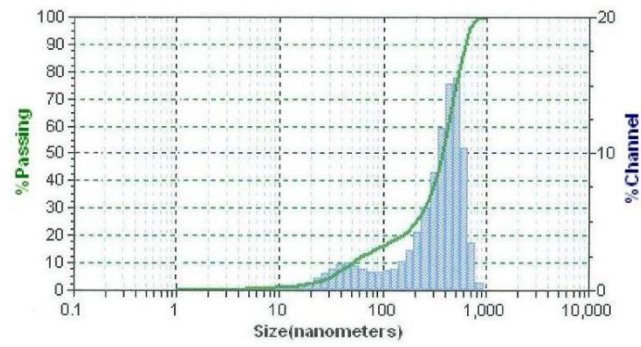


Figure 3.2 (a) Tension test on a flat dumbbell-shaped cement specimen to measure the Young's modulus and Poisson's ratio of the cement specimen, (b) schematic diagram and dimension of the flat dumbbell-shape specimen, (c) schematic diagram and dimension of the single edge sandwiched bone-cement specimen, and (d) tension test setup for the measurement of the interface fracture toughness of bone-cement specimen

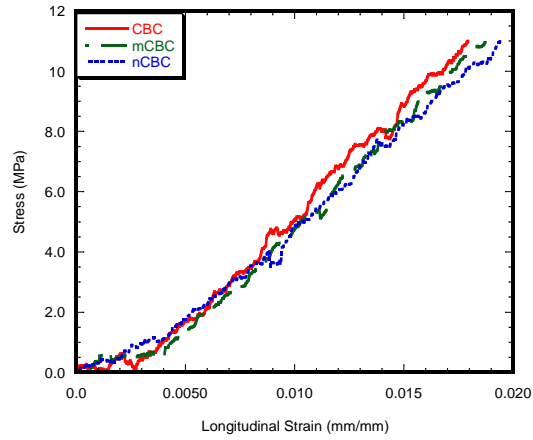


(a)

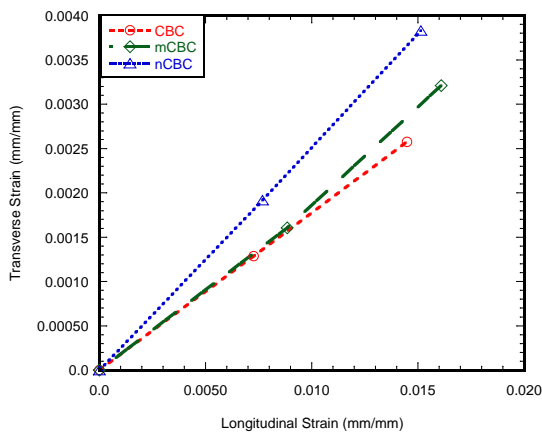


(b)

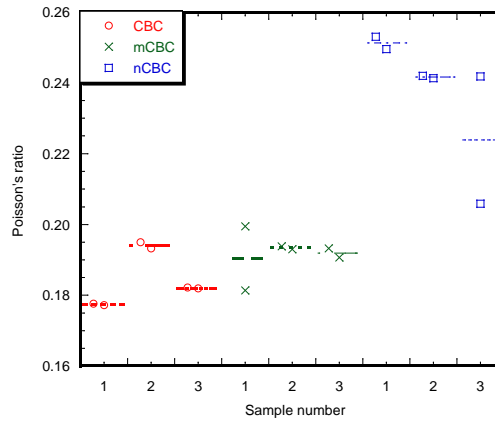
Figure 3.3 Particle-size distribution of the MgO powders: (a) micro size and (b) nano size



(a)



(b)



(c)

Figure 3.4 (a) Longitudinal stress vs. longitudinal strain plots of a CBC, mCBC and nCBC specimen (b) transverse strain vs. longitudinal strain plots of a CBC, mCBC and nCBC specimen calculated at 30 sec and 60 sec test time (c) dot plots of the Poisson's ratios of three CBC, mCBC and nCBC samples

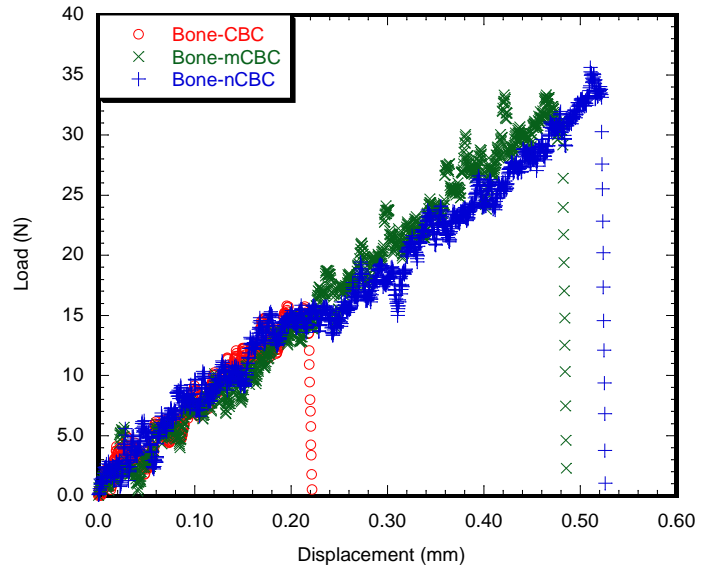


Figure 3.5 Load versus displacement graphs of (a) bone-CBC, (b) bone-mCBC and (c) bone-nCBC specimens

3.7 Tables

Table 3.1 Some particle-size parameters and specific surface of the two MgO powders used

Types	$D(10)^a$	Median size, $D(50)$	$D(90)^b$	Particle size volume average	Particle size number average	Particle size diameter average	Specific surface area (m^2/cc)
Micro	1.458 (μm)	2.778 (μm)	4.92 (μm)	3.04 (μm)	1.481 (μm)	2.417 (μm)	2.483
Nano	50 (nm)	382 (nm)	614 (nm)	362 (nm)	4.07 (nm)	116.2 (nm)	51.62

^a $D(10)$ means 10% of the powder particles are smaller than this value.

^b $D(90)$ means 90% of the powder particles are smaller than this value.

Table 3.2 Experimental parameters determined for the tensile test on the flat dumbbell-shaped cement CBC (n=3), mCBC (n=3) and nCBC (n=3) specimen

Experimental parameters	Specimen type			Significance test
	CBC	mCBC	nCBC	
Young's modulus, E_1 (Mpa)	740.41 \pm 16.41	696.93 \pm 16.83	662.02 \pm 19.37	p=0.0124
Poisson's ratio, ν_1	0.183 \pm 0.002	0.196 \pm 0.006	0.239 \pm 0.01	p<0.0001

Table 3.3 Descriptive statistics of the experimental single edge sandwiched bone-cement specimen data

Specimen type	No of specimen	Demension of the test specimen				Interface fracture toughness ($KPa.m^{1/2}$)			
		Width, W (mm)	Height, H (mm)	Thickness, B (mm)	Pre-crack length, a (mm)	average	St. dev.	Max.	Min.
Bone-CBC	6	21.48 \pm 0.04	1.77 \pm 0.16	11.94 \pm 0.03	5.38 \pm 0.15	9.71	2.23	12.85	6.87
Bone-mCBC	6	21.65 \pm 0.29	1.67 \pm 0.15	11.95 \pm 0.04	5.33 \pm 0.18	25.05	5.00	30.04	16.18
Bone-nCBC	6	21.59 \pm 0.13	1.69 \pm 0.10	11.98 \pm 0.07	5.27 \pm 0.15	27.24	5.25	35.24	20.71

CHAPTER 4

EFFECT OF SPECIMEN HOLDER ON STATIC AND FATIGUE TESTS ON TITANIUM/CEMENT INTERFACES

4.1 Summary

A tension or compression load was applied onto the Ti rod to test the fracture strength and fatigue life of Ti-cement interface under static and fatigue loadings, respectively. These tests are referred as static and fatigue in this study. A customized holder for the cement is required for the static and fatigue experiments, since the typical wedge, pneumatic, or hydraulic gripper are not suitable for static and fatigue tests on the fracture tests of bi-material samples. The objectives of this study are (1) to evaluate the effect of cement thickness on the fracture strength and fatigue life on Ti-cement union by finite element analysis; (2) to evaluate the effect of plastic cement holder and aluminum cement holder on fracture strength and fatigue life on Ti-cement union by experiment and finite element analysis. Ti-cement union model with 0.22 inch and 0.11 inch cement, Ti-cement-holder union with plastic and aluminum holders were created and validated using ANSYS in this study to develop a suitable specimen holder for static and fatigue tests. Experimental static tests of Ti-cement with both plastic and aluminum specimen holders were conducted as well. The result clearly showed that both plastic and aluminum holders can be used for static test whereas aluminum holder required much larger fracture load compared to the fracture load on plastic holder. Plastic holder is not suitable for fatigue test, because fatigue test required a stronger and more rigid holder such as aluminum.

4.2 Introduction

4.2.1 Static and fatigue tests specimen holder

The bond of an ideal implant with surrounding tissue must maintain certain fracture strength, σ_f , due to static loads (e.g. body weight, carry weight) as well as fatigue

life, N , due to cyclic loads (e.g. walking, running) [56]. Accordingly setup for fracture strength and fatigue life test, especially the specimen holder, was needed in this research. To the author's best understanding, there were no static and fatigue test gripper for bi-material samples that can be suitable for Test Resources Machines (UTM). Finite element analysis on customized specimen holder for static and fatigue tests were executed in this study to validate the application of the holder for these tests.

4.2.2 Factors that affect Ti-cement interface

Cement holder material is one of the main factors to consider before the cement holder design. The elastic properties of cement holder material may affect the fracture of Ti-cement interface under the static tests. If the cement holder is not strong enough, the damage will occur on the cement holder other than the Ti-cement interface. Cement thickness is also an important factor that affects Ti-cement interface. Fisher *et al.* [57] found out increasing cement mantle thickness caused substantial strain reductions in the distal cement which may eventually increase the fatigue life of a bone-implant system. In this study, effects of the cement holder material and cement thickness on the fracture of Ti-cement interface were investigated to determine a suitable cement holder design for the static and fatigue test of Ti-cement interface.

4.2.3 Motivation and Objectives

The objectives are (1) to evaluate the effect of cement thickness on the static and fatigue tests on Ti-cement union by finite element analysis; (2) to evaluate the effect of plastic cement holder and aluminum cement holder on static and fatigue tests on Ti-cement union by experiment and finite element analysis.

4.2.4 Scope of work

The scope of work for this study was: (1) to conduct static experiment test of Ti-cement with plastic holder and aluminum holder; (2) to determine the frictional coefficient of Ti-cement interface and cement-aluminum holder interface based on the experiment result; (3) to determine the cement thickness by comparing the deformation of Ti at Z axis, Von-Mises stress of cement and fatigue life of cement in models of Ti-cement union with 0.11 inch cement and 0.22 inch cement through ANSYS; (4) to evaluate the effect of the cement holder on the fracture of Ti-cement interface by comparing the deformation of Ti at Z axis, Von-Mises stress of cement and fatigue life of cement in models of Ti-cement-holder union with plastic and aluminum holder.

4.3 Material and Method

4.3.1 Static Test Experiment

Titanium (Ti) bars (6Al-4V ELI, ASTM B 348 standard, grade 23, biocompatible) of dimension (3" length and 3/8" diameter) were purchased from Titanium Metal Supply, Inc., Poway, CA. Cobalt™ HV bone cement (Biomet Inc., Warsaw, IN) [58] was used as the polymethyl methacrylate (PMMA) cement. The titanium rod is encapsulated by a 3D printed (Dimension elite 3D printer) [59] cylindrical holder or aluminum holder in order to cure the rod to the cement without being contaminated. Figure 4.1 shows these two holders for the production of titanium/cement sample. Static and fatigue tests were performed under static compression load condition using Test Resources 800LE4 universal testing machine (UTM) [60] to test the breaking load of the Ti-cement specimen under static test. During the test, Ti rod samples were fixed in the UTM. After that, the PMMA cement was prepared and poured into the bottom holder as shown in Figure 4.2(a). According to Biomet HV PMMA cement preparation protocol, PMMA cement was prepared by hand mixing 1.25 grams of PMMA powder with 0.625 ml of methyl methacrylate (MMA) monomer using powder: monomer ratio of 2:1. PMMA was

poured on top of the different titanium samples during doughy phase in the mold. A 60Kpa weight (clinically achievable range[36]) was placed onto the top of the cement and cured for 15 minutes (Figure 4.2(b)). After cured, the weight was taken out and run the static test to find σ_f of Ti/PMMA samples at strain rate 0.05 mm/sec. The maximum push-down force was determined and fracture strength was calculated by dividing the force at the point of failure by the surface area of the implant in contact with the cement. The surface area of the implant, A , was calculated using: $A = 2\pi rl$. r refers to the diameter of the Ti rod which is 3/8" and l is the height of the Ti implant surrounding with the cement, which can be obtained from the height of the cement.

4.3.2 Finite Element Analysis

Finite element 3D models of a cemented Ti rod and a cemented Ti rod with a cement holder surrounding the cement were created to study the debonding process of the stem-cement interface according to the dimension of the experimental model. The geometric FEA model was modeled and analyzed in ANSYS Workbench R15 [61]. The deformation of Ti rod at Z axis, Von-Mises stress and fatigue life of Ti-cement union with two different cement thicknesses and Ti-cement holder with two different materials were used to find the suitable cement holder thickness and material for static and fatigue tests. Deformation of Ti rod at Z axis was applied in the FEA model, which is the experimental displacement of Ti rod break from the cement in the direction normal to the Ti rod top surface. Von-Mises stress, also referred as equivalent tensile stress, is used to check whether the design will withstand a given load condition. This is accomplished by comparing the Von Mises stress to the material's yield stress. Fatigue test in this simulation was analyzed for the Ti-cement model as shown in Figure 4.2(a) under static structural analysis. Fatigue life suggests the number of cycles of fluctuating stress and strain that a material will sustain before failure occurs. Modified Goodman theory was used for the prediction of life in this study. Materials used in the analysis were titanium alloy (rod), PMMA cement, ABS plastic which corresponds to the 3D printer holder and

aluminum alloy which corresponds to the CNC machining holder in the experimental model. Table 4.1 shows the properties of materials used for FEA analysis. A normal stiffness factor of 1 was used for the Ti-PMMA interface, and ANSYS program controlled stiffness factor was used for PMMA-ABS plastic interface.

Huiskes [62] recommended a non-uniform thickness of cement ranging from 3 to 6mm (0.118inch to 0.236inch) for the proximal part of the canal. Ti-cement models with two different cement thicknesses 0.22 inch and 0.11 inch were created and analyzed in this study to evaluate the effect of cement thickness on the fracture of Ti-cement interface. It is assumed that there is no momentum of Ti rod and the outside surface of the cement is fully constrained. Figure 4.3(a) shows the meshed FE models of Ti with 0.22 inch cement with the element size of $0.8E-3$ meters. There were 174205nodes and 41501elements for Ti-cement model. For Ti-cement models, a compression load that corresponds to the failure load for the experimental model discussed in the section 4.2.1 was applied on the top surface of the Ti rod. Only displacement normal to the top surface was allowed for the Ti rod. The outside surface of the cement was constraint in all directions (Figure 4.6(a)).

Ti-cement-holder models with two different holder materials (plastic and aluminum) were created and analyzed to evaluate the effect of cement holder on the fracture of Ti-cement interface. Figure 4.3 (b) shows the Ti-cement-holder model with the element size of $3.0E-3$ meters, which has 8242.6nodes and 8002elements. It is also assumed that there is no momentum of Ti rod and the outside surface of the cement holder is fully constrained. Only displacement normal to the top surface was allowed for the Ti rod and the bottom surface of the cement holder was constraint in all direction (Figure 4.6(b)). A compression load that corresponds to the failure load for the experimental model discussed in the section 4.2.1 was applied to the top surface of the titanium rod. The contact of the plastic holder and the cement was set as bonded while the contacts of aluminum-cement interface and cement-Ti interface were both set as frictional contacts. The frictional coefficient would be analyzed based on the experiment

result of displacement-load plot. According to displacement-load plot, the maximum failure load was applied on to the Ti rod in the model of Ti-cement and multiple frictional coefficient of Ti-cement interface would be input to find out the corresponding displacement of Ti-rod. When the displacement of Ti rod in Ti-cement union obtained from the ANSYS simulation result matched the experiment result, the input frictional coefficient was set as the frictional coefficient of Ti-cement interface and used to continue test the frictional coefficient of aluminum-cement. Similarly, the load was applied onto the Ti rod of Ti-cement-holder model and multiple frictional coefficients of aluminum-cement were input to find out the displacement of Ti rod matching the corresponding experimental result.

4.4 Results and discussion

4.4.1 Control Experiment

Based on our observation of the force required to break the cement and Ti rod, the fracture load of Ti-cement interface with aluminum holder is much higher than the cement with plastic holder (Table 4.2). The most likely reason may be the difference of contact load applied from the holder to the cement. From Table 4.1, Young's modulus and shear modulus of ABS plastic is 2.2GPa and 0.81481, while aluminum has 71GPa for Young's Modulus and 26.692GPa for Shear Modulus. Thus it can be seen that ABS is more elastoplastic material and when the load applied on the Ti rod transferred to cement and the plastic holder, the holder deformed more. From load-displacement result for Ti-cement interface with the aluminum holder has a higher stiffness comparing the result with the plastic holder. The other possible reason to explain the different fracture load would be the different thermal conductivities between plastic and aluminum holders. As reported by Nuno, N. A., G. [63], time-temperature profiles of bone cement were sensitive to the mold material. Poor conductive material, like ABS plastic, decreases the cement heat transfer generating from PMMA cement curing and have higher thermal

expansion of the cement. The thermal expansion of the cement would have generated large residual stress which would affect the cement stress distributions at the stem cement interface [64]. Thus the difference of thermal expansion of the cement can be presented for different holders that may produce different the preload value during static tests. Figure 4.4(a) and (b) show the example of preload of the static test with plastic holder and the aluminum holder. Table 4.2 shows the observation of preload during the experiment. With the plastic holder, the maximum preload before the test was from 110N to 150N, which is around two times more than the preload of the test with the aluminum holder.

4.4.2 Finite Element Analysis

4.4.2.1 Mesh sensitivity analysis

Two models of Ti-cement union with the cement thickness 0.22 inch and 0.11 inch were designed. Different element size of 0.8mm, 0.9mm, 1mm and 2mm were analyzed since the nodes number with element size 0.8mm is the maximum nodes number the academic version of ANSYS R15 can go.

Table 4.5 shows life and stress at different element size. Figure 4.8 compares the fatigue life result with different meshing sizes. The mesh size at 0.8 mm is used due to the limitation of the ANSYS academic version.

Two models of Ti-cement union with the cement thickness 0.22 inch and 0.11 inch were created and analyzed with different element size of 2.8mm, 2.9mm, 3mm and 4mm. Table 4.6 shows convergence of FEA results. Figure 4.12 compares the fatigue life result with different meshing sizes. The mesh size at 3mm is used since the node number with 2.8mm mesh size is the maximum node number of ANSYS academic version.

4.4.2.2 Frictional coefficient for stem-cement and holder-cement interfaces

The frictional coefficients of Ti-cement and cement-aluminum were calculated based on the experiment load-displacement graph (Figure 4.5). The failure load of 241.14N has corresponding displacement 0.03002mm for plastic holder. In finite element analysis, the load of 241.14N was applied onto the Ti rod and frictional coefficients from 0 to 10 was tried to find the displacement of 0.03mm in Z axis. Table 4.3 showed the corresponding displacements for the frictional coefficients 4 to 10. From Figure 4.7(a), frictional coefficient 7 is the best fit for the coefficient because the Z-displacement of it 0.029703mm is the closest to the experimental displacement 0.3002. The frictional coefficient 7 was used in the continuing the frictional coefficient analysis of the aluminum holder and cement. Also, Ti-cement-aluminum holder was analyzed under the load similar to the load applied for the model of Ti-cement-plastic holder. From the original data recorded and the experiment load-displacement graph for aluminum holder (Figure 4.5), under 240N load the displacement of the cement from Ti was 0.016444mm. In the same way, the load of 240N was applied onto the Ti rod and a frictional coefficient from 10 to 50 was tried to find the deformation closest to 0.016444mm in Z axis. From the result shown in Table 4.4 and Figure 4.7(b), the frictional coefficient was found as 14 because the Z-displacement of it 0.01649 is the closest to the experimental displacement 0.016444.

4.4.2.3 FEA static and fatigue results for cement with different thickness

Since the objective of the FEA was to evaluate the effect of the cement thickness on the fracture performance of Ti-cement interface, constrains applied on the Ti-cement model should be the same for different cement thickness. A downward load of 240N that was closest to the minimum experimental failure load of the Ti-cement-holder model was applied to the top surface of the titanium rod. The frictional coefficients of Ti-cement were input as 7 and the static and fatigue simulations were performed.

For the 0.22 inch cement, the Ti rod slipped from the cement 0.008mm (Figure 4.9(a)) under the maximum Von-Mises stress of 8.8166 MPa and minimum Von-Mises stress of 0.042002 MPa (Figure 4.10(a)). The Ti rod has displacement of 0.0091945mm at Z-axis from the 0.11 inch cement, 0.001mm more than result of the thicker cement (Figure 4.9(b)). The Von-Mises stress of the 0.11 inch cement has the maximum value of 13.719MPa and the minimum value of 0.029224MPa (Figure 4.10(b)). The minimum fatigue life of the 0.22 inch cement is 1.6949×10^9 while the life of 0.11 inch cement is 2.5623×10^8 (Figure 4.11). Thus the Ti-cement with less cement would fracture faster, which is actually more suitable for observation in the experiment. However, if the cement is too thin, more loads would be transferred to the cement holder. In this case, the impact of the cement holder on the fracture of implant-cement interface will become stronger. Furthermore, a thin cement holder is also a big challenge for the experimental machining. Thus the 0.22 inch cement model was used to continue the analysis in the following analysis.

4.4.2.4 FEA static and fatigue results for plastic and aluminum holders

Based on the static experiment setup and the result, the bottom surface of the cement holder model was constraint in all direction (Figure 4.6(b)). A downward load of 240N that corresponds to the failure load for the experimental model was applied to the top surface of the titanium rod. The frictional coefficients of Ti-cement and cement-aluminum holder were input as 7 and 14 and the static and fatigue simulations were performed.

Figure 4.13 and Figure 4.14 show the displacement contour plot of the Ti-cement-holder union model and the cement only under the compressing load of 240N. Figure 4.15(a) & (b) display the Von-Mises stress contour plot of cement for both plastic and aluminum holders. For plastic holder, Ti rod has displacement of 0.030457mm at Z-axis from the cement (Figure 4.13(a)) under the minimum stress of 0.5967kPa and maximum

stress of 8.9579MPa (Figure 4.15(a)). Under the same load as plastic model, the deformation and the stress was lower for aluminum holder. The displacement of Ti rod was 0.01649mm (Figure 4.13(b)) under the minimum stress of 0.25352kPa and maximum stress of 7.5824 MPa (Figure 4.15(b)). Comparing the results of plastic holder and aluminum holder, Ti rod of the plastic holder transfer more load to the cement so the cement of the plastic holder has a displacement of 0.013529mm (Figure 4.14(a)), which is much larger than that of the cement with aluminum holder 0.0088523mm (Figure 4.14(b)). According to the analysis, the fracture strength of Ti-cement interface with plastic holder has a lower value than the result of Ti-cement in aluminum holder, which is consistent with the experiment result.

For plastic or aluminum holders, the cement holder has the minimum design life of the whole setup (Figure 4.16). Plastic holder has only 8242.6cycles (Figure 4.16(a)), which suggested the plastic holder is the most subject to damage. The cement in the plastic holder has the minimum design life of the 1.0443e8 cycles (Figure 4.17(a)). For the aluminum holder, the cement holder also has the minimum design life of the whole setup, 1e8 (Figure 4.16(b)), much more than the plastic holder. Moreover, the cement of the aluminum holder has a longer fatigue life of 2.9317e9 cycles (Figure 4.17(b)), around 20 times more than the cement of the plastic holder. Based on the result, plastic holder is not suitable for fatigue test. To avoid the cement holder damaged before the fracture of the Ti-cement interface, aluminum is the better option as the cement holder.

4.5 Conclusions

This study evaluated the effect of cement thickness and cement holder material on the fracture of Ti-cement interface by experiment and FEA. This result shows the following:

1. The cement thickness of 0.22 inch has more fracture strength and fatigue life than the cement thickness of 0.11 inch.

2. Either plastic or aluminum holder can be used for static test. However, the fracture strength result got from the model with plastic holder was much less than the result with aluminum holder. The plastic holder is the most subject to damage during the fatigue test. Thus plastic holder is not better than aluminum holder for fatigue test.

4.6 Figures

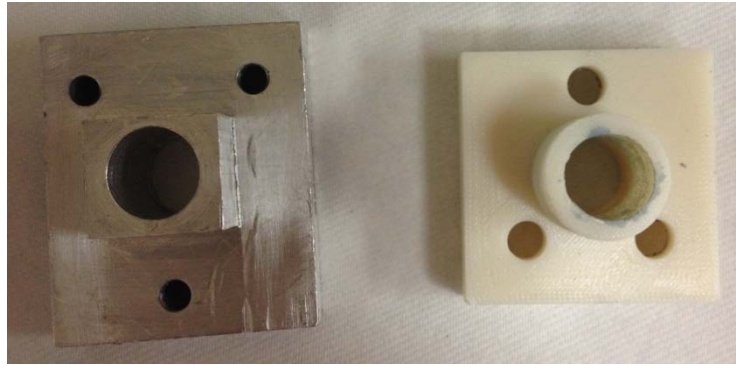


Figure 4.1 Fabricated aluminum and plastic cement holder using CNC machining and 3D printer



Figure 4.2 (a) Static tests setup in UTM before curing; (b) during curing

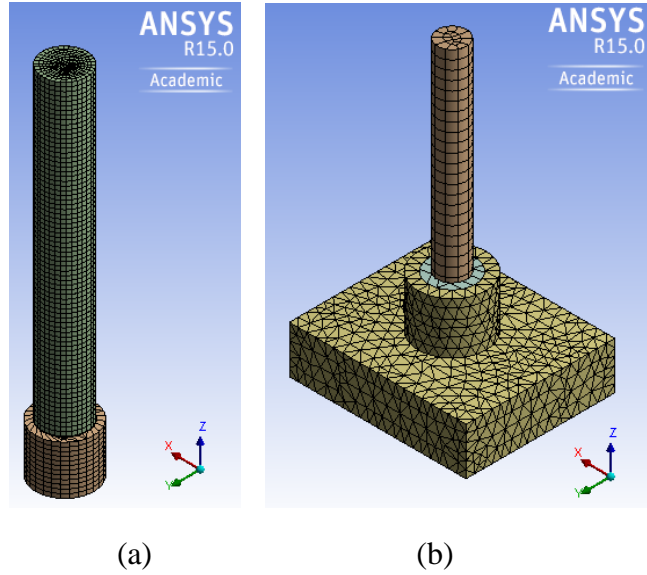


Figure 4.3 (a) Meshed model of Ti-cement samples with element size of 0.8mm; (b) meshed model of Ti-cement-holder samples with element size of 3mm

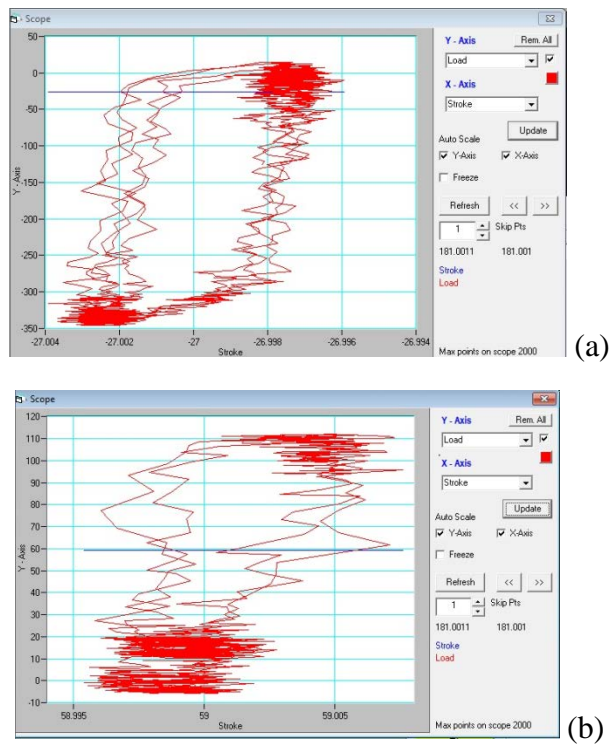


Figure 4.4 Load vs displacement plot before static test to determine preload caused by curing (a) with plastic holder; (b) with aluminum holder

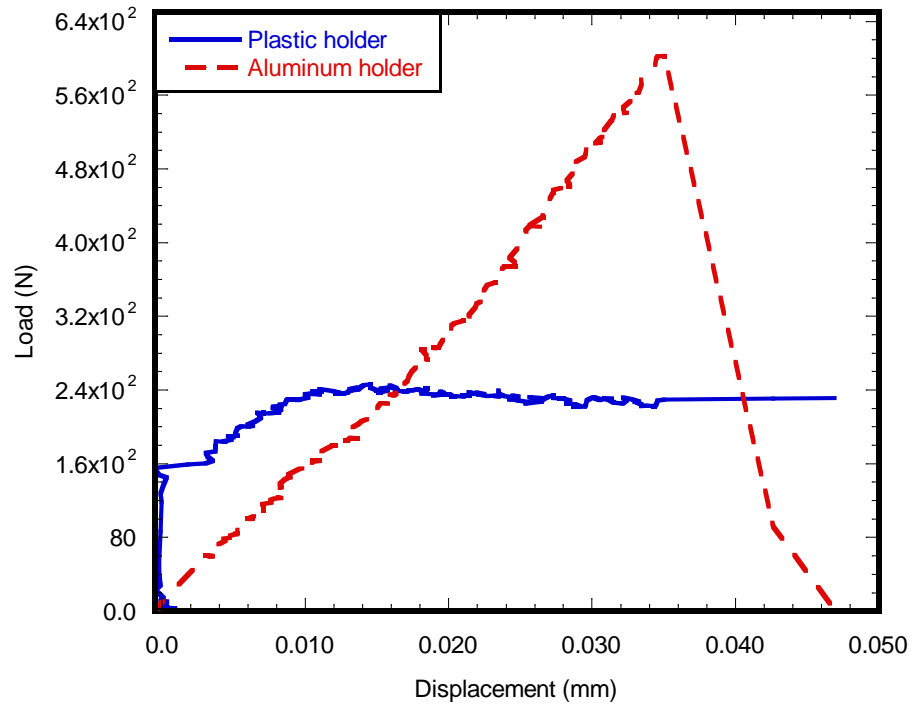


Figure 4.5 Load vs displacement plot for plastic and aluminum cement holder

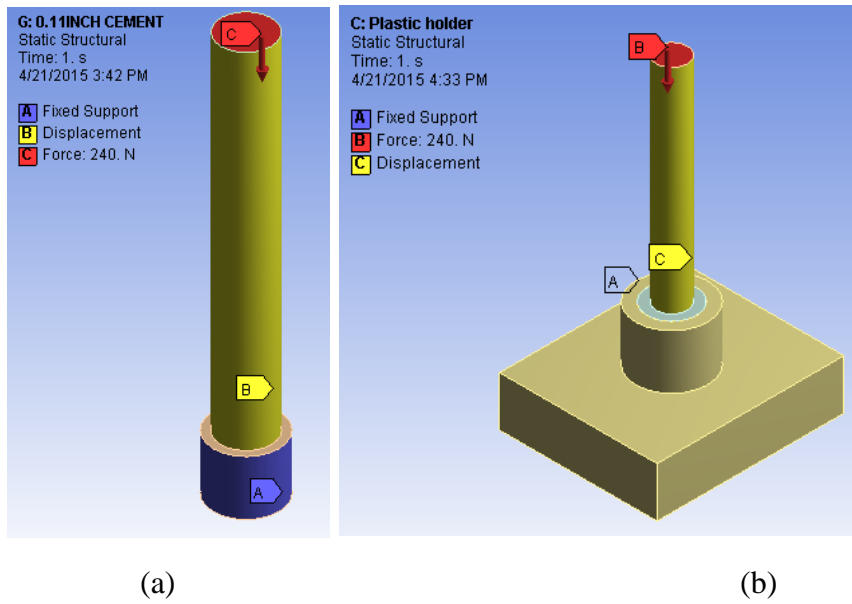


Figure 4.6 (a) Boundary conditions of the Ti-0.11 inch cement model; (b) boundary conditions of the Ti-cement-holder model

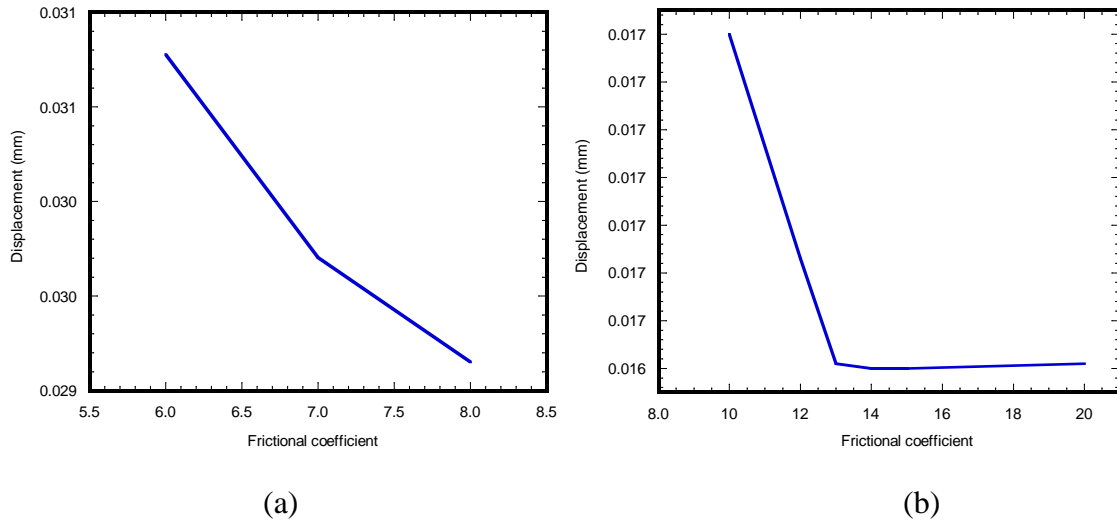


Figure 4.7(a) Frictional coefficient of Ti-cement interface (b) frictional coefficient of cement-aluminum interface

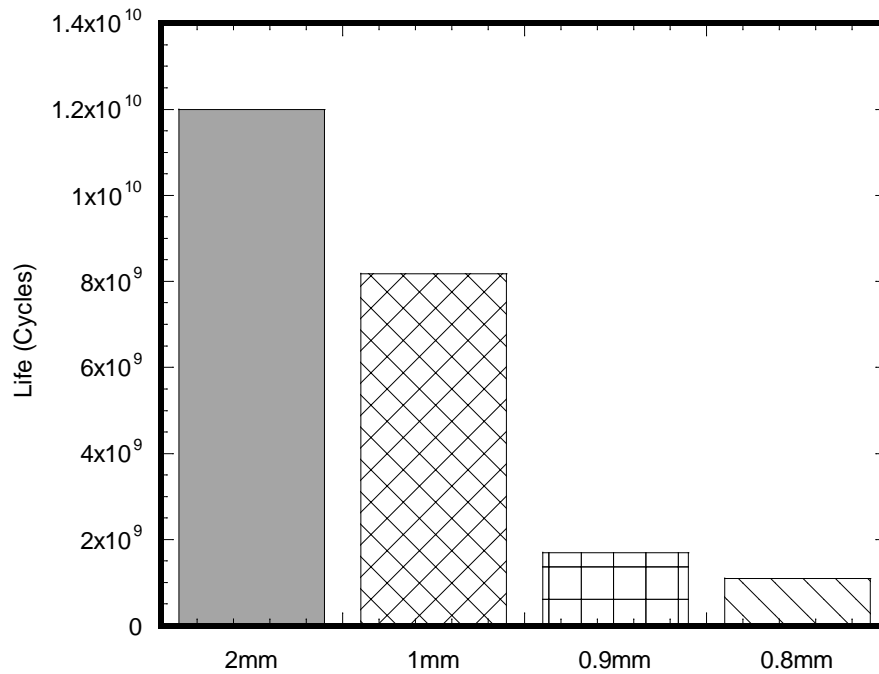
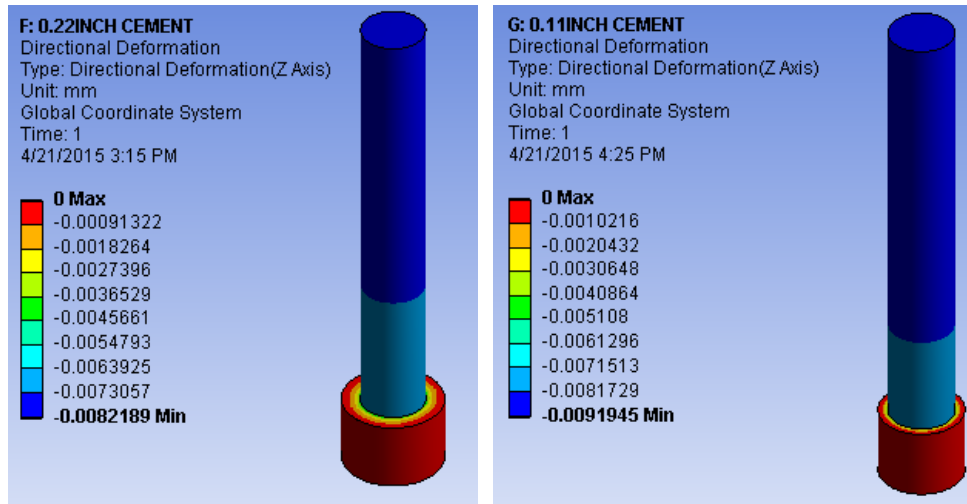


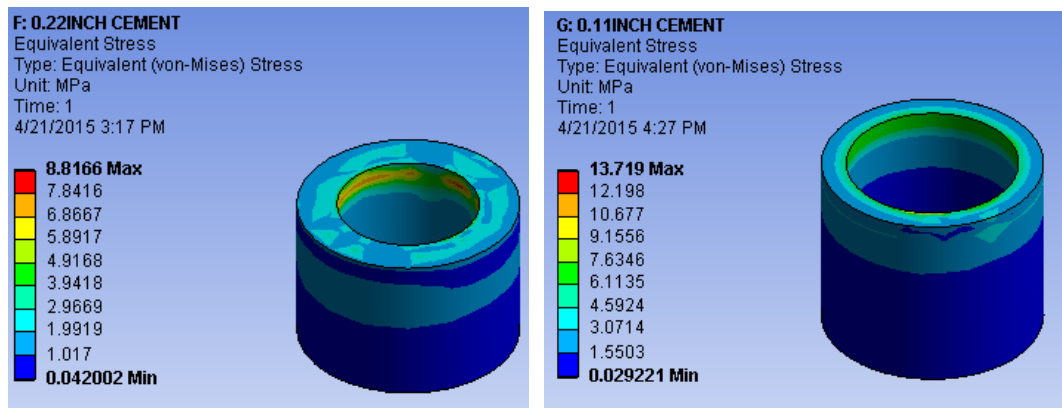
Figure 4.8 Ti-cement union fatigue life variations with different meshing element sizes



(a)

(b)

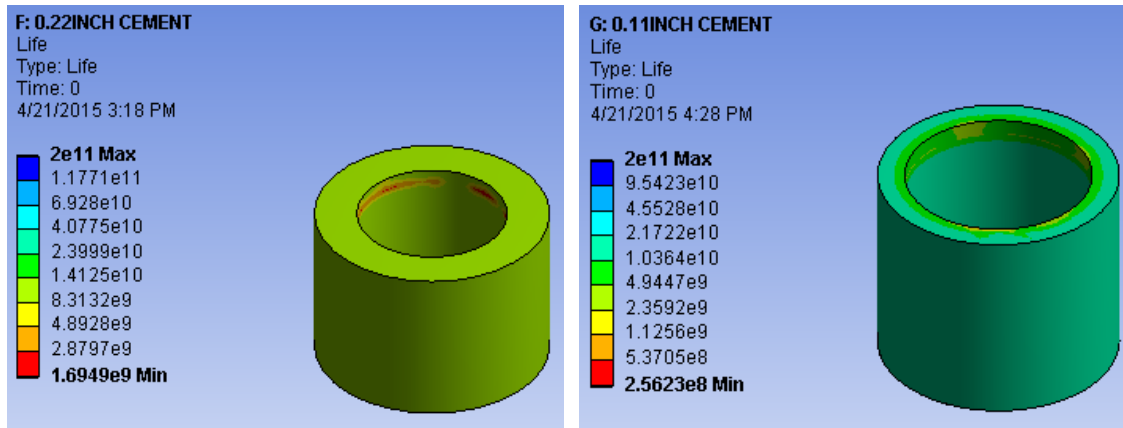
Figure 4.9 (a) Displacement contour plot in Z direction of Ti-0.22 inch cement interface;
 (b) displacement at Z axis contour plot of Ti-0.11 inch cement interface



(a)

(b)

Figure 4.10(a) Von-Mises stress contour plot of 0.22 inch cement; (b) Von-Mises stress contour plot of 0.11 inch cement



(a)

(b)

Figure 4.11 (a) Fatigue life contour plot of 0.22 inch cement; (b) fatigue life contour plot of 0.11 inch cement

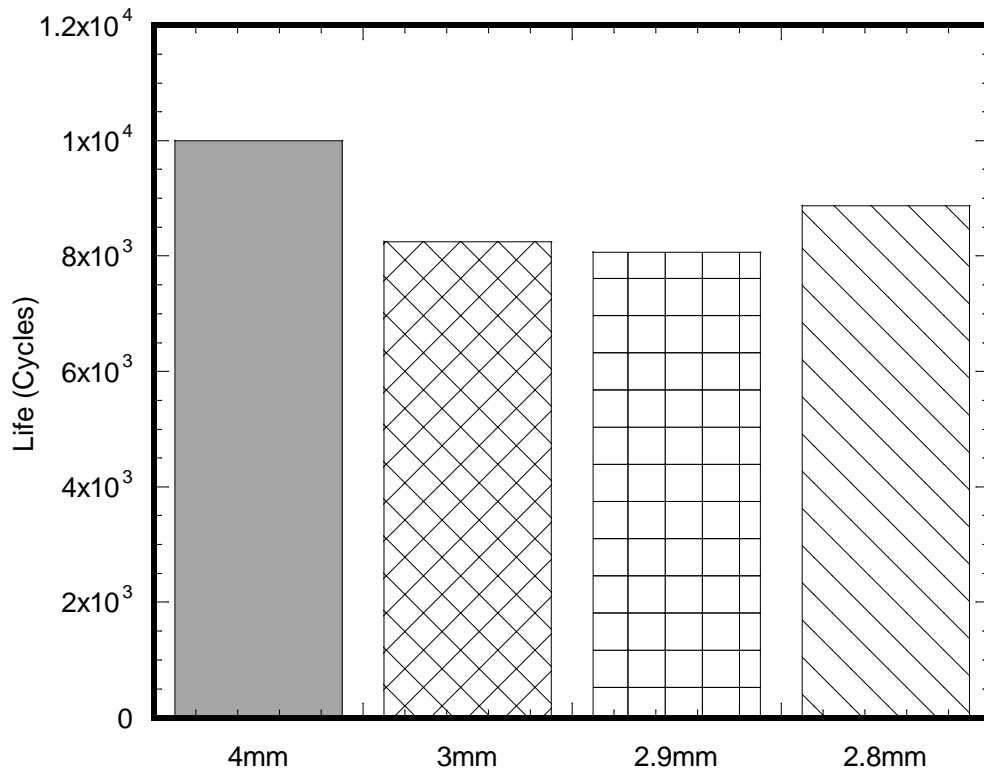
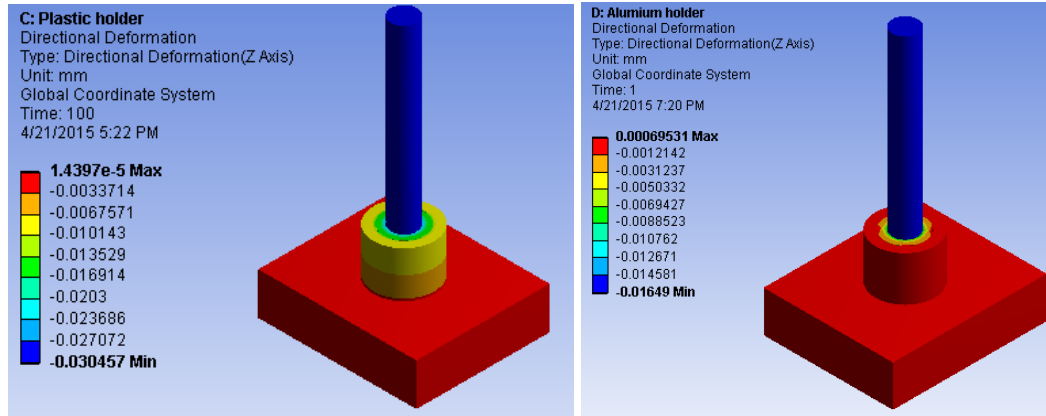


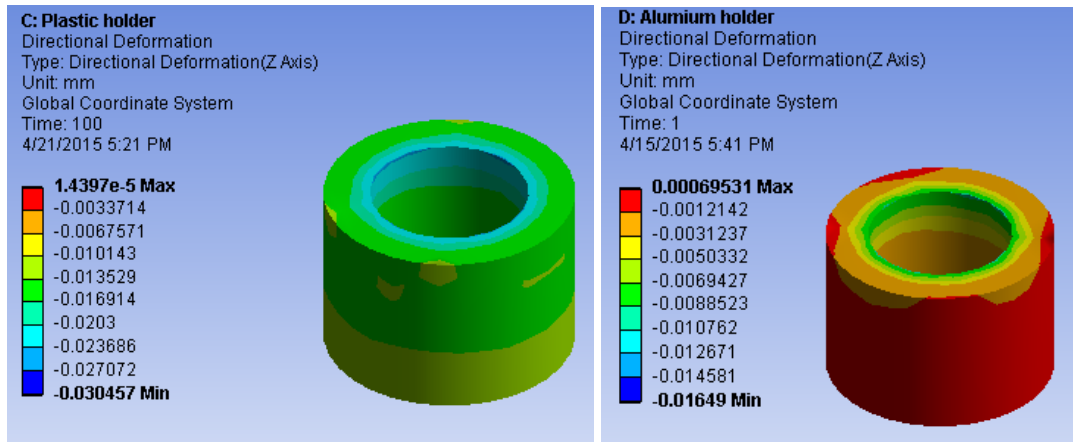
Figure 4.12 Ti-cement-holder union fatigue life variations with different meshing element sizes



(a)

(b)

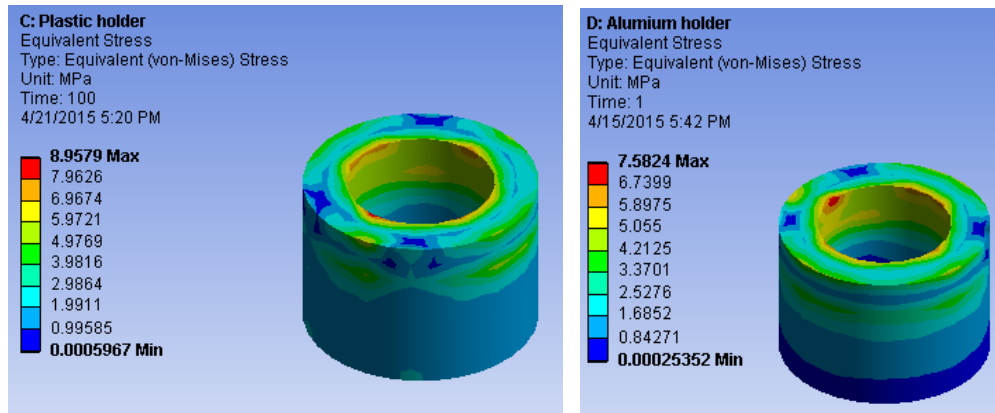
Figure 4.13(a) Displacement contour plot in Z direction of the Ti-cement-plastic holder union; (b) displacement contour plot in Z direction of the Ti-cement-plastic holder union



(a)

(b)

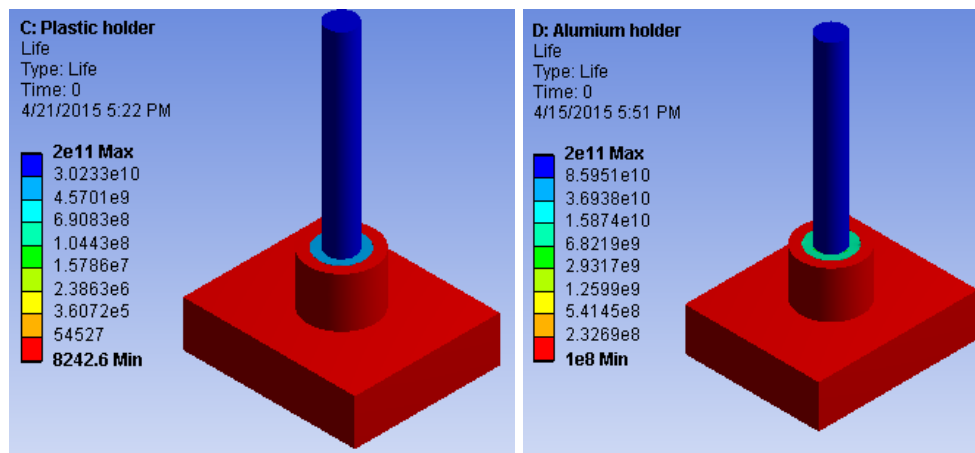
Figure 4.14(a) Displacement at Z axis contour plot of cement in plastic holder; (b) displacement at Z axis contour plot of cement in aluminum holder



(a)

(b)

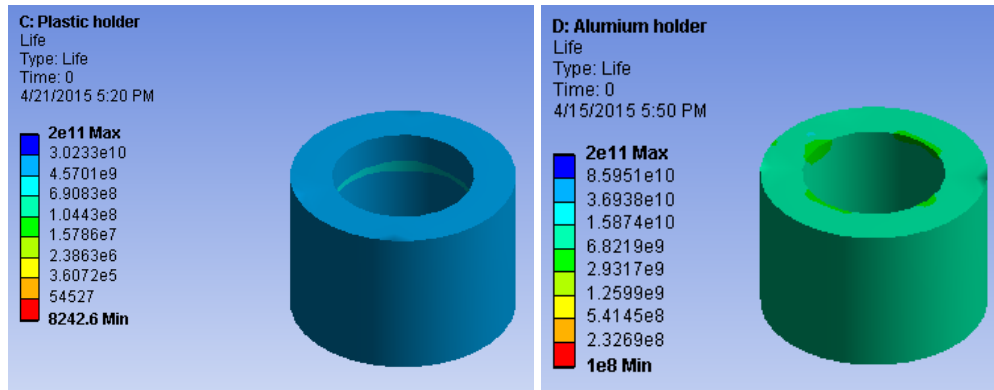
Figure 4.15 Von-Mises stress contour plot of cement in plastic holder; (b) Von-Mises stress contour plot of cement in aluminum holder



(a)

(b)

Figure 4.16(a) Fatigue life contour plot of the Ti-cement-plastic holder union; (b) fatigue life contour plot of the Ti-cement-aluminum holder union



(a)

(b)

Figure 4.17 (a) Fatigue life contour plot of the cement in plastic holder; (b) fatigue life contour plot of the cement in aluminum holder

4.7 Tables

Table 4.1 Material Properties used for the fatigue test of bi-material samples

Properties	Titanium alloy	PMMA Cement	ABS plastic	Aluminum
Young's Modulus (GPa)	116	3.3	2.2	71
Poisson's ratio	0.32	0.39	0.35	0.33
Shear Modulus (GPa)	43.939	1.1871	0.81481	26.692
Density (kg/m ³)	4507	1190	1040	2770
Compressive Ultimate Strength (MPa)	120	120	50	310
Compressive Yield Strength (MPa)	970	120	65	280
Tensile Ultimate Strength (MPa)	950	69	40	0
Tensile Yield Strength (MPa)	880	70	43	280

Table 4.2 Static result of plastic and aluminum fatigue holders (n=3)

Sample Groups	Method	L (mm)	Contact area (mm ²)	Fracture load (N)	Stiffness (KN/mm)	Fracture strength ((N/mm ²))	Max Preload (N)
1	Plastic specimen holder	10.233 ±0.170	307.344± 5.106	298.619 ±13.350	1.679± 0.041	0.967± 0.025	0~ 300
2	Aluminum specimen holder	10.208 ±0.035	306.810± 1.051	617.531 ± 168.483	7.893±2. 602	2.014± 0.485	0~110

Table 4.3 Relations between implant-cement contact frictional coefficient and displacement

Frictional Coefficient	6	7	8
Displacement (mm)	0.030777	0.029703	0.029151

Table 4.4 Relationship between cement-aluminum holder frictional coefficient and displacement

Frictional Coefficient	10	12	13	14	15	20	50
Displacement (mm)	0.01656	0.016513	0.016491	0.01649	0.01649	0.016491	0.016492

Table 4.5 Mesh sensitive of FEA model at the Ti-cement union

Element size (mm)	Element number	Node number	Life (cycles) (e9)	Alternating Stress (MPa)		
				Minimum Stress	Maximum Stress	Mean Stress
2	1274	6446	12	0.10	3.9442	2.0221
1	19855	84825	8.1803	0.041997	7.3591	3.7005
0.9	22944	98232	1.6949	0.042002	8.8166	4.4293
0.8	41501	174205	1.0942	0.05221	9.5146	4.7834

Table 4.6 Mesh sensitive of FEA model at Ti-cement-holder union

Element size (mm)	Element number	Node number	Life (cycles)	Alternating Stress (MPa)		
				Minimum Stress	Maximum Stress	Mean Stress
4	7490	3793	10000	6.5206e-16	46.569	23.2845
3	8002	8242.6	8242.6	0.0005967	8.9579	4.4792
2.9	8486	16557	8071.5	0.00062356	8.1314	4.0660
2.8	9360	17733	8869.7	0.00025352	7.5824	3.7913

CHAPTER 5

EFFECT OF FIBER ARCHITECTURE ON THE FRACTURE STENGTH OF IMPLANT/CEMENT INTERFACES

5.1 Summary

Titanium (Ti) and Ti-based alloys are widely used as implants for hard tissue repair. However, the optimal surface properties for ideal integration of Ti implant with native tissues have not yet been achieved. The goal of this study was to improve the bio-mechanical performances of titanium (Ti) implant by implant surface modification such as coating fiber on the implant surface. It is hypothesized that deposition of fiber with certain architecture can increase mechanical interlock of Ti surface which leads to the increment of in vitro bonding of Ti-cement interfaces. It is common facts in electrospun fibers technique the implant translation and rotation controls fiber deposition (i.e. topography) of the coating on Ti. In addition, fiber material and temperature controls the coating material (i.e. stiffness) and thickness. There is no study conducted for evaluating the fiber topography and thickness on the fracture strength of Ti-implant interface. The research objectives were to (1) test the fracture strength of Ti-cement with one round, two rounds and five rounds of PCL fiber under static load to determine the topography effect of electrospun fiber material on the Ti/PMMA cement interface; (2) test the fracture strength of Ti-cement with PCL fiber and PCL-PMMA fiber, with and without heating up Ti before fiber under static load to determine the stiffness effect of electrospun fiber material on the Ti/PMMA cement interface; (3) test the fracture strength of Ti-cement with PCL fiber and PCL-PMMA fiber, with and without heating up Ti before fiber under static load to determine the thickness effect of electrospun fiber material on the Ti/PMMA cement interface.

PCL and PCL-PMMA fibers coated on the Ti surfaces were produced by electrospinning technique using PCL-acetone fiber solution and PCL-PMMA-acetone solution respectively. Under static conditions, Ti/PMMA union specimen with and

without fiber were tested to determine the fracture strength. The result showed one round of PCL fiber has higher fracture strength than two rounds and five rounds of fiber, which suggested that more fibers on the surface were not beneficial to the fracture strength of Ti-cement interface. With PMMA added into the polymer fiber solution, the fracture strength of Ti-fiber-cement increased. Heating up the Ti implant to 50°C before coating PCL fiber can help the PCL fiber become stickier to the Ti implant which leads to the increasing of the fracture strength of Ti-cement interface. However, for PCL-PMMA fiber, heating up Ti implant before fiber doesn't help improve the quality of Ti-cement interface as PCL fiber.

5.2 Background and Specification

5.2.1 Joint replacement implant

In the United States of America, five types of total joint replacement devices are currently used with different bearing surfaces [65] which are: metal-on-polyethylene, ceramic-on-polyethylene, metal-on-metal, ceramic-on-ceramic and ceramic-on-metal. Various hip implants have different drawbacks and attributes. A more suitable hip implant device which decreases the number of risks is needed [66]. As an effective implant, it primarily should have enough surface energy and mechanical interlock [25, 67-69] to ensure long lasting bond between implant and cement interface. Specifically, the fracture strength, σ_f , under static loads (e.g. body weight, carry weight) of an implant with cement interface should maintain certain values.

Our previous research [40] has reported the addition of micron- or nano-size magnesium oxide particles to poly(methyl methacrylate) (PMMA) can increase the fracture toughness of bone-cement union through increasing the surface roughness. Based on this, we were assuming deposition of micron fibers on an implant, similar to incorporation of micron particles, can improve the fracture strength of implant-cement interfaces by changing micro architecture at the interface. Moreover fiber may increase

the bonding strength of metal/cement since the fiber increases surface area of the implant. In addition, research [11] showed that fiber could prevent imperfections of implants: toxic particles and loosening/breakage. In this chapter, the effect of micro-fiber on the bio-mechanical performances of conventional Ti implant was studied. To the best of the present author's knowledge, no study of this aspect has been published.

5.2.2 Electrospinning

Electrospinning technology is used to fabricate fiber with different morphologies and multidimensional structures and the fiber are widely applied in medical diagnosis, tissue engineering, replica molding and other applications [1]. By electrospinning, fibers have a high surface area to volume ratio, which have numerous engineering applications. The present study was based on the hypothesis that the differences of the surface properties at implant/cement interface due to incorporation of micro and sub-micron diameters fiber may have significant influence on the quality of implant-cement union. Polycaprolactone (PCL) is one kind of synthetic polyesters and compatible with many types of polymers. It is bio-compatible, cheap, easy to process, thus PCL is being considered as bio-materials for bone tissue [70], nerve tissue [71] and drug delivery systems [72]. Poly(methyl methacrylate) (PMMA) is known for its good mechanical as bone cement material. It is also being tested as a fiber material to achieve long-term mechanical stability after implantation [73].

5.2.3 Factors that affects the quality of fiber coatings on implant

Fiber architectures, particularly fiber topography, stiffness and thickness, may control the union between Ti and joint biomaterial. Firstly, topography of the fibers was varied with different quantities of the fibers. Different coating time can produce different amount of the fibers, which makes different fiber topography. The motor used to control the Ti rod moving forward and backward was also used to control the coating time. Ti

rod moving forward and backward was considered as one round of fibers in this study. Secondly, the stiffness of the fiber depends on the fiber solution material. PCL-acetone fibers and PCL-PMMA-acetone fibers were produced and studied in this research. Thirdly, the thickness of the fiber is basically referred to the width of the fibers. It may depend on the environment and Ti rod temperature, the electrospinning needle diameter and the fiber solution. Heating up Ti rod before fibers and without heating up were studied in this research.

5.2.4 Motivation and Objectives

Optimal surface properties for an ideal implant with native tissues have not yet been achieved. The objective of this thesis was to evaluate the fiber architecture (topography and thickness) that will improve the bio-mechanical performances of conventional Ti implant. In vitro static test has been conducted on Ti/biomaterial interfaces with different architecture of fiber.

5.2.5 Scope of Work

The scope of work was two-fold. Firstly the topography and diameter of the fiber coated on Ti implant was observed and measured. Secondly in vitro static tests were conducted on Ti/biomaterial interfaces to determine the effect of fiber with different architecture (topography, stiffness and thickness) on the fracture strength of cement-implant interface.

5.3 Material and Method

5.3.1 Material

Ti rods (6Al-4V ELI, ASTM B348 standard, grad 23, bio-compatible) were purchased with 3" length X 3/8" diameter from Titanium Metal Supply, Poway, CA, USA. There were three Ti rods for each group of experiment. All Ti rods samples were polished before experiment using a custom polishing disc (Figure 5.1 (a)) with the polishing pads around the disc. Buehler isomet low speed cutter (Figure 5.1(b)) at speed level 6 was used to provide and control the rotation speed of the Ti rods. Ti rods were fixed in a customized holder and provided voltage of 6.8V (Figure 5.1(c)). The polishing process was recommended by Buehler. There were three steps for polishing all the Ti rods. The first step was to polish using Buehler CarbiMet 2 Abrasive Discs for 5mins. During the first step polishing, 9um MetaDi Supreme Diamond Suspension was used to spray on the contact surface of the Ti rod and the polishing disc. The second step of polishing was using Ultra Pad with 0.05um MetaDi Supreme Diamond Suspension from Buehler for 5mins as well. The last step was using MicroCloth and MasterPrep Alumina for 5mins as well. After each step, Ti rods were cleaned by Ethanol.

PMMA bone cement was prepared by hand-mixing the PMMA powder and methyl methacrylate monomer (MMA) with the powder: monomer ratio of 2g: 1ml. PMMA powder was bought in a gas-permeable packet. It consists of 40 g powder (copolymer) with the following composition: 1) 33.42-33.86grams of Methylmethacrylate-methylacrylate copolymer with FD&C Blue No. 2 Aluminum Lake; 2) 0.20- 0.64grams of Benzoyl peroxide, hydrous 75%; 3) 5.94grams of Zirconium dioxide; 4) 0.84grams of Gentamicin sulfate (equivalent to 0.50g Gentamicin). MMA monomer was supplied in a flexible pouch. It consists of 20ml of liquid (monomer) with the following composition: 1) 18.424grams of Methylmethacrylate (stabilized with hydroquinone); 2) 0.376grams of N,N-dimethyl-p-toluidine.

PCL fiber solution was mixed with PCL beads which were purchased from Sigma-Aldrich (St Louis, MO, USA) and acetone. The amount of PCL beads and acetone were 0.5g and 6ml. SONIC Vitro-Cell (Figure 5.2(a)) was used to mix the PCL beads and acetone for 30minutes with the amplitude 60%. To produce PCL-PMMA fiber solution, firstly PMMA powder and acetone was mixed with the amount of 0.5g and 2ml using Sonicator for 2 hours and with the amplitude of 40%. Then PCL beads and acetone was mixed using the same ratio and process as making the PCL fiber solution. After that, the two kinds of solution was blended together using the stirring cell (Figure 5.2(b)) for 1hour with the speed of 85.

5.3.2 Fiber Deposition

The schematic process of electrospinning fiber is shown in Figure 5.3(a). A customized electrospinning unit (Figure 5.3(b)) was fabricated to deposit PCL and PCL-PMMA fiber on Ti rod on a motor. The solution was poured into a glass syringe in an infusion pump (PHD Ultra™; Harvard Apparatus, Holliston, MA, USA) (Figure 5.3(c)) for fiber production. Fiber was injected from the glass syringe via charged needle (23 G blunt needle, aluminum hub, 1" length). The needle was charged by a high-voltage power source (ES 30 series; Gamma High Voltage Research, Ormond Beach, FL, USA) (Figure 5.3(d)). The fiber was hitting onto a grounded custom-made drum collector and then collected on Ti rod on a motor. The Ti rod was mounted on a motor. A direct-current motor with the drum was mounted on a precision linear stage (model 426; Newport, Irvine, CA, USA). The motion of the stage was controlled by a linear actuator (LTA-HS; Newport) to produce fiber on the Ti rods. SMC Tool was used to control the Ti rods moving forward and backward. The fibers were collected on the Ti surface area. A carbon tape was attached around the rod. Carbon tapes were used for the visualization of fiber distribution and measurement of fiber dimension using a Nikon (Tokyo, Japan) SMZ stereo-microscope and a Hitachi (Tokyo, Japan) TM3000 scanning electron microscope (SEM), respectively.

5.3.3 Static Test

Six groups of samples were prepared and tested with the process shown in Figure 5.4. To evaluate the effect of the fiber topography on the fracture strength of Ti-cement interface, samples of group #1 to group #4 (without fiber, 1 round, 2 rounds and 5 rounds of fibers) were tested. Moving forward 35mm and backward 35mm controlled by SMC tool was referred as 1 round in this study. To evaluate the effect of the fiber thickness on the fracture strength of Ti-cement interface, fracture strength of group #1, group #5 and group #3 (heating up before PCL_acetone fiber and without heating), group #6 and group #7 (heating up before PCL-PMMA-acetone fiber and without heating), group #6 and group #3 (PCL-acetone fiber and PCL-PMMA-acetone fiber) were compared and analyzed. Since the melting point of PCL fiber is 60°C, Ti rods were only heated up to 50°C.

Topography and thickness of the produced fiber samples coated on the carbon tape were observed and measured using Hitachi TM 3000 scanning electron microscope (SEM). A custom made mold was used for the fabrication of the samples, as shown in Figure 5.5. Pulling static and fatigue tests were performed using Test Resources 800LE4 universal testing machine (UTM). During static test, Ti rod samples with or without fiber were fixed in the UTM, as shown in Figure 5.6(a). After that, prepare the PMMA cement and pour it into the bottom holder. A 60Kpa weight was placed onto the top of the cement and cured for 15 minutes (Figure 5.6(b)). After cured, the weight was taken out and run the static test to find σ_f of Ti/PMMA samples at strain rate 0.05 mm/sec. The maximum push-down force was determined and fracture strength was calculated by dividing the force at the point of failure by the surface area of the implant in contact with the cement. For all statistical analysis, statistical significance was considered as p-value<0.5.

5.4 Results

5.4.1 Relation between fiber topography and interface fracture strength

During the experiments of coating PCL-acetone fibers, it was found that the fiber were not sticky to the Ti rods and very easy to go to the bottom when pouring the cement into the bottom holder. Experiment has also shown that heating up the Ti rods makes the fiber stick to the Ti rods better. Fiber distribution was measured using Scanning electron microscope (SEM) images (Figure 5.7). The topography of 5rounds fibers is denser than that of 5rounds fiber. The result (Table 5.1) showed that the ranges of diameter of fibers and distances between two adjacent fibers are mainly micrometer ranges.

Figure 5.8 shows the typical load-displacement plot of Ti-cement samples found from the static experiment. The load-displacement characteristics of all Ti-cement specimens with or without fiber exhibited a long elastic and inelastic region before catastrophic failure. Table 5.2 shows the effect of deposition of fiber on the fracture load of Ti-cement interface. Specifically, the Ti-cement without fiber, which is called control experiment as well, has the fracture load of $298.619\text{N} \pm 13.350\text{N}$ (n=3) while with 1 round of fibers, the load increased to $345.896\text{N} \pm 46.157\text{N}$ (n=3). Figure 5.9 compares the fracture loads of Ti-cement and Ti-PCL fiber-cement with different amount of fiber, 1 round, 2 rounds and 5 rounds respectively. The fracture strength of Ti-cement interface with 1 round of fibers is much higher than the result with 2 rounds and 5 rounds coating fibers. Thus PCL-acetone fibers can increase the fracture strength of Ti-cement union, however, the effect is not significant (p-value=0.225).

5.4.2 Relation between fiber thickness and interface fracture strength

Figure 5.11 exhibits the typical load-displacement plot of Ti-cement samples with Ti heated up before coating PCL fiber. The load-displacement characteristics of all Ti-cement specimens with PCL-PMMA fiber exhibited less elastic comparing to the result

without fiber. Figure 5.12 and Table 5.3 shows the fracture strengths of Ti-cement interface with heating up Ti rods before coating fiber has around two times more than the result without heating up (p -value=0.0000183). According to the result, heating up the Ti before coating the PCL fiber can obviously help improve the quality of Ti implant.

Same as PCL fiber, heating up Ti rod before PCL-PMMA fiber was trying as well to test the fracture strength of Ti-cement union. Figure 5.12 and

Table 5.6 compares the fracture strengths of Ti-PCL-PMMA fiber-cement with and without heating up. Different from PCL only fiber, heating up the Ti-rods didn't help increase the fracture strength of Ti-PCL-PMMA fiber-cement (p =0.0544).

5.4.3 Relation between fiber stiffness and interface fracture strength

Fiber distribution was measured using Scanning electron microscope (SEM) images (Figure 5.10). The results (Table 5.4) show that the ranges of diameter of fibers and distances between two adjacent fibers are mainly micrometer ranges.

Figure 5.11 also demonstrates the typical load-displacement plot of Ti-cement samples with PCL-PMMA fiber coated. Only 1 round fiber was tested for PCL-PMMA fiber. Results show that with PMMA added, fiber can significantly increase the fracture strength of Ti-cement union. Table 5.5 shows the static result of Ti-cement without fiber, with PCL and PCL-PMMA fiber. Figure 5.12 compares the fracture strengths of Ti-cement, Ti-PCL fiber-cement and Ti-PCL-PMMA fiber-cement. The PCL-PMMA-acetone fibers has the larger fracture strength comparing to the result with PCL-acetone fibers (p =0.0399). With PMMA added into the fiber solution, the fracture load of Ti-cement union increases from 298.619 ± 13.350 ($n=3$) to 542.610 ± 26.449 ($n=3$), which is about two time increased.

5.5 Conclusions

This study evaluated the fracture strength of Ti-cement interface without and with fiber, PCL-fiber and PCL-PMMA fiber. This result shows the following:

1. Compared to Ti-cement without fiber, PCL fiber can slightly increase the fracture strength of Ti-cement interface. However, more fiber on the Ti surface makes the fracture strength of Ti-cement interface less. Heating up Ti before fiber can greatly help increase the fracture strength, which is around 2 times increasing.

2. Compared to Ti-PCL-cement, PCL-PMMA fiber can improve the quality of Ti implant much more than PCL fiber. The fracture strength of Ti-PCL-PMMA fiber-cement is around 2 times as the value of Ti-cement without fiber. Different from PCL fiber, heating up Ti before fiber doesn't help increase the Ti-cement interface.

5.6 Figures

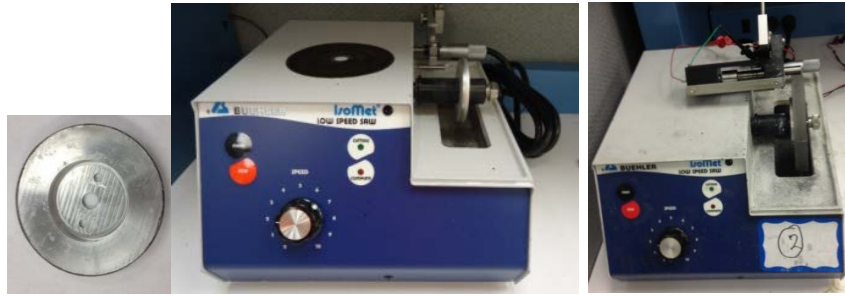


Figure 5.1 (a) Customized made dis used for polishing round sample using Buehler isomet low speed cutter; (b) Buehler isomet low speed cutter; (c) polishing setup



Figure 5.2 (a) Sonic vitro & sonication device used for sonication; (b) Corning heating & magnetic stirring cell

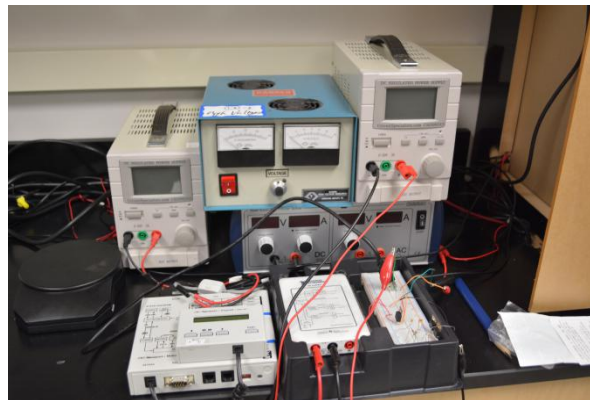
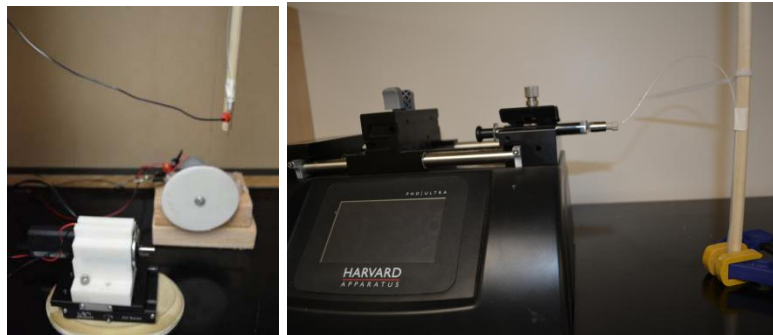
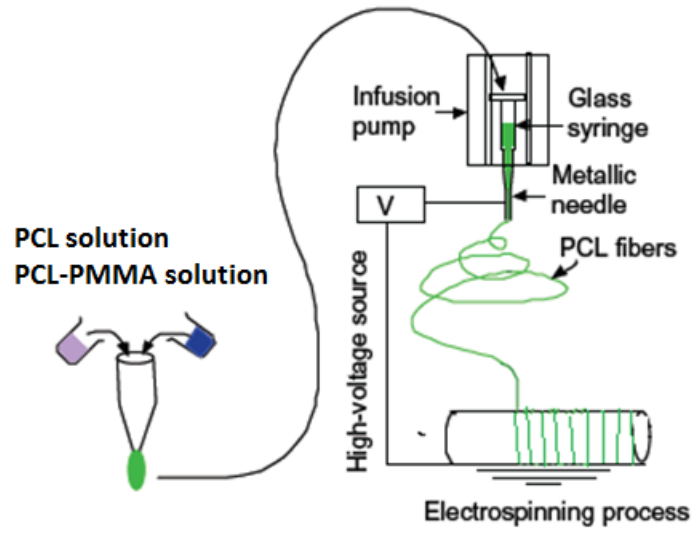


Figure 5.3 (a) Schematic representation of the electrospinning process; (b) electrospinning unit; (c) infusion pump; (d) power supplies

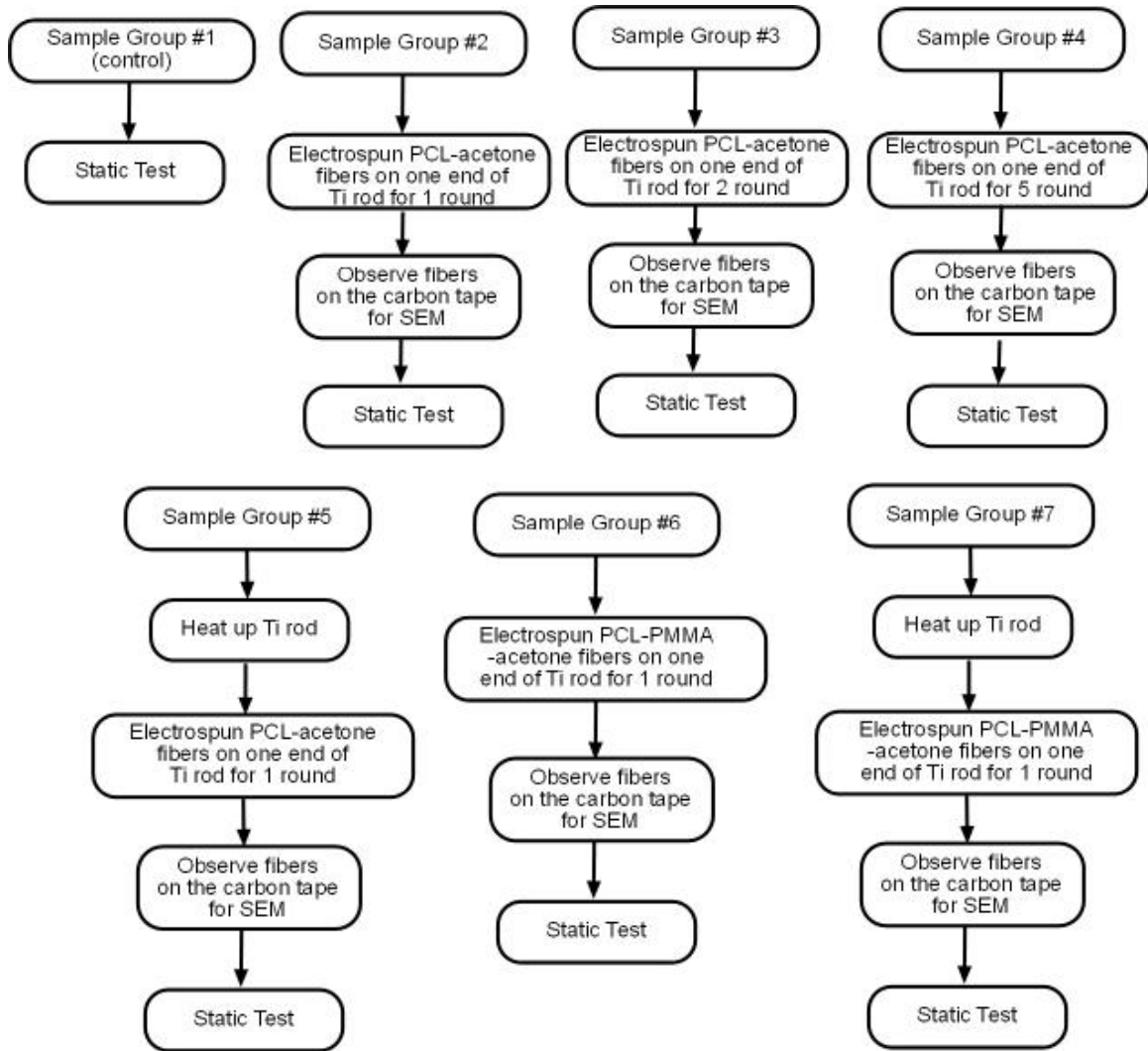


Figure 5.4 Flowchart showing the steps of determining the topography, stiffness and thickness effect on the fracture of Ti-cement interface

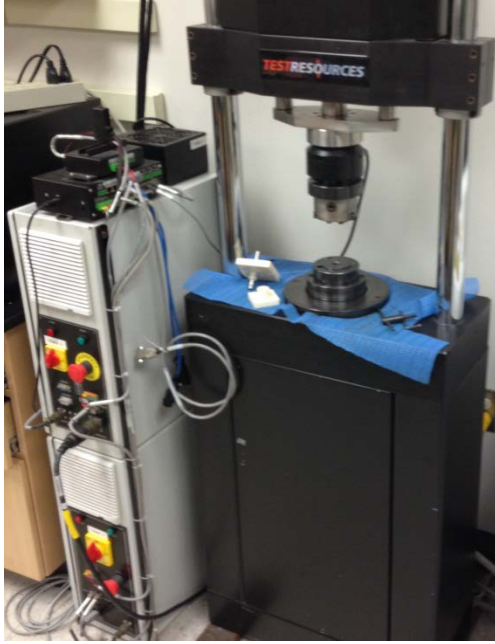
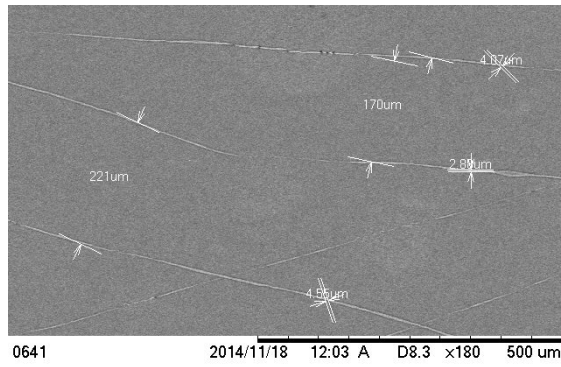


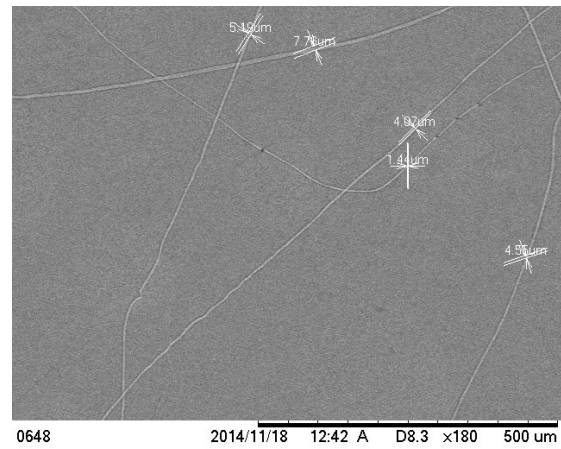
Figure 5.5 Universal Test Resources (UTM)



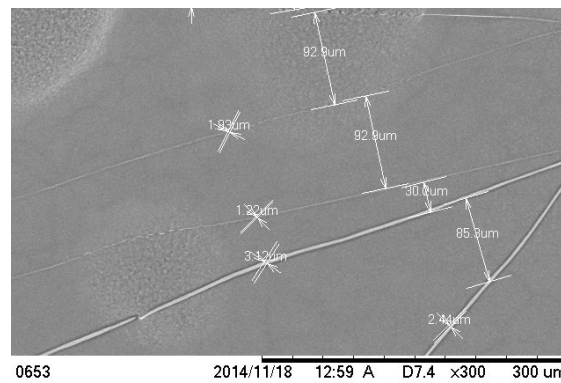
Figure 5.6 Static test setup in UTM (a) before curing; (b) during curing



(a)



(b)



(c)

Figure 5.7 (a) Scanning electron microscope images (SEM) of with 1 rounds of PCL-acetone fiber sample (sample #1); (b) SEM of 2 rounds of PCL-acetone fiber sample; (c) SEM of 3 rounds of PCL-acetone fiber sample

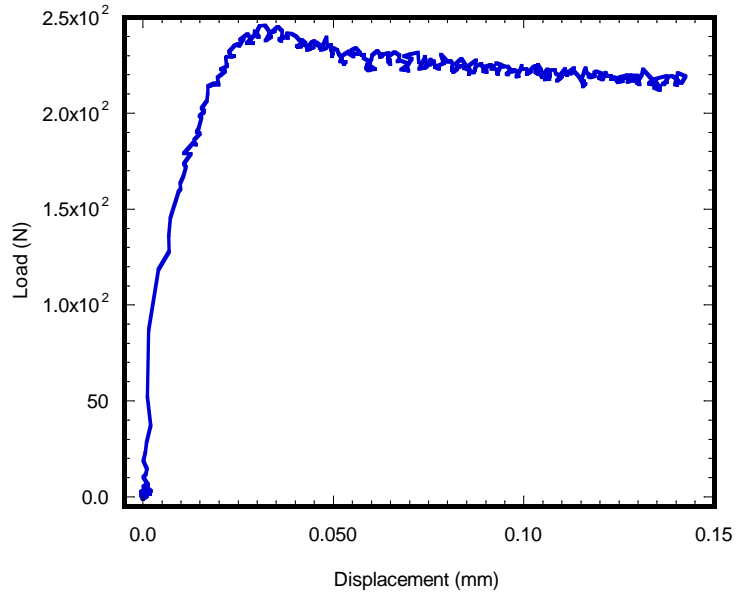


Figure 5.8 Typical load-displacement plot of Ti-cement interface without fibers

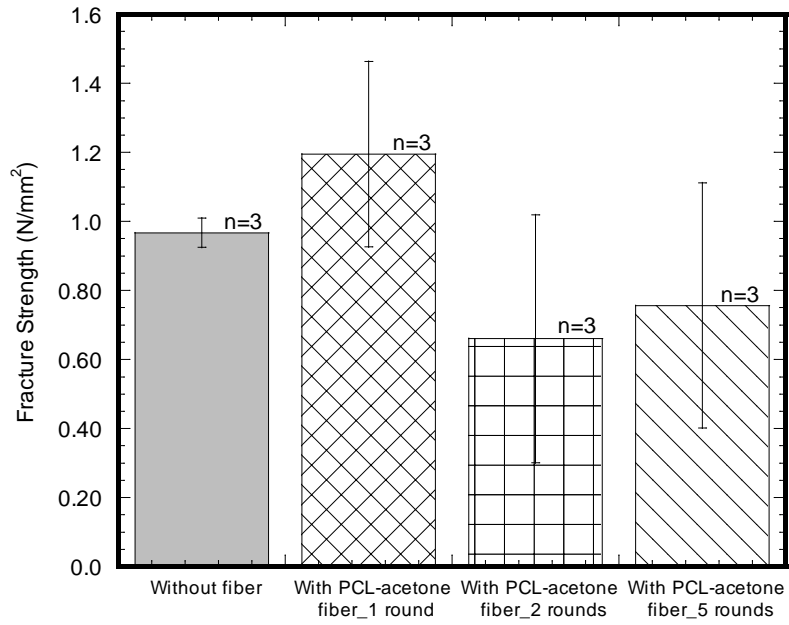


Figure 5.9 Comparison of fracture load of Ti-cement interface with different round of fiber

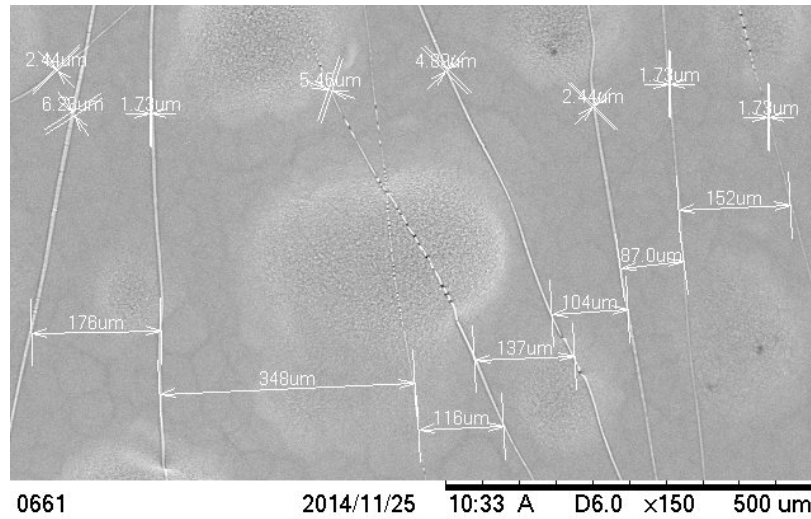


Figure 5.10 Scanning electron microscope images of PCL-PMMA-acetone fiber samples

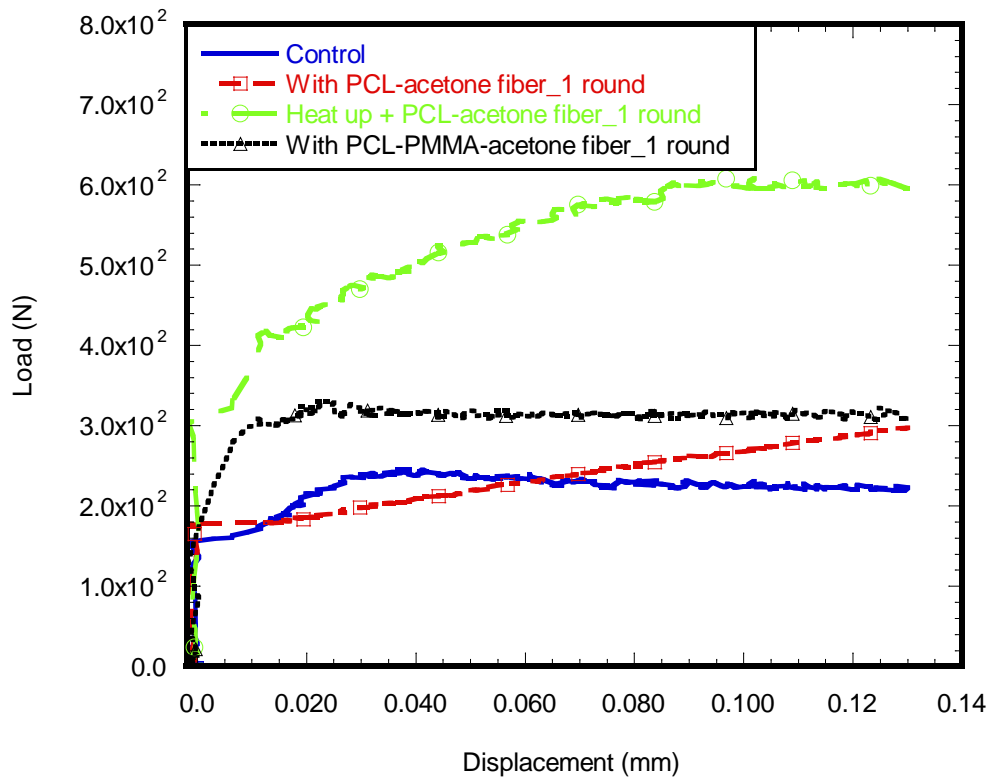


Figure 5.11 Typical load-displacement plot of Ti-cement union with and without fiber under static test

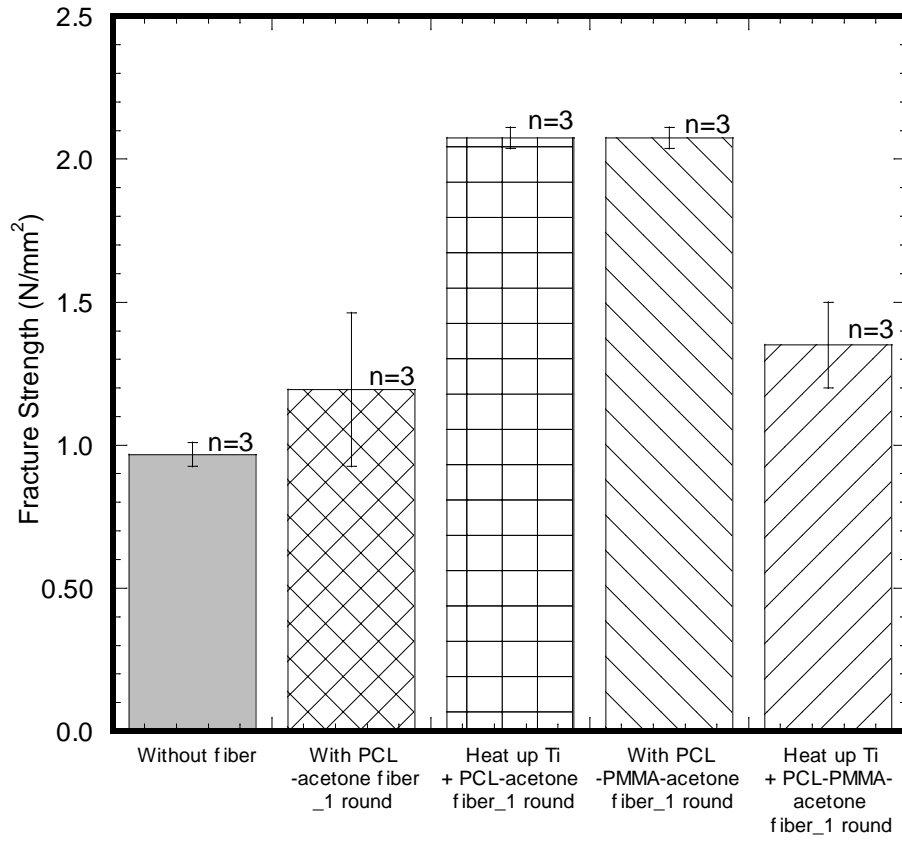


Figure 5.12 Comparison of fracture load of Ti-cement union with different fiber and with or without heating

5.7 Tables

Table 5.1 SEM image of produced PCL-acetone 1 round fiber distribution

Description	Sample number		
	1	2	3
Number of fibers intersects 500um length line (PCL-Acetone)	3	3	5
Range of diameter of fibers (PCL-Acetone)	2.88um~ 4.55um	1.89um~ 2.30um	1.17um~ 1.30um

Table 5.2 Static results of Ti-cement union with and without PCL-acetone fiber (n=3)

Sample Groups	Method	L (mm)	Contact area (mm ²)	Fracture load (N)	Stiffness (KN/mm)	Fracture strength (N/mm ²)
1	Without Fiber	10.233±0.170	307.344±5.106	298.619±13.350	1.679±0.041	0.967±0.025
2	With PCL fiber_1 round	9.490±0.235	276.640±9.058	345.896±46.157	2.114±0.208	1.195±0.379
3	With PCL fiber_2 rounds	9.211±0.114	285.019±7.058	177.0364±95.06156	1.0169±0.1297	0.6603±0.3588
4	With PCL fiber_5 rounds	9.445±0.147	283.668±6.125	225.9119±108.0264	0.93075±0.15435	0.7564±0.3555

Table 5.3 Static results of Ti-cement union with and without heating up Ti before PCL-acetone fiber (n=3)

Sample Groups	Method	L (mm)	Contact area (mm ²)	Fracture load (N)	Stiffness (KN/mm)	Fracture strength (N/mm ²)
1	Without Heating Up Ti	9.49±0.235	285.019±7.058	345.896±46.157	2.114±0.208	1.195±0.379
2	Heat up Ti (50°C) + PCL-acetone fiber	9.267±0.29	278.312±8.71	577.484±34.085	7.848±1.936	2.074±0.058

Table 5.4 SEM image of produced PCL-PMMA-acetone fiber distribution

Description	Sample number		
	1	2	3
Number of fibers intersects 500um length line (PCL-PMMA-Acetone)	12	9	5
Range of diameter of fibers (PCL-PMMA-Acetone)	1.44um~ 5.94um	2.07um~ 6.56um	1.44um~ 4.07um

Table 5.5 Static results of Ti-cement union with PCL or PCL-PMMA fiber and without fiber (n=3)

Sample Groups	Method	L (mm)	Contact area (mm ²)	Fracture load (N)	Stiffness (KN/mm)	Fracture strength (N/mm ²)
1	Without Heating Up Ti	8.995±0.108	269.021 ±3.257	542.610 ±26.449	8.580±0.041	2.013±0.074
2	Heat up Ti (50°C) + PCL-PMMA-acetone fiber	9.016±0.019	270.933 ±0.584	419.005 ±104.355	5.862±2.358	1.548±0.389

Table 5.6 Static results of Ti-cement union with and without heating up Ti rod before PCL-PMMA fiber (n=3)

Sample Groups	Method	L (mm)	Contact area (mm ²)	Fracture load (N)	Stiffness (KN/mm)	Fracture strength (N/mm ²)
1	Without Fiber	10.233±0.170	307.344±5.106	298.619±13.350	1.679±0.041	0.967±0.025
2	With PCL fiber_1 round	9.490±0.235	276.640±9.058	345.896±46.157	2.114±0.208	1.195±0.379
3	With PCL-PMMA fiber_1 round	8.995±0.108	269.021±3.257	542.610±26.449	8.580±0.041	2.013±0.074

CHAPTER 6

DESIGN OF GRIPPERS FOR FATIGUE TESTS ON BI-MATERIAL INTERFACES

6.1 Summary

Apart from fracture strength, the bond of an ideal implant with surrounding tissue must maintain certain fatigue life, N , due to cyclic loads (e.g. walking, running)[56]. Fatigue failure of the bone cement is the primary cause of loosening of cemented implant. The research goal was to determine the fatigue life of the Ti and PMMA cement interface. Based on the analysis in chapter 4, the cement holder is more prone to deform and damage during the fatigue test. Thus a suitable gripper for fatigue test is essential. Various fatigue test setups have been tried in this study. Cyclic tests (amplitude = 50 N) were conducted to find fatigue life of Ti/PMMA samples at 1 Hz using stepwise load (100 N) for 1000000 cycles starting from 250 N until the failure of the interfaces. Based on the observation during the experiment, using a customized gripper to avoid clamping one end of Ti rod directly with the load cell could effectively overcome the preload issue. However, the results of the fatigue life were still very inconsistent, which may be due to the variable surface property of Ti rods.

6.2 Specification and Background

6.2.1 Introduction

Fatigue failure of the cement mantle in terms of cement cracking is one of the causes of aseptic loosening in cemented hip reconstructions[74]. Under the influence of dynamic loading, it has been demonstrated that the implant–cement interface is a debonded interface, which enables gapping and sliding between the implant and cement[13, 14]. Fatigue test for Ti-cement interface is essential to understand the debonded mechanism and develop a solution for improve the fatigue performance of Ti-

cement interface. To author's best knowledge, there is little study about the fatigue test gripper.

6.2.2 Problems of conventional gripper

Conventional UTM grippers (wedge, hydraulic, pneumatic) are designed for signal material, where alignment of gripper center and center of specimen is not critical for static and fatigue tests. It is very crucial to have perfect alignment of sample with gripper in case of bi-material samples. Multiple gripper designs have been tested and analyzed. There are two parts of the test gripper, gripper to clamp the Ti rod and cement holder. The load cell of Test Resources 800LE4 universal testing machine (UTM) will be used to provide the cyclical load for fatigue test in this study. The gripper connecting from the load cell to the Ti rod should be able to transfer the load to Ti rod without much preload. From the finite element analysis in chapter 5, the cement holder used in static test is more prone to fatigue fail than the Ti-cement interface. A sufficient cement holder design should have higher fatigue life than the Ti-cement interface fatigue life.

6.2.3 Motivation and Objectives

The goal of this project is to develop a more efficient fatigue test solution for Ti-cement union. The objectives of this research were: (1) to design a suitable gripper for fatigue test on bi-material samples; (2) to conduct the fatigue tests to evaluate the suitability of the gripper for fatigue test on biomaterial sample; (3) to conduct the fatigue test for polished Ti rod to evaluate the effect of polishing technique on the fracture of Ti-implant interface.

6.3 Material and Method

6.3.1 Material

Surgical Simplex P Radiopaque bone cement (Distributed by Stryker Howmedica Osteonics) was used as the polymethyl methacrylate (PMMA) cement. Titanium (Ti) rods (6Al-4V ELI, ASTM B348 standard, grad 23, bio-compatible) were purchased with 3”length X 3/8” diameter from Titanium Metal Supply, Poway, CA, USA. There were three Ti rods for each group of experiment. All Ti rods samples were polished using Geared Head Milling & Drilling Machine (Figure 6.1(a)) at high speed before experiment. Ti rods were fixed in a geared head. The polishing pad was fixed by the vice of the machine (Figure 6.1(b)).

Two kinds of different polishing technology have been tried in this study. The polishing process was recommended by Buehler. For the first technique, there were three steps for polishing all the Ti rods. The first step was to polish using Buehler CarbiMet 2 Abrasive Discs for 3mins. During the first step polishing, 9um MetaDi Supreme Diamond Suspension was used to spray on the contact surface of the Ti rod and the polishing disc. The second step of polishing was using Ultra Pad with 0.05um MetaDi Supreme Diamond Suspension from Buehler for 3mins as well. The last step was using MicroCloth and MasterPrep Alumina for 3mins as well. After each step, Ti rods were cleaned by Ethanol. For the second technique, only the first step and the second step have been conducted for 1 min for both. Before testing, the surface roughness of Ti rod for two different polishing technique was measured by Leica DCM8 microscope.

6.3.2 Fatigue Test

The titanium rod is encapsulated by a cylindrical holder in order to cure the rod to the cement without being contaminated. Multiple holders based on the different setup design discussed in chapter 5.3.3 have been tried for the production of titanium/cement sample. The test setup was placed in the Test Resources 800LE4 dynamic universal

testing machine to be put the titanium/PMMA specimen under cyclic loading for a fatigue test. According to Surgical Simplex P Radiopaque bone cement preparation protocol, PMMA cement was prepared by hand mixing 1.25 grams of PMMA powder with 0.625 ml of methyl methacrylate (MMA) monomer using powder: monomer ratio of 2:1. PMMA was poured to surround different titanium samples during doughy phase in the mold. Cyclic tests (amplitude = 100 N) were conducted at 1 Hz using stepwise load (100 N) for 1000 cycles starting from 350 N until the failure of the interfaces.

6.3.3 Setup Design Concept Evaluation

6.3.3.1 Concept I

The first setup was designed based on the static test discussed in Chapter 4. A customized rectangular plastic holder with a cylinder in the middle (made from 3D-printer) was shown in Figure 6.2(a). There were three holes which were used to fix with the top. The testing procedure is similar as the static test. Firstly, the Ti rod is held into the plastic test setup and fixed in the test resource machine as Figure 6.2(b). Secondly, PMMA and MMA was mixed and poured into the holder and press the top plate. Then a metal plate with 60KPa pressure was placed on top of the cement for 30mins to help the cement cured (Figure 6.2(c)). After 30mins of curing, the fatigue test started.

6.3.3.2 Concept II

Given that the cement holder was not usable at the first concept, concept II was modified from concept I. The cylinder hole of the cement holder was drilled through. A channel was cut at the bottom side to allow an aluminum plate placed in to support the cement when the cement became solid (Figure 6.3(a) and (b)). Similar to concept I, the Ti rod is held in the cement holder with the plate at the bottom and clamped at the top in the test resource machine as Figure 6.3(c). PMMA and MMA was mixed and poured into the

holder and press the top plate. Then a metal plate with 60KPa pressure was placed on top of the cement (Figure 6.3(c)). After 5mins, the aluminum plate was taken out and the cement was continued curing for 25mins more before running the test.

6.3.3.3 Concept III

Concept III was using aluminum for the top and the bottom holder which were made by CNC. Even so, the cement holder was still not fixed enough. When the load applied, the whole setup displaced other than breaking the Ti rod from the cement. The cyclic load was applied on the three bolts which were used to fix the cement holder.

To get rid of these three bolts of the cement holder, the cement holder was combined by two pieces (Figure 6.4(a)) using three bolts in concept III. The hollow cylinder at the rear (Figure 6.4(b)) was used for clamping into the test machine through three corner support (Figure 6.4(c)). The surface of hollow cylinder was grooved to increase the roughness so that it can be clamped tighter. In addition, the aluminum plate was difficult to take out during the previous trial because the Ti rod pined on the plate. To solve this problem, two aluminum plates were used to hold the cement at the bottom. The bottom plate was added a handle (Figure 6.4(d) and Figure 6.4(f)). After taking out the bottom plate, it became very easy to take out the top plate which wouldn't affect the cement curing. Both of the plates were taken out after the cement got 5minutes cured. The total curing time will still be 30minutes.

6.3.3.4 Concept IV

Consolidating the concepts above, the preload was still the main problem. The preload was considered coming from the cement curing and the clamping at the top of the Ti rod. When cement was curing, the Ti rod will displace when the cement became solid so that a force will transfer to the load cell of the machine. This preload was in a range,

normally from 150N to -150N, which can't be offset. To overcome the preload, the Ti rod can't be directly clamped by the gripper of the machine. A customized gripper (Figure 6.5(b)) was used to hold the Ti rod with a drill hole (Figure 6.5(a)) at the top. This top specimen holder includes two hollow cylinders. The smaller cylinder was fixed in the machine gripper while the bigger cylinder was holding the Ti rod at one end (Figure 6.5(c)). A through hole was drilled in the bigger cylinder of the cap with the same diameter as the hole drilled at one end of the Ti rod. A pin was hung through these two holes to assemble the Ti rod and the cap together. The bottom specimen holder is same as the design of concept III (Figure 6.4 (a) and (b)).

6.4 Results

6.4.1 Surface Roughness for different polishing technique

Figure 6.6 and Figure 6.7 displayed the surface roughness of Ti rod with different polishing technique. Table 6.1 present the R_a of Ti rod with 2-step polished is around two times of that with 3-step polished.

6.4.2 Control Experiment

6.4.2.1 Concept I

During the fatigue test, the cyclical load was applied on the Ti rod. However, the whole setup was lifting up instead of the Ti rod. The Ti rod didn't break from the cement, which suggested the bottom of the setup was not fixed enough. The other concern was the 3D printer plastic holder. It was not reusable, which would cost a lot of material.

6.4.2.2 Concept II

After the test, the cement was pushing out since the cylinder was a through hole. In spite of that, the cement was still stick to the side of the cylinder. Likewise, this concept didn't solve the problem that the displacement happened at the whole setup. Besides, the rectangular side of the cement holder bended after many cycles of load, which may be caused by the channel at the bottom surface of the holder.

6.4.2.3 Concept III

This concept works better. When load was applied, the Ti would be broken from the cement. However, the preload every time was inconsistent which lead to inconsistent result.

6.4.2.4 Concept IV

Through employing this setup, the preload problem has been solved successfully. Various compression cyclical tests based on all the concepts mentioned above have been performed. Comparing to the Cobalt HV bone cements used in the previous chapters, Simplex bone cement takes more working time because of the lower viscosity. Based on our observation, concept IV can be the suitable fatigue test solution because it overcame the preload issues. Table 6.2 shows the fatigue test results for the Ti rod of 3-step polishing using concept IV. From the result, the Ti rod with 3-step polished is too smooth to attach with the cement. Thus, 2-step polishing is used for the control experiment in this chapter.

There were three out of ten tests failed. Moreover, from the result got from concept IV (Table 6.3) is very inconsistent, for example, fatigue life was varied from 39128cycles to 67cycles. Furthermore, there were some tests which the bone cement

cracked at the interface between cement and aluminum specimen holder other than the interface of Ti-cement. Thus the fatigue test tried in this study was not working.

The failure of the fatigue test was possibly initiated by a few reasons. The factors affecting the fatigue fracture strength include the stress concentration, surface roughness, surface condition and environment [75]. In a stress concentration, firstly the fatigue strength is reduced considerably in a place where the stress is concentrated, such as notches, holes, keyways and places where there are sudden changes in cross-section. For this test, the surface roughness of the inside surface of aluminum cement holder is not enough which lead to the bonding strength between the holder and cement is not strong and eventually the cement will break from aluminum holder. Secondly, the fatigue strength is reduced considerably in a place where the stress is concentrated, such as notches, holes, keyways and places where there are sudden changes in cross-section. The aluminum holder is reusable, which is possible to generate stress concentration areas. Besides, the surface roughness and surface condition of the Ti rod samples was variable which leads to different fracture strength of Ti-cement union, even though all the Ti rods were bought at the same batch. Moreover, the test machine has the alignment problem. If the machine is misaligned, either at a small angle, the machine will exert a bending force on the specimen. This is especially bad for brittle materials, because it will dramatically skew the results. The initial portion of the stress–strain graph we got was curved and not linear, which indicates the specimen is misaligned in the testing machine.

6.5 Conclusions

Aluminum cement holder can be a suitable cement holder for fatigue test because it is reusable and not prone to deform as plastic. The customized gripper used in concept IV can successfully get rid of the preload issue.

6.6 Figures

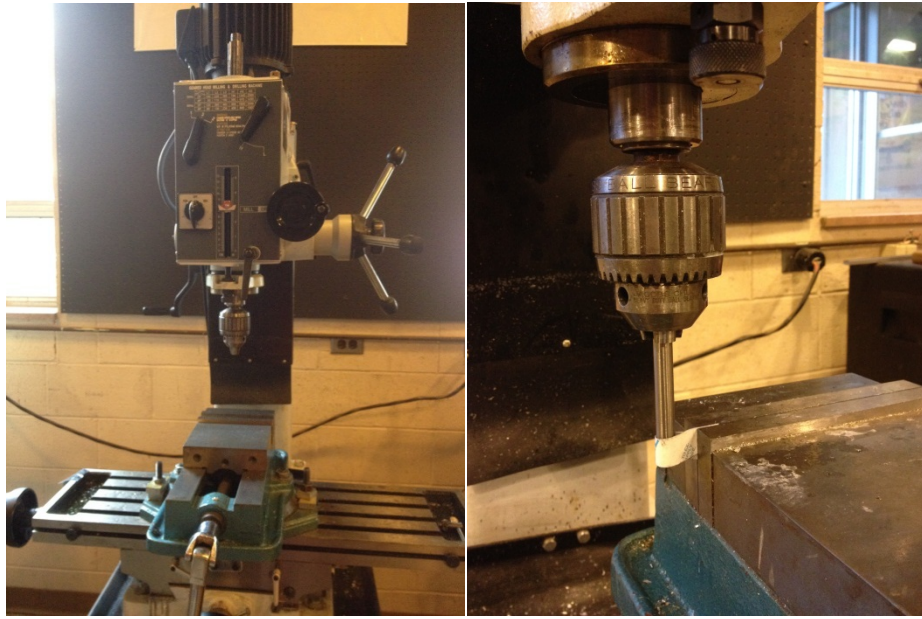


Figure 6.1(a) Geared Head Milling & Drilling Machine; (b) polishing setup

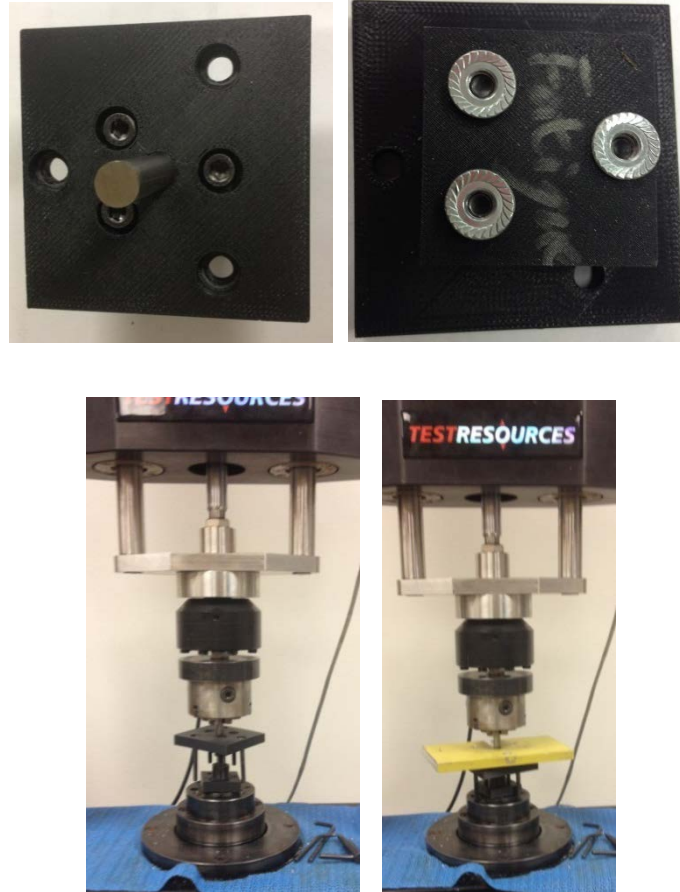


Figure 6.2 (a) Top side of the cement holder of concept I; (b) bottom side of the cement holder of concept I; (c) fatigue test setup before cemented; (d) setup during curing the cement

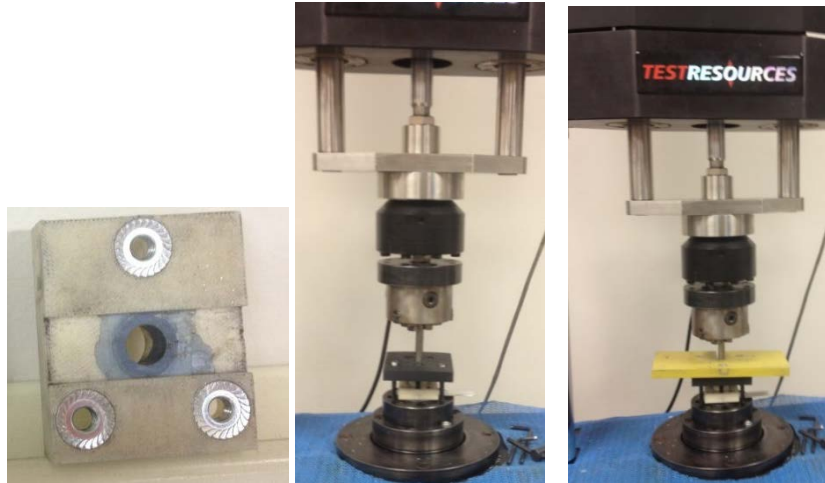


Figure 6.3 (a) Bottom side of the cement holder of concept II; (b) fatigue test setup before cemented; (c) setup during curing the cement

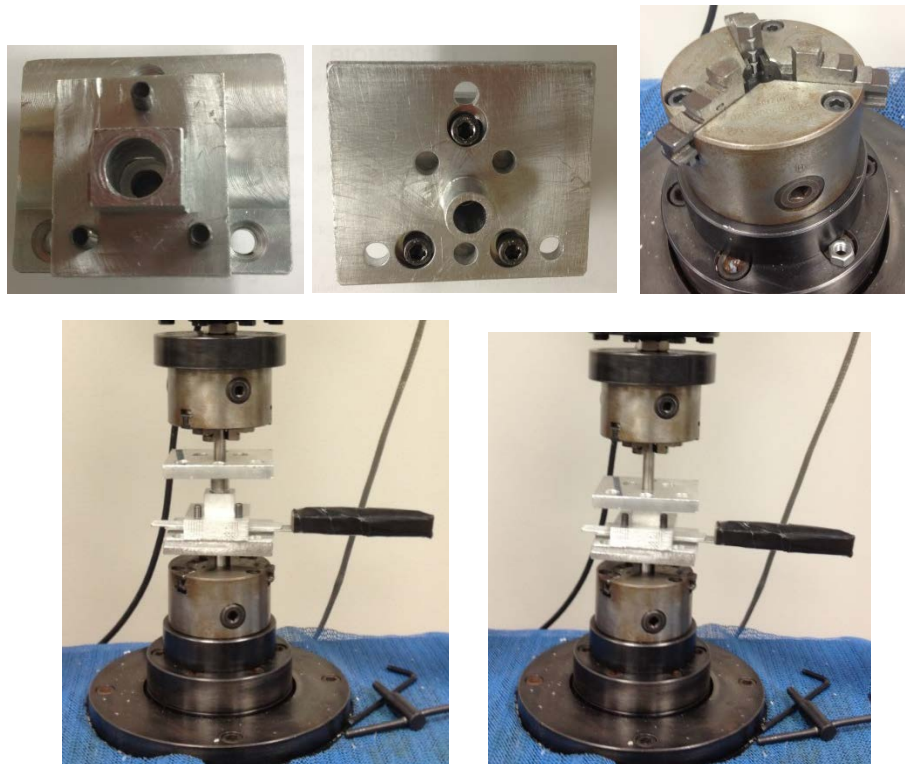


Figure 6.4 (a) Top side of the aluminum cement holder of concept III; (b) bottom side of the cement holder of concept III; (c) corner support for the cement holder; (d) fatigue test setup before cemented; (f) setup during curing the cement

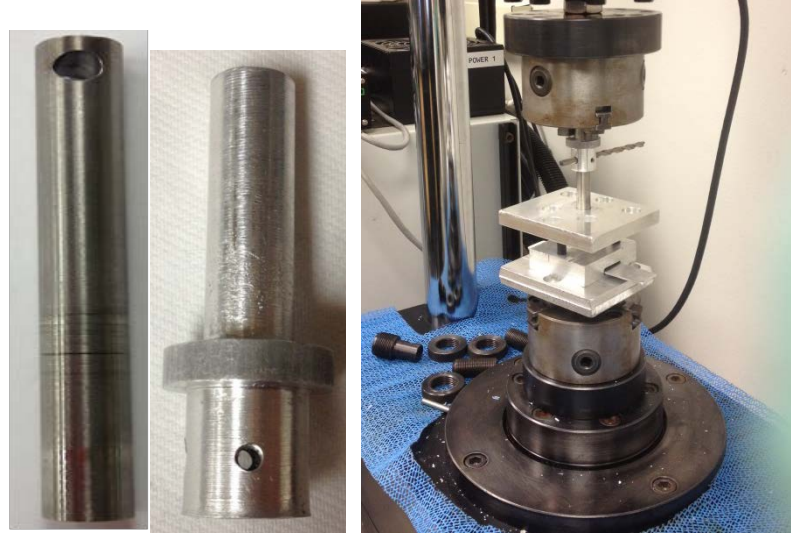


Figure 6.5 (a) Titanium rod sample with a drill hole; (b) fabricated top specimen holder for fatigue test; (c) fatigue test setup of Concept IV

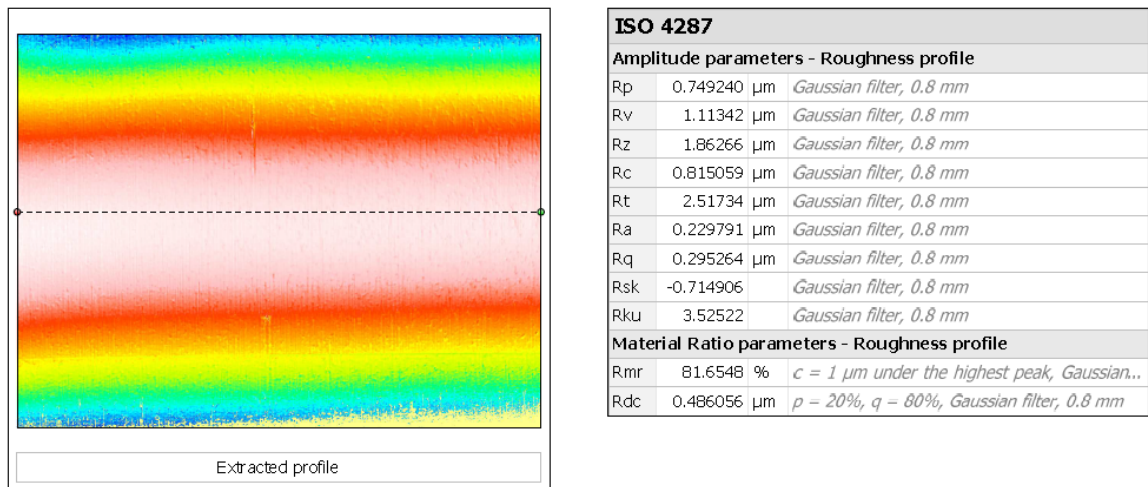
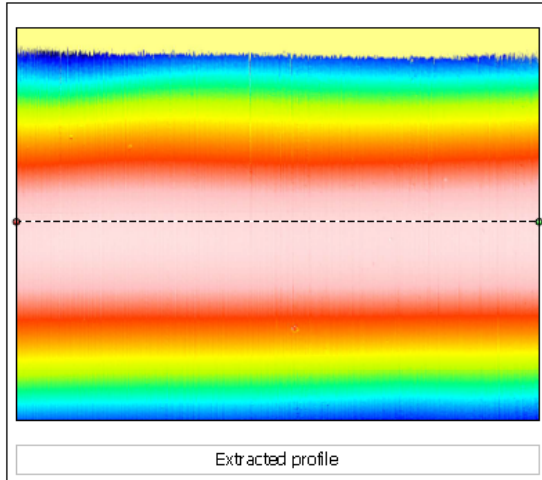


Figure 6.6 Surface roughness respond to Ti with 2-step polished using Geared Head Milling & Drilling machine generated by Leica



ISO 4287		
Amplitude parameters - Roughness profile		
Rp	0.372044 μm	Gaussian filter, 0.8 mm
Rv	0.906368 μm	Gaussian filter, 0.8 mm
Rz	1.27841 μm	Gaussian filter, 0.8 mm
Rc	0.340261 μm	Gaussian filter, 0.8 mm
Rt	1.27841 μm	Gaussian filter, 0.8 mm
Ra	0.0988855 μm	Gaussian filter, 0.8 mm
Rq	0.132893 μm	Gaussian filter, 0.8 mm
Rsk	-1.09617	Gaussian filter, 0.8 mm
Rku	8.07555	Gaussian filter, 0.8 mm
Material Ratio parameters - Roughness profile		
Rmr	99.7297 %	$c = 1 \mu\text{m}$ under the highest peak, Gaussian...
Rdc	0.184731 μm	$p = 20\%$, $q = 80\%$, Gaussian filter, 0.8 mm

Figure 6.7 Surface roughness respond of Ti with 3-step polished using Geared Head Milling & Drilling machine generated by Leica

6.7 Tables

Table 6.1 Surface roughness for different polishing technique

Properties	2 step polishing	3-step polishing
R_a (um)	0.229791	0.0988855
R_q (um)	0.295264	0.132893

Table 6.2 Control experiment result of fatigue test_3 step polishing using concept IV

Sample #	Control_3 step polishing	
	Breaking load (N)	Fatigue life (cycles)
1	60	9
2	40	14.5
3	60	9.5
4	80	11
5	60	33

Table 6.3 Control experiment result of fatigue test for Ti_2 step polishing using concept IV

Sample #	L (mm)	Contact area (mm ²)	Breaking load (N)	Fatigue life (cycles)	Fatigue strength (N/mm ²)
1	10.07333	302.5386235	250	39128	0.826340773
2	9.803	294.4196334	220	3283.5	0.747232776
3	9.63	289.2238161	350	8221.5	1.210135475
4	10.18	305.7423103	350	17034	1.144754874
5	10.3	309.3463454	420	67	1.357701509
6	10.01	300.6365939	350	4866	1.164196266
7	10.08333	302.8389597	350	33332.5	1.155729766

CHAPTER 7

CONCLUSION AND FUTURE WORKS

7.1 Conclusions

The goal of this research is to develop an efficient bond interface between the Ti and PMMA through micron architectural modification by applying micron particles to the surface of the cement mantle and electrospinning fibers to the surface of the implant. For research question (1), the study found that flexural strength and fracture toughness of the CBC specimens that contain GMA is significantly greater than the flexural strengths of all other specimens. For research question (2), CBC-SiO₂ specimen that do not contain GMA is significantly greater than the flexural strengths of all other specimens. For research question (3), it has been demonstrated that the incorporation of micron size or nanosize particles of MgO to PMMA enhanced the fracture toughness of bone-PMMA interfaces. For research question (4), the result showed that the fracture strength and fatigue life of 0.11 inch thick cement is much less than 0.22 inch thick cement. For research question (5), the FEA analysis and static test showed that the fracture strength of Ti-cement interface using plastic cement holder has less value that using aluminum cement holder. Additionally, plastic holder is not suitable for fatigue test due to its poor fatigue life. For research question (6) to (8), it has been manifested that the adhesion and strength of fiber is controlled by the type of the electrospinning material. The static test results showed one round of fibers coated on the surface can improve the quality of Ti implant surface more than two rounds or 5 rounds of fiber. The fracture strength of Ti-cement interface with coating PCL-PMMA-acetone fibers on Ti surface is more than that of Ti-cement interface with coating PCL-acetone fibers. Heating up Ti rod before coating PCL-acetone fibers can significantly increase the fracture strength of Ti-cement interface. However, heating up Ti rod before coating PCL-PMMA-acetone is not benefit to increase the fracture strength of Ti-cement interface. For research question (9), concept IV discussed in chapter 6 is the suitable fatigue test fixture which can conduct the fatigue test on bi-material interface such as Ti -cement interface. In conclusion, micron

architectural modification can be an effective solution to improve the fracture properties of implant-cement interface.

7.2 Future works

The future works of all the chapters are listed. (1) The future work for chapter 2 is to develop alternative bone cement using the optimal nanoparticles and alternative monomer. The result on chapter 3 shows the fracture toughness of bone cement with nanosize MgO added is significantly higher than the result of bone cement without MgO and bone cement with micron MgO. Based on this result, the suggestion is to use the nano-size particles instead of micron size particles to modify the bone cement. (2) The future work for chapter 3 is to see the effect of MgO and other nanoparticle on bone-cement interface and implant-cement interface. Specifically, HA, CT, Chitosan, BaSO₄ and SiO₂ can be added into the PMMA beads to modify the bone cement and then the interface between the modified cement and bone as well Ti implant can be tested to see the effect of these particles on the bone-cement interface and implant-cement interface. (3) The future work for chapter 4 is to validate the FEA frictional coefficient values for Ti-cement interface and Aluminum-cement interface using experiment. (4) The future work for chapter 5 is to evaluate the effect of the PCL-acetone nanofiber and PCL-PMMA-acetone nanofibers on the fracture of Ti-cement interface. It is assumed the fracture strength of implant-cement interface can be increased by coating nano-fiber on the implant surface according to chapter 3. The main concern is the electrospinning process because the nano-size needle will be used. If the viscosity of the fiber solution is too higher, it may block in the needle without fibers coming out. Thus the primary object may be finding a suitable fiber solution with sufficient viscosity. The other concern is the cleaning of the needle due to the small hole of the needle. A high pressure pump may be able to clean the needle. (5) The future work for chapter 6 is to conduct the fatigue test for Ti-cement interface using the gripper of concept IV. It has been proved that the customized gripper in concept IV can overcome the preload issue, which is the main

issue for the fatigue test. It is believed that the inconsistency of fatigue result is caused by the varying of the surface roughness of Ti rod surface. The suggestion for it is using a higher polishing technique. As discussed in chapter 6, higher polishing leads to the implant-cement fracture before the testing. In this case, increasing the height of the cement mantle or the cement thickness can be considered.

REFERENCES

1. W. Lu, J.S., and X. Jiang, *Recent advances in electrospinning technology and biomedical applications of electrospun fiber*. Journal of Materials Chemistry B, 2014. **2**: p. 2368-2380.
2. E.P. Lautenschlager, P.M., *Titanium and titanium alloys as dental materials*. International dental journal, 1993. **43**(3): p. 245-253.
3. Elias CN, L.J., Valiev R, Meyers MA, *Biomedical applications of titanium and its alloys*. JOM, 2008. **60**(3): p. 46-49.
4. O. Okuno, H.H., Dent. Jpn., 1989. **26**: p. 101-104.
5. G. Cunin, H.B., H. Petite, C. Blanchat, G. Guillemin, *Experimental vertebroplasty using osteoconductive granular material*. Spine, 2000. **25**(9): p. 1070-1076.
6. J.X. Lu, Z.W.H., P. Tropiano., *Human biological reactions at the interface between bone tissue and polymethylmethacrylate cement*. J Mater Sci Mater Med, 2002. **13**(8): p. 803-809.
7. J.E. Barralet, T.G., A.J. Wright, I.R. Gibson, J.C. Knowles, *Effect of porosity by compaction on compressive strength and microstructure of calcium phosphate cement*. J Biomed Mater Res (Appl Biomater), 2002. **63**(1): p. 1-9.
8. Lennon, A.B., B.A.O. McCormack, and P.J. Prendergast, *The relationship between cement fatigue damage and implant surface finish in proximal femoral prostheses*. Medical Engineering and Physics, 2003. **25**(Compendex): p. 833-841.
9. Lombardi AV, J., Berasi CC, Berend KR, *Evolution of tibial fixation in total knee arthroplasty*. J Arthroplasty 2007. **22**(4 suppl 1): p. 25.
10. Bishop, J.A., et al., *Assessment of compromised fracture healing*. J Am Acad Orthop Surg, 2012. **20**: p. 273-282.
11. U.S., F. *Food and Drug Administration*.
<http://www.fda.gov/medicaldevices/productsandmedicalprocedures/implantsandprosthetics/metalonmetalhipimplants/ucm241770.htm>.
12. J.R. Jeffers, M.B., A.B. Lennon, P.J. Prendergast, M. Taylor, *Cement mantle fatigue failure in total hip replacement: experimental and computational testing*. Journal of Biomechanics, 2007. **40**: p. 1525-1533.
13. Ramos, A.S., J.A., *The influence of cement mantle thickness and stem geometry on fatigue damage in two different cemented hip femoral prostheses*. Journal of Biomechanics, 2009. **42**(15): p. 2602-2610.
14. Gravius, S.W., D.C. ; Siebert, C.H. ; Andereya, St. ; Mueller-Rath, R. ; Maus, U. ; Mumme, T., *In vitro interface and cement mantle analysis of different femur stem designs* Journal of Biomechanics, 2008. **41**(9): p. 2021-2028.

15. Ohashi, K.L., et al., *Adhesion and reliability of interfaces in cemented total joint arthroplasties*. Journal of orthopedic research, 1998. **16**: p. 705-714.
16. Hosein, Y.K.K., Graham J. W. ; Dunning, Cynthia E., *The Effect of Stem Circumferential Grooves on the Stability at the Implant-Cement Interface*. Journal of Medical Devices, 2014. **8**(1): p. 014504.
17. M.T Manley, L.S.S., J Gurtowski, *The load carrying and fatigue properties of the stem–cement interface with smooth and porous coated femoral components*. J. Biomed Mater. Res. (Applied Biomaterials), 1985. **19**: p. 563-575.
18. Fritsche, A.H., Maximilian ; Zietz, Carmen ; Mittelmeier, Wolfram ; Neumann, Hans-Georg ; Heidenau, Frank ; Finke, Birgit ; Bader, Rainer, *Mechanical characterization of anti-infectious, anti-allergic, and bioactive coatings on orthopedic implant surfaces*. Journal of Materials Science, 2009. **44**(20): p. 5544-5551.
19. Lewis, G., *Alternative acrylic bone cement formulations for cemented arthroplasties: Present status, key issues, and future prospects*. Journal of Biomedical Materials Research - Part B Applied Biomaterials, 2008. **84**(2): p. 301-319.
20. Heo, S.J., et al., *Evaluation of bonding stress for the newly suggested bone cement: comparison with currently used PMMA through animal studies*. Key Engineering Materials, 2007. **342-342**: p. 373-6.
21. Khang, D., et al., *Enhanced fibronectin adsorption on carbon nanotube/poly(carbonate) urethane: Independent role of surface nano-roughness and associated surface energy*. Biomaterials, 2007. **28**(32): p. 4756-4768.
22. Liu, H. and T.J. Webster, *Nanomedicine for implants: A review of studies and necessary experimental tools*. Biomaterials, 2007. **28**(2): p. 354-369.
23. Ricker, A., P. Liu-Snyder, and T.J. Webster, *The influence of nano MgO and BaSO4 particle size additives on properties of PMMA bone cement*. International Journal of Nanomedicine, 2008. **3**(1): p. 125-1.
24. Gbureck, U., et al., *Modified PMMA cements for a hydrolysis resistant metal–polymer interface in orthopaedic applications* Acta Biomaterialia, 2005. **1**: p. 671-676.
25. Travan, A., et al., *Polysaccharide-coated thermosets for orthopedic applications: From material characterization to in vivo tests*. Biomacromolecules, 2012. **13**(5): p. 1564-1572.
26. Khandaker, M., et al. *BIOACTIVE ADDITIVES AND FUNCTIONAL MONOMERS AFFECT ON PMMA BONE CEMENT: MECHANICAL AND BIOCOMPATIBILITY PROPERTIES*. in *2011 ASME International Mechanical Engineering Congress and Exposition*. 2011. Denver, Colorado.

27. Barralet, J.E., et al., *Cements from nanocrystalline hydroxyapatite*. Journal of Materials Science: Materials in Medicine, 2004. **15**(4): p. 407-411.
28. Mann, K.A., et al., *Fracture toughness of CoCr alloy-PMMA cement interfaces*. J. Biomed Mater. Res. (Applied Biomaterials), 1997. **38**: p. 211-219.
29. Serbetci, K., F. Korkusuz, and N. Hasirci, *Thermal and mechanical properties of hydroxyapatite impregnated acrylic bone cements*. Polymer Testing, 2004. **23**(2): p. 145-155.
30. Tunney, M.M., et al. *Incorporation of chitosan in acrylic bone cement: Effect on antibiotic release, bacterial biofilm formation and mechanical properties*. in *Special Section: Selected Papers from the 21st European Conference on Biomaterials, Brighton, UK, 9-13 September 2007. Guest Editors: Andrew Lloyd and Matteo Santin*. 2008. Van Godewijckstraat 30, Dordrecht, 3311 GZ, Netherlands: Kluwer Academic Publishers.
31. Hong, R.Y., et al., *Surface-modified silica nanoparticles for reinforcement of PMMA*. Journal of Applied Polymer Science, 2007. **105**(4): p. 2176-84.
32. Walsh, W.R., et al., *Cemented fixation with PMMA or Bis-GMA resin hydroxyapatite cement: Effect of implant surface roughness*. Biomaterials, 2004. **25**(Compendex): p. 4929-4934.
33. Ni, G.X., et al., *Nano-mechanics of bone and bioactive bone cement interfaces in a load-bearing model*. Biomaterials, 2006. **27**(9): p. 1963-1970.
34. Elizalde-Pena, E.A., et al., *Synthesis and characterization of chitosan-g-glycidyl methacrylate with methyl methacrylate*. European Polymer Journal, 2007. **43**(Compendex): p. 3963-3969.
35. Flores-Ramirez, N., et al., *Hybrid natural-synthetic chitosan resin: Thermal and mechanical behavior*. Journal of Biomaterials Science, Polymer Edition, 2008. **19**(Compendex): p. 259-273.
36. Ries, M.D., et al., *Intramedullary pressure and pulmonary function during total knee arthroplasty*. Clinical Orthopaedics and Related Research, 1998(356): p. 154-160.
37. Graham, J., M. Ries, and L. Pruitt, *Effect of bone porosity on the mechanical integrity of the bone-cement interface*. Journal of Bone and Joint Surgery-American Volume, 2003. **85A**(10): p. 1901-1908.
38. Cowin, S.C., *Bone Mechanics Handbook*,. Second ed. 2001.
39. Lucksanasombool, P., et al., *Fracture toughness of bovine bone: influence of orientation and storage media*. Biomaterials, 2001. **22**(23): p. 3127-3132.
40. Khandaker, M., Y. Li , and T. Morris, *MgO micro/nano particles for the improvement of cement–bone interface*. journal of biomechanics, 2013. **46**(5): p. 1035–1039.

41. Wood, J.D., et al. *Mechanical behavior of the dentin-enamel interface*. in *9th Intl. Cong. Soc. Experimental Mech.* 2000. Orlando, FL.
42. Mann, K.A., et al., *Mixed-mode failure response of the cement–bone interface*. *Journal of Orthopaedic Research*, 2001. **19**(6): p. 1153-1161.
43. Wang, X.D. and C.M. Agrawal, *A mixed mode fracture toughness test of bone-biomaterial interfaces*. *Journal of Biomedical Materials Research*, 2000. **53**(6): p. 664-672.
44. ASTM, *Annual book of ASTM standards: section 3 - Metals test methods and analytical procedures* 1994. **03.01**.
45. Athanasiou, K.A., et al., *Fundamentals of biomechanics in tissue engineering of bone*. *Tissue Engineering*, 2000. **6**(4): p. 361-381.
46. Dundurs, J., *Edge-bonded dissimilar orthogonal elastic wedges under normal and shear loading* *Journal of applied mechanics*, 1969. **36**: p. 650.
47. Cowin, S.C., *Bone Mechanics Handbook*. Second ed. 2001.
48. Lasaygues, P. and M. Pithioux, *Ultrasonic characterization of orthotropic elastic bovine bones*. *Ultrasonics*, 2002. **39**(8): p. 567-573.
49. Khandaker, M., Y. Li , and S. Tarantini, *INTERFACIAL FRACTURE STRENGTH MEASUREMENT OF TISSUE-BIOMATERIAL SYSTEMS*, in *2011 ASME International Mechanical Engineering Congress and Exposition 2011*: Denver, Colorado.
50. Ramaniraka, N., L. Rakotomanana, and P. Leyvraz, *The fixation of the cemented femoral component. Effects of stem stiffness, cement thickness and roughness of the cement-bone surface*. *J Bone Joint Surg Br.*, 2000. **82**(2): p. 297-303.
51. Wang, C.X. and J. Tong, *Interfacial strength of novel PMMA/HA/nanoclay bone cement*. *Bio-Medical Materials and Engineering*, 2008. **18**(6): p. 367-375.
52. Zelle, J., et al., *Mixed-mode failure strength of implant–cement interface specimens with varying surface roughness*. *Journal of Biomechanics*, 2011. **44**(4): p. 780-783.
53. Funk, M.J. and A.S. Litsky, *Effect of cement modulus on the shear properties of the bone–cement interface*. *Biomaterials*, 1998. **19**(17): p. 1561-1567.
54. Zor, M., M. Küçük, and S. Aksoy, *Residual stress effects on fracture energies of cement–bone and cement–implant interfaces*. *Biomaterials*, 2002. **23**(7): p. 1595-1601.
55. Gillani, R., et al., *Nanofunctionalized zirconia and barium sulfate particles as bone cement additives*. *Int J Nanomedicine*, 2010 **5**(1-11).

56. Davies, J. and W. Harris, *Strength of cement-metal interfaces in fatigue: comparison of smooth, porous and precoated specimens*. *Clinical Materials*, 1993. **12**(2): p. 121-6.
57. D. A. Fisher, A.C.T., N. Paydar, S. Milionis and C. H. Turner, *Cement-mantle thickness affects cement strains in total hip replacement*. *J. Biomechanics*, 1997. **30**(11/12): p. 1173-1177.
58. Biomet, I. *Cobalt™ HV Bone Cement*. 2010; Available from: http://www.biomet.com/wps/portal/internet/Biomet/Healthcare-Professionals/products/orthopedics/cement/cobalt%20hv%20bone%20cement/79129bed-6e70-45fb-9344-07abfa553910!/ut/p/a1/zVLbbtpAEP0V-mC_mV1fALuSVRISCCiBOijB9ku0Xq8v1HjNeoHQR--YJBKVkkLfamm1O-MzoznnDIpQgKKK7luMyIJXpGzjqP889_B3PLSM2eRWH2Fv6vVnd5OJsVgYAAg_B9jjwaX6FYpQRCtZyxvFRSWZqJh8phxeldRYpeCckVLmlAjWqQVPWdOcRmsUDGGyoxJeXMic1ywpKASUBaAWbh5DZSffd2Jesc57euDohhOzROuzAdasXhprjmlZGh6QOCW9nunouB2qpkWCwqvQryLgTz4PXxJhdoXKhrgrf3WcwFpG5VIQpR8E7fxSc8UfBK1G4P-KPgmsZFEvtNvLAnNaLFyj8f9w5Lc2FtTsB_mJJCJ4NzjrMsQMdZtb4wZgY110PLf9xCcDErGxJteJ5VWza4JZgKRNMDhcC0rmU9VcFK_hwOHQzrOSdSnfKBj-fmuIK1VBpbtWt67KGkHdRm34TIDmHlisOsTV1T1LXDwa2v547XkqLLtT0U3PUU3xu1pW8cF3zB5ag2Zc_UhfLPlhklSIF2aAsYcUyJZxsUR3jeGA7D-G-yU6GGVFfa6Puf4Uk2AerkzuL4tsOvGHMESTud7YX4_mk4HxlATL_e2PRTCdLW36y3jQfqrVfXof6RJzhvYqj-1QPXmcWObRy0KPVs6U43E9tEssy-ASF9joo!/dl5/d5/L2dBISEvZ0FBIS9nQSEh/?urile=wcm%3Apath%3A%2Finternet_content-en%2Fhealthcare%20professionals%2Fproducts%2Forthopedics%2Fcement%2Fcobalt%20hv%20bone%20cement%2F79129bed-6e70-45fb-9344-07abfa553910.
59. Stratasys, *Dimension Elite*.
60. resources, T., *800LE4*.
61. ANSYS, I., www.ansys.com, 2011.
62. R., H., *The various stress patterns of press-fit, ingrown and cemented femoral stems*. *Clin orthop* 1990. **261**: p. 27-38.
63. Li C1, M.J., Yakimicki D, *Thermal characterization of PMMA-based bone cement curing*. *J Mater Sci Mater Med*, 2004. **15**(1): p. 85-9.
64. Nuño, N.A., G. *Journal of Biomechanics, Residual stresses at the stem–cement interface of an idealized cemented hip stem* 2002. **35**(6): p. 849-852.
65. U.S., F. *Food and Drug Administration*. <http://www.fda.gov/MedicalDevices/ProductsandMedicalProcedures/ImplantsandProsthetics/MetalonMetalHipImplants/ucm241594.htm#risks>.

66. A. Ramos, A.C., C. Relvas, and J. A. Simões, *Design process of a novel cemented hip femoral stem concept*. *Materials & Design*, 2012. **33**: p. 313-321.
67. Biggs, M., et al., *The influence of nanoscale biomimetic structures on osteoblast adhesion*. *Comparative Biochemistry and Physiology - Part A: Molecular & Integrative Physiology*, 2007. **146**(4, Supplement): p. S64.
68. Im, B.J., et al., *Texture direction of combined microgrooves and submicroscale topographies of titanium substrata influence adhesion, proliferation, and differentiation in human primary cells*. *Archives of Oral Biology*, 2012(0).
69. Zankovych, S., et al., *The effect of polyelectrolyte multilayer coated titanium alloy surfaces on implant anchorage in rats*. *Acta Biomaterialia*, 2013. **9**(1): p. 4926-4934.
70. Yoshimoto, H.S., Y.M. ; Terai, H. ; Vacanti, J.P., *A biodegradable nanofiber scaffold by electrospinning and its potential for bone tissue engineering* *Biomaterials*, 2003. **24**(12): p. 2077-2082.
71. Salerno, A.D.M., E. ; Iannace, S. ; Netti, P., *Tuning the microstructure and biodegradation of three-phase scaffolds for bone regeneration made of PCL, Zein, and HA* 2011. **47**(3): p. 245-260.
72. Kim, G., *Micro/Nanofibrous Scaffolds Electrospun from PCL and Small Intestinal Submucosa* *Journal of Biomaterials Science, Polymer Edition*, 2010. **21**(5): p. 553-562.
73. Downes S, A.R.S., Kayser M V, Patel M P and Braden M, *The regeneration of articular cartilage using a new polymer system*. *Journal of Materials Science: Materials in Medicine*, 1994 **5**(2): p. 88-95.
74. M. Jasty, W.J.M., C.R. Bragdon, D.O. O'Connor, T. Haire, W.H. Harris, *The initiation of failure in cemented femoral components of hip arthroplasties*. *Journal of Bone and Joint Surgery [Br]*, 1991. **73**: p. 551-558.
75. Callister, W.D., *Materials Science and Engineering An Introduction (fifth ed.)*. 2000, New York. 222.